Studies on torsional motions of flexible molecules in condensed phase(Dissertation_全文)

AUTHOR(S):

Hayashi, Haruhisa

(2)

STUDIES ON TORSIONAL MOTIONS OF FLEXIBLE MOLECULES IN CONDENSED PHASE

Haruhisa HAYASHI

Division of Molecular Engineering
Graduate School of Engineering
Kyoto University

1994

ACKNOWLEDGEMENTS

The present thesis is a summary of the author's studies from 1989 to 1994 at the Division of Molecular Engineering, Faculty of Engineering, Kyoto University.

The author would like to express his greatest gratitude to Professor Koichiro Nakanishi and Dr. Hideki Tanaka for their valuable advice and constant encouragement throughout this thesis. Especially, he deeply owes the accomplishment of his studies to the stimulating discussion and discerning suggestions by Dr. Hideki Tanaka.

He also would like to express the gratitude to the Associate Professor Tsuyoshi Nakajima, Dr. Osamu Kitao and other members of Professor Nakanishi's laboratory for their kind help and useful suggestions.

It was a great pleasure for the author to become acquainted with a lot of people both officially and privately through his study-life over seven years in Professor Nakanishi's laboratory. He would like to thank them for their encouragement and friendship. Above all, he also feels thankful to all my friends for their helpful encouragement and heartfelt friendship.

Finally, he expresses his sincere gratitude to his parents for their financial supports, generous understanding and affectionate encouragement.

Kyoto, winter 1994 Haruhisa HAYASHI

CONTENTS

GENERAL INTRODUCTION

Many computer simulation studies for liquids and liquid mixtures composed of rigid molecules have been carried out for the last three decades. The structure and dynamics for classical liquids have been studied by using computer simulation (e.g., Allen and Tildesley, 1987). Little attention has, however, been paid to the molecules having the degrees of freedom of internal rotation around dihedral angle, because these motions in flexible molecules are not easy to treat and distinguish from other motions such as the rotational motion and translational motion. The physical properties of chain molecules are somewhat related to their flexibility. A complicated nature of the liquid structures arising both from intermolecular and intramolecular interactions prevented us from understanding the roles played by the degrees of freedom of internal rotation.

It is well-known that the distribution of dihedral angle depends significantly on the density and temperature. The dynamical feature of the torsional motion is also sensitive to such external conditions. The dihedral angle distribution is a measure of solvent effects typical to liquid states, and the mechanism of torsional motion of the dihedral angle in the liquid is expected to differ from that in dilute gas state. However, this difference has not yet been accounted for. The interactions between the solvent and the solute alter the topography of potential energy hypersurface which is different from that in vacuum. This, in turn, affects the conformational equilibrium of the solute. Conformational changes in liquid state, which occur less frequently than the relaxation process of surrounding solvent molecules, are closely related to this topography.

In the series of present studies, molecular dynamics (MD) simulations for flexible molecules, have been performed to examine the liquid

structure in connection with the coupling between intra- and intermolecular interactions and its effect on the torsional motions. Two flexible molecules are adopted: butane (n-butane) as the simplest flexible molecule and ethylene glycol (ethane-1,2-diol, EG) as the simplest polyol. Butane is one of n-alkanes which are high theoretical and industrial interest substances. Polyols are well known characteristic of some interesting phenomena such as the prevention of denaturating protein and the presence of 'non-freezable water' in aqueous solution at subzero temperatures (Franks, 1982). The effects in terms of the torsional motions are examined since these complicated static and dynamical properties arise from the coupling mentioned above.

I. Conformational equilibria of n-butane molecules

It is believed that the distribution of the dihedral angle of flexible molecule in the liquid state is fairly different from that in the ideal gas state. However, the origin of this difference is not clear. The distribution of dihedral angle is a measure of the effect of intermolecular interaction on the internal degree of freedom. Historically, this distribution in the condensed phase has been discussed in terms of the random distribution or the short range packing effect. The former view proposed by Flory (1969) was based on the consideration that the distribution is dominated by random packing, and therefore, it should be the same as that in the ideal gas state. On the other hand, statistical mechanical theory predicted that the distribution shifted to the *gauche* form in favor of the short range packing. In fact, various methods such as the packing fraction theory, and superposition approximation have been proposed to evaluate the distribution of the dihedral angle. According to these approximate methods, an increase in the population of the *gauche* conformation is estimated to be as large as 10 % (e.g.,

Jorgensen *et al.*, 1981; Jorgensen, 1981). In a more realistic treatment with the reference interaction-site model (RISM) by Pratt and Chandler (Chandler and Pratt, 1976; Pratt and Chandler, 1977; Pratt, Hsu and Chandler, 1978), the increase is 7 %. The recent computer simulation studies (Edberg *et al.*, 1986, 1987; Wielopolski and Smith, 1986; Brown and Clarke, 1990) support the latter view. However, the results are likely to be dependent on the models used, the simulation time, the existence of the attractive forces, and other simulation conditions. Therefore, n-butane as the simplest molecule is adopted, in which only a single degree of freedom of internal rotation is included and other stretching and bending vibrational motions are ignored. Furthermore, the effect of the attractive forces on the dihedral angle distribution for n-butane has been examined by the molecular dynamics (MD) simulations.

II. The torsional dynamics of n-butane molecule

The chemical reaction rate and its mechanism in liquid state are somewhat different from that in the ideal gas state. However, the origin of this difference has not been accounted for. It is believed that the interaction between the solvent and the solute forces to alter the topography of potential energy hypersurface. The dynamics of infrequent molecular events are closely related to this topography. In the case that the system has stronger interaction between the solvent and the solute, we must consider the whole effects of many solvent molecules to interact concurrently with the solute molecules. In the opposite case, the existence of the solvent molecules also plays a significant role in the conformational equilibrium of solute molecules. The interactions between the solvent molecules and the solute molecules are 'co-operative' effects which affect indirectly the equilibrium and the reaction path of internal rotation of the flexible molecule.

The conformational equilibrium of flexible molecule is considered to be one of chemical reaction in a condensed phase (Chandler, 1978). The intramolecular rearrangement is regarded as energy transformation process. The *trans-gauche* isomerization of n-butane is a simple model for first-order chemical reaction since the torsional potential for n-butane is one-dimensional. Many investigations have been carried out in order to evaluate the rate constants from molecular dynamics of n-butane using statistical mechanical approaches (Rosenberg *et al.*, 1980) and transition state theory (TST) (Edberg *et al.*, 1986,1987; Brown and Clarke, 1990).

In this work, to clarify the torsional motion of the flexible molecule, n-butane molecule is adopted as the simplest flexible molecule among n-alkanes. Only a single degree of freedom for torsional motion is included and other stretching and bending vibrational motions are ignored. The molecular dynamics (MD) simulations of the n-butane molecule in non-polar molecules Xe are carried out, which is spherical but has a fairly high melting point. To analyze the torsional motion of n-butane, the kinetic energy of n-butane is divided into three terms, which are arising from the translational, rotational and torsional motions. By analyzing the time development of these kinetic and potential energies of n-butane, we investigate how the reaction path of internal rotation of n-butane molecule changes under the influence of the solvent molecules.

III. Aqueous Solution of Ethylene Glycol

Protein in polyol solvents is not easily denatured, while most proteins are not stable against heating, cooling or pH changes and easily undergo rearrangements to other stable states. The proteins in polyol solvents or aqueous polyol solutions, however, seem to retain a highly ordered

structure than those in pure water. Non-freezing glassy water is a very interesting example in which pure water does not become glassy upon cooling. A recent proton NMR study (Forsyth and MacFarlane, 1990) has shown that diol molecules can interact strongly with water by means of hydrogen bonds. However, it is not possible to say whether or not the diol solutes reduce the ability of water to form hydrogen-bonded networks and thus prevent the water molecules from nucleating to form ice. Many investigations have been carried out in order to clarify the origins of these phenomena, but their mechanisms are still unclear.

These characteristic properties undoubtedly arise from the coupling of intermolecular interactions with intramolecular interactions in the polyol molecules as well as from hydrogen bonding between the polyol hydroxy groups and water molecules. The torsional motions of flexible molecules are dependent on the nature of the solvent species in a condensed phase as well as on the torsional potential. The dynamics of the torsional motions are highly cooperative in the liquid state. The conformational equilibrium is somewhat different from that in a vacuum. Therefore, investigations of the role of solvent molecules on the equilibrium properties and dynamics of torsional motions are very important.

Ethylene glycol is the simplest of polyols and a biologically important substance. Because each EG molecule has two OH groups, three-dimensional (3D) networks can be formed with water, with other EG molecules, and with itself by hydrogen bonding in aqueous EG solutions. Some of the physical properties of EG are different from those of other monohydric alcohols (Podo *et al.*, 1974) which can form only linear hydrogen bonds. The internal equilibrium configuration of the EG molecule has been measured by electron diffraction (Bastiansen, 1949) and IR spectroscopic methods (Krueger and Mettee, 1965; Buckley and Giguère, 1967), and has been calculated using energy minimiza-

tion of rotational isomers (Podo *et al.*, 1974; van Alsenoy *et al.*, 1984). Recently, conformational analyses have been performed using MC perturbation simulations (Nagy *et al.*, 1991) and the Potential Mean Force (PMF) was also calculated (Hooft *et al.*, 1992).

In the present molecular dynamics (MD) simulation, we aim to clarify the torsional motion of EG in aqueous solutions of finite EG composition in connection with inter- and intra-molecular hydrogen bonds. To this end, we make a comparison of this system with an EG+Xenon mixture. In order to investigate how the intramolecular interaction affects intermolecular hydrogen bonds, some rigid-EG models are also examined.

Scope of the Present Study

MD simulations on n-butane and aqueous solutions of EG have been carried out in the present study. In the next chapter, the scheme of constraint-MD method is given with some improvements. In chapter II, the conformational equilibria of n-butane molecules are discussed. Chapter III deals with the torsional dynamics of n-butane molecule to analyze the motion of n-butane. Chapter IV is devoted to MD calculations for aqueous solution of EG. The torsional motions of EG in aqueous solutions of finite EG composition are presented and clarified in connection with inter- and intra-molecular hydrogen bonds. General conclusion of this work is given in the final chapter.

CHAPTER I

CONSTRAINT MOLECULAR DYNAMICS SIMULATION

ALGORITHM OF MD SIMULATION

Molecular Dynamics (MD) simulation is one of methods using computer for numerical solution of equations of motion (EOM), which are ordinary differential equations.

Theory

In the monoatomic molecule system, the Lagrangian equations of motion (EOM) with the degree of freedom f become

$$\frac{d}{dt}\frac{\partial \mathcal{L}}{\partial \dot{q}_k} - \frac{\partial \mathcal{L}}{\partial q_k} = 0, \quad (k = 1, \ldots, f) \tag{1}$$

where the Lagrangian function $\mathcal{L}(\mathbf{q}, \dot{\mathbf{q}})$ is defined by the difference between kinetic energy term $\mathcal{K}$ and potential energy term $\mathcal{V}$,

$$\mathcal{L} = \mathcal{K} - \mathcal{V}. \tag{2}$$

For Cartesian coordinates, eqn (1) becomes

$$m_i \ddot{\mathbf{r}}_i(t) = \mathbf{F}_i(t) \tag{3}$$

where $\mathbf{r}_i$ is the position and m_i is the mass of atom i and $\mathbf{F}_i(t)$ is the force on that atom,

$$\mathbf{F}_i(t) = \nabla_{\mathbf{r}_i}\mathcal{L} = -\nabla_{\mathbf{r}_i}\mathcal{V}. \tag{4}$$

Given the molecular positions, velocities, and other dynamic information at time t, 3N second-order differential equations, EOM (3),

are solved on a step-by-step basis. In classical mechanics, the estimation of the next positions $\mathbf{r}_i$ at time $t + \delta t$ may be obtained by Taylor expansion around time t:

$$\mathbf{r}_i(t + \delta t) = \mathbf{r}_i(t) + \delta t \dot{\mathbf{r}}_i(t) + \frac{1}{2}(\delta t)^2 \ddot{\mathbf{r}}_i(t) + O((\delta t)^3) \tag{5}$$

and also the previous positions $\mathbf{r}_i$ at time $t - \delta t$:

$$\mathbf{r}_i(t - \delta t) = \mathbf{r}_i(t) - \delta t \dot{\mathbf{r}}_i(t) + \frac{1}{2}(\delta t)^2 \ddot{\mathbf{r}}_i(t) - O((\delta t)^3) \tag{6}$$

The central-difference prediction is obtained by adding and deleting these two expressions to give

$$\mathbf{r}_i(t + \delta t) + \mathbf{r}_i(t - \delta t) = 2\mathbf{r}_i(t) + (\delta t)^2 \ddot{\mathbf{r}}_i(t) + O((\delta t)^4) \tag{7}$$

$$\mathbf{r}_i(t + \delta t) - \mathbf{r}_i(t - \delta t) = 2\delta t \dot{\mathbf{r}}_i(t) + O((\delta t)^2) \tag{8}$$

The velocities are not to be computed from the trajectories, but they are useful for estimating the kinetic energy. They may be obtained from the formula.

$$\mathbf{r}_i(t + \delta t) = 2\mathbf{r}_i(t) - \mathbf{r}_i(t - \delta t) + (\delta t)^2 \ddot{\mathbf{r}}_i(t) + O((\delta t)^4) \tag{9}$$

$$\mathbf{v}_i(t) = \dot{\mathbf{r}}_i(t) = \frac{1}{2\delta t}\{\mathbf{r}_i(t + \delta t) - \mathbf{r}_i(t - \delta t)\} + O((\delta t)^2) \tag{10}$$

This algorithm is the most widely used and simple method of integrating the EOM, is adopted by Verlet (1967).

MD FOR RIGID NON-SPHERICAL BODIES

In polyatomic molecule systems, however, it becomes necessary to consider intramolecular freedoms such as

- stretching of interatomic bonds
- bending motions
- torsional (twisting) motions.

Therefore, the equations of motion for polyatomic molecules are very complex. In addition, the time step by which EOM are solved numerically using computer has to be very short since these frequencies are much high.

The torsional motions are, of much lower frequency than bond vibrations, and are very important in long-chain organic molecules: they lead to conformational interconversion and have a direct influence on polymer dynamics. Clearly, these effects must be treated properly in molecular dynamics, within the classical approximation. It would be quite unrealistic to assume total rigidity of such molecules, although bond lengths and bond bending angles can be thought of as fixed.

CONSTRAINT MD METHODS

In MD simulations of long chain molecules, the fast intramolecular vibrations are frozen. The bond lengths are fixed by use of geometrical constants, and the bond angles are kept fixed by use of holonomic constants. In generalized coordinates, it is difficult to write down explicitly the EOM of flexible molecules since inertial terms are not omitted. Therefore, usually the cartesian EOM is used for long chain molecules. Under the existence of these geometrical and holonomic constraints, the EOM becomes linear equations. There are two efficient methods to solve the linear equations: the direct matrix method and the iterative method (van Gunsteren, 1980). The former method is used to calculate inverse matrix by using Gaussian elimination (e.g., Edberg *et al.*, 1986). However, for long and complicated molecules, this method is required for long computer run times to compute the large inverse matrix, since the dimension of this matrix is equal to the number of constraints. The latter method is used to calculate approximate solution iteratively to be converged to real solution until all the constraints are satisfied. Some algorithms to be applied this iterative method to

MD simulation are advocated: most popular algorithm is named Shake (Ryckaert *et al.*, 1978) and its modificative algorithms are Rattle (Andersen, 1983), CFR (Ciccotti *et al.*, 1982), modified-Shake (Lambrakos *et al.*, 1989), Settle (Miyamoto and Kollman, 1992) and so on.

SHAKE

Scheme of Shake algorithm

Flexible molecules can be treated as an extension of the case of the molecule without degree freedom of internal rotation. Not only the force of inter- and intra-molecular interactions, but the force acting on atom pertaining to the molecule with constraints is also taken into account.

No direct route to solve the constraint force is traced at all the time and therefore we are forced to use an iterative process where each loop treats all constraints individually and successively. This method called SHAKE (Ryckaert *et al.*, 1977; Ciccotti and Ryckaert, 1986), has been devised for molecules with bond constraints.

In a system containing $\mathcal{N}$ molecules, the Lagrangian equations of motion with the degree of freedom f and ℓ holonomic constraints become

$$\frac{d}{dt}\frac{\partial \mathcal{L}}{\partial \dot{\mathbf{r}}_{i\alpha}} - \frac{\partial \mathcal{L}}{\partial \mathbf{r}_{i\alpha}} = \mathbf{G}_{i\alpha} \quad i = 1, \ldots, n, \quad \alpha = 1, \ldots, \mathcal{N} \tag{11}$$

where $\mathbf{G}_{i\alpha}$ is constraint force interacted on particle (i, α).

The force of constraint $\mathbf{G}_{i\alpha}$ acting on atom (i, α) pertaining to a molecule with ℓ constraints, has the general form

$$\mathbf{G}_{i\alpha} = -\sum_{k=1}^{\ell} \lambda_k^{(\alpha)} \nabla_{i\alpha} \sigma_k^{(\alpha)} = -\sum_{k=1}^{\ell} \lambda_k^{(\alpha)} \Big(\frac{\partial \sigma_k^{(\alpha)}}{\partial \mathbf{r}_{i\alpha}} \Big) \tag{12}$$

where the Lagrange multiplier ${\lambda_k}^{(\alpha)}$ is a function of the coordinates and velocities of the atoms of that molecules, associated with the constraint $\sigma_k^{(\alpha)}$. The explicit expression for this Lagrange multiplier is obtained by requiring that for all k, $\ddot{\sigma}_k^{\alpha}$ vanishes at all the time.

Consider the example, as the simple case of the heteronuclear rigid diatomic molecule such as N_2 and CO, which constrain one of the bonds to be of fixed length,

$$\mathbf{r}_{12}{}^2 - d^2 = 0 \tag{13}$$

where $\mathbf{r}_{12} = \mathbf{r}_1 - \mathbf{r}_2$, so d is the fixed bond length. The constraint forces are eqn (2)

$$\mathbf{G}_1 = -\mathbf{G}_2 = -2\lambda(t)\mathbf{r}_{12}. \tag{14}$$

In the usual NVE-MD, the Verlet algorithm for both atoms is

$$\mathbf{r}_1(t+\delta t) = \mathbf{r}_1'(t+\delta t) - 2 \cdot \big(\frac{\lambda(t)}{m_1}\big) \cdot \mathbf{r}_{12}(t) \tag{15}$$

$$\mathbf{r}_2(t+\delta t) = \mathbf{r}_2'(t+\delta t) + 2 \cdot \big(\frac{\lambda(t)}{m_2}\big) \cdot \mathbf{r}_{12}(t) \tag{16}$$

where

$$\mathbf{r}_i'(t+\delta t) = -\mathbf{r}_i(t-\delta t) + 2\mathbf{r}_i(t) + \big(\frac{(\delta t)^2}{m_i}\big) \cdot \mathbf{F}_i(t) \tag{17}$$

are the predicted positions at time $(t+\delta t)$ according to all forces in the system except the constraint one. Combining eqns (13), (15) and (16) in which Lagrange multiplier $\lambda_k(t)$, which is depended on time, is substituted formally by parameter γ_k, we get a quadratic equation in γ_k giving

$$\gamma_k(\delta t)^2 = \frac{-(\mathbf{r}_{12} \cdot \mathbf{r}_{12}') + \sqrt{(\mathbf{r}_{12} \cdot \mathbf{r}_{12}')^2 - \mathrm{d}^2(\mathrm{d}^2 - \mathbf{r}_{12}'{}^2)}}{2\mu^{-1}\mathrm{d}^2} \tag{18}$$

where $\mathbf{r}_{12}' = \mathbf{r}_1' - \mathbf{r}_2'$ and

$$\mu = \frac{1}{m_1^{-1} + m_2^{-1}} \tag{19}$$

is the reduced mass of this molecule.

In general, the position of an atom i on a molecule with ℓ constraints is

$$\mathbf{r}_i(t+\delta t) = \mathbf{r}_i'(t+\delta t) - \frac{(\delta t)^2}{m_i}\sum_{k=1}^{\ell}\gamma_k\Big(\frac{\partial\sigma_k}{\partial\mathbf{r}_i}\Big)_{\{\mathbf{r}_i(t)\}}. \tag{20}$$

If the γ_k is evaluated, the position $\mathbf{r}_i$ can be evaluated from $\mathbf{r}_i'$. A given constraint k at the $\mathcal{N}$th iterative loop is focused on.

$$\mathbf{r}_j{}^{\mathrm{NEW}} = \mathbf{r}_j{}^{\mathrm{OLD}} - (\delta t)^2\frac{\gamma_k^{(\mathcal{N})}}{m_j}\frac{\partial\sigma_k}{\partial\mathbf{r}_j}, \quad (j=1,\ldots,n_k) \tag{21}$$

The single parameter $\gamma_k{}^{(\mathcal{N})}$ is now evaluated as the first order solution of the scalar equation

$$\sigma_k(\{\mathbf{r}_j{}^{\mathrm{NEW}}\}) = 0. \tag{22}$$

This is obtained by expanding this last equation in power of $\gamma_k{}^{(\mathcal{N})}$ and neglecting all term of order lager than unity. Therefore we get

$$\gamma_k^{(\mathcal{N})} = (\delta t)^{-2}\sigma_k(\{\mathbf{r}_j{}^{\mathrm{OLD}}\})/\sum_{j=1}^{n_k} m_j^{-1}\Big(\frac{\partial\sigma_k}{\partial\mathbf{r}_j}\Big)_{\mathbf{r}^{\mathrm{OLD}}}\cdot\Big(\frac{\partial\sigma_k}{\partial\mathbf{r}_j}\Big)_{\mathbf{r}(t)} \tag{23}$$

where the sum in the denominator runs over the n_k atoms involved by σ_k.

If the iterative procedure is started with the 'unconstrained' positions as eqn (17), the coordinates after completion of step eqns (21) and (23) for the σ_k constraint at the Nth loop can be written

$$\mathbf{r}_i{}^{\mathrm{NEW}} = \mathbf{r}_i'(t+\delta t) - \frac{(\delta t)^2}{m_i}\sum_{k'=1}^{\ell}\beta_{k'}^{k\mathcal{N}}\Big(\frac{\partial\sigma_{k'}}{\partial\mathbf{r}_i}\Big)_{\mathbf{r}(t)} \tag{24}$$

where

$$\beta_{k'}^{k\mathcal{N}} = \sum_{\mathcal{N}'=1}^{\mathcal{N}}\gamma_{k'}^{(\mathcal{N}')}, \quad k'\le k, \tag{25}$$

$$\beta_{k'}^{k\mathcal{N}} = \sum_{\mathcal{N}'=1}^{\mathcal{N}-1}\gamma_{k'}^{(\mathcal{N}')}, \quad k'>k. \tag{26}$$

In order to solve γ_k, these schemes mentioned above are calculated iteratively regarding all the constraints as a continuative procedure.

In practice, the set of Lagrange parameters γ_k is adjusted by the iterative method until all the constraints are satisfied within a tolerance value.

$$\sigma_k(\{\mathbf{r}_j(t+\delta t)\}) \le tol., \quad k=1,\ldots,\ell \tag{27}$$

The tolerance value was set to 1.0×10^{-8}, all the constraints are satisfied for the adjusted positions less than $\pm0.01\%$ error.

Application and Improvement

Most of computational time was spent calculating the force between sites and iterating shake routine in every MD and MC simulation. The simulations become increasingly time consuming as the number of particles increases. Furthermore, properties of long-chain molecules occur over a wide range of time scales. In order to study these properties, long computer run times are needed.

Vector processor (VP) computer works by taking the whole vector operation and logically executing it as one instruction. The use of the VP computer and the coding program suitable for VP machine are able to be fast and efficient computing by the control of flow dependencies. Efficient vector and parallel algorithms for MD simulation are still in development. The routine for calculating the force between all interaction sites is easy to be vectorized by regarding each coordinate of interaction sites as an element of vector array.

The Shake algorithm is applied originally to the molecule one by one and is subsequently iterated until all the constraints of each molecule are satisfied. Unfortunately, this procedure is not suitable for

VP machine since this algorithm is a regressive calculation. The Shake routine is essentially an iterative method that considers all constraints of all molecules in succession. Therefore, we coded this algorithm as the iterative calculation is implemented until all the molecules are satisfied own constraints simultaneously. These improvements led the Shake routine to be vectorized easily. Thus MD simulations with the improvement SHAKE routine can be executed on VP machine very quickly.

CHAPTER II

PURE LIQUID n-BUTANE

For liquid n-butane, molecular dynamics simulations have been performed in order to understand liquid structures in terms of both inter- and intra-molecular interactions. Each n-butane molecule consists of four sites interacting with LJ potential and only a dihedral angle is taken into account as the internal degree of freedom (LJ model). The population of *gauche* conformations with respect to the ideal gas state is found to increase in the liquid state. To investigate how the intermolecular interaction affects the dihedral angle distribution, we also adopt repulsive LJ potential (RLJ) model. It is found that the nearest neighbor packing of the methyl and/or methylene groups can be represented roughly by using only the repulsive interaction. From the dihedral angle distribution, however, the rate of the shift of RLJ model to *gauche* is larger than that of LJ model and the attractive force also plays a significant role in the conformational equilibrium.

MODEL AND POTENTIAL

Since we pay attention to the torsional motion of the dihedral angle, both intra- and intermolecular interactions are taken into account. Our model for n-butane is the same as that used by Ryckaert and Bellemans (1978). Each n-butane molecule consists of four interaction sites centered on each carbon atom having the same mass ($m = 2.408 \times 10^{-23}$ g). All the hydrogen atoms of n-butane are neglected. The site-site distance is fixed at 1.53 Å and the bond angles are also fixed at 109.47°.

The intramolecular conformation of n-butane is defined by the dihedral angle, $\alpha, (-180° < \alpha \leq +180°)$ and the torsional potential is

given as a function of α by

$$\mathcal{V}^{DIH}(\alpha)/k_B = \{+1.116 + 1.462\cos\alpha - 1.578\cos^2\alpha - 0.368\cos^3\alpha + 3.156\cos^4\alpha - 3.788\cos^5\alpha\} \times 10^3\mathrm{K} \quad (1)$$

(k_B = Boltzmann's constant). This intramolecular potential has been proposed by Scott and Scheraga on the basis of IR and Raman spectroscopic measurements and the *ab-initio* calculations for an n-butane molecule in vacuum (Scott and Scheraga, 1966; Woller and Garbisch, 1972). The potential energy for *trans* conformation ($\alpha = 0°$) is set equal to 0 kJ mol^{-1} and that for $\pm$*gauche* conformation ($\alpha = \pm 120°$) is 2.93 kJ mol^{-1}. The potential barrier from *trans* to $\pm$*gauche* is 12.35 kJ mol^{-1}.

The site-site intermolecular potential is described by the Lennard-Jones 12-6 potential with multiplification by the switching-function $\mathcal{SF}(R)$ (Ohmine *et al.*, 1988) (we call this LJ-model).

$$\mathcal{V}^{\mathcal{SF}\text{-LJ}}(\mathbf{r}, \mathbf{r}') = \mathcal{SF}(R) \cdot \sum_{i,j} \mathcal{V}^{\mathrm{LJ}}(r_{ij}) \quad (2)$$

$$\mathcal{SF}(R) = \begin{cases} 1 & , \quad (R < r_d) \\ \frac{(R-r_c)^3}{(r_d-r_c)^5}\{10(R-r_d)^2 + (R-r_c)^2 & \\ \quad -5(R-r_c)(R-r_d)\} & , \quad (r_d \le R < r_c) \\ 0 & , \quad (r_c \le R) \end{cases} \quad (3)$$

$$\mathcal{V}^{LJ}(r) = 4\varepsilon\left\{\left(\frac{\sigma}{r}\right)^{12} - \left(\frac{\sigma}{r}\right)^{6}\right\} \quad (4)$$

where R stands for the separation of the centers of mass, $\mathbf{r}$ (also $\mathbf{r}'$) denotes the Cartesian coordinates of all atoms on each molecule, r_{ij} is the distance between i and j sites. Size parameter σ and energy parameter ε are 3.923 Å and 72 K, respectively.

In the present MD calculation, all the n-butane molecules have

initially the *trans* conformation ($\alpha = 0°$) and their orientations are random. Initial temperatures and densities are set equal to the experimentally observed values of liquid n-butane (system A: 200 K, $\rho^* = 0.419$; system B: 291 K, $\rho^* = 0.365$) (Ryckaert and Bellemans, 1978). Equations of motion are solved by the Verlet method (e.g., Allen and Tildesley, 1987) and the constraints of bond angles and length are treated by the Shake algorithm (Ryckaert *et al.*, 1977). A time step, Δt, for the integration of equations of motion is 1.93×10^{-15} sec. 108 n-butane molecules are confined in a cubic cell imposing the periodic boundary condition and the systems in the MD simulation correspond to the NEV-ensemble. The MD simulation is extended to 900,000 time steps (1737ps) for each system. This simulation time is long enough to evaluate the dihedral angle distribution with better statistics than that of previous studies (Ryckaert and Bellemans, 1978; Wielopolski and Smith, 1986).

In order to understand how the attractive part of the LJ interaction from other molecules affects the dihedral angle distribution, another potential, repulsive LJ (RLJ) model which has only the repulsive part is also examined. The repulsive part of the potential was evaluated by adopting the Weeks-Chandler-Andersen (W.C.A.) type separation (Weeks *et al.*, 1971).

$$\mathcal{V}^{\mathrm{RLJ}}(r) = \begin{cases} \mathcal{V}^{\mathrm{LJ}}(r) + \varepsilon, & (\text{for } r < r_{min}) \\ 0, & (\text{for } r \ge r_{min}) \end{cases} \quad (5)$$

where r_{min} is set equal to $2^{1/6}\sigma$.

RESULTS AND DISCUSSION

The energy and dihedral angle distribution obtained from the present MD simulations are given in Table 1. The *trans* conformation is defined by the region of the dihedral angle α , $-60° < \alpha < +60°$, and the *gauche*

Table 1. Conditions of MD simulations for n-butane interacting LJ and RLJ potential. The temperature, energies and the percentage of *trans* state (X^T) are given. Standard deviations of X^T are also given in the parentheses. The temperature T, the density ρ^* are in Kelvin, LJ reduced unit, respectively. The unit of energy is kJ/mol.

	System	Average Temp.(K)	Total Energy	Potential Energy	Intra Energy	X^T (%) (dev.)
LJ-A	T = 200.00 K $\rho^* = 0.419$	192.79	-14.763	-20.372	+1.685	73.995 (3.826)
LJ-B	T = 291.00 K $\rho^* = 0.365$	279.21	-8.228	-16.352	+2.521	63.842 (3.771)
RLJ-A	T = 200.00 K $\rho^* = 0.419$	194.89	+10.499	+4.828	+1.885	67.581 (3.142)
RLJ-B	T = 291.00 K $\rho^* = 0.365$	286.23	+13.446	+5.118	+2.729	56.875 (3.603)

conformation by that of $-180° < \alpha \leq -60°$ and $+60° \leq \alpha \leq +180°$. X^T and X^G $(= 1.0 - X^T)$ stand for the fraction of *trans* and *gauche* conformational populations, respectively. Standard deviations are also given in the parentheses of this table. The deviations are calculated by dividing whole simulation run into several blocks comprising consecutive 10000 steps (19.3ps). In the RLJ model, the total energy of the system is positive. This is simply because the RLJ potential does not have the attraction term and is positive in all regions.

Time evolution of the dihedral angle

We can obtain the time evolution of the dihedral angles of individual molecules in the LJ model. Figures 1 to 4 show the typical examples of the time evolution of the dihedral angles for both the LJ model and the RLJ model. The higher the temperature is, the more frequently the rotation of the dihedral angle in n-butane molecule takes place. Moreover, various patterns of rotation are observed; *trans* $\rightarrow \pm$*gauche* transformation, $\pm$*gauche* $\rightarrow$ *trans* transformation, and $\pm$*gauche* $\rightarrow \mp$*gauche* direct transformation. In the case of RLJ model, we can obtain the similar results to that of LJ model.

Radial Distribution

Although the temperatures for both the LJ and the RLJ systems are different slightly with each other, the difference in the radial distribution function (RDF) arising from the temperature difference is expected to be small. No correction due to the difference is made for RDF's, when they are compared. Figures 5 and 6 show the End-End (E-E), Inner-Inner (I-I), End-Inner (E-I), and centers of mass (G-G) RDF's for the LJ and the RLJ models, respectively. As seen from these figures, the first peak of G-G RDF in either system is rather broad compared

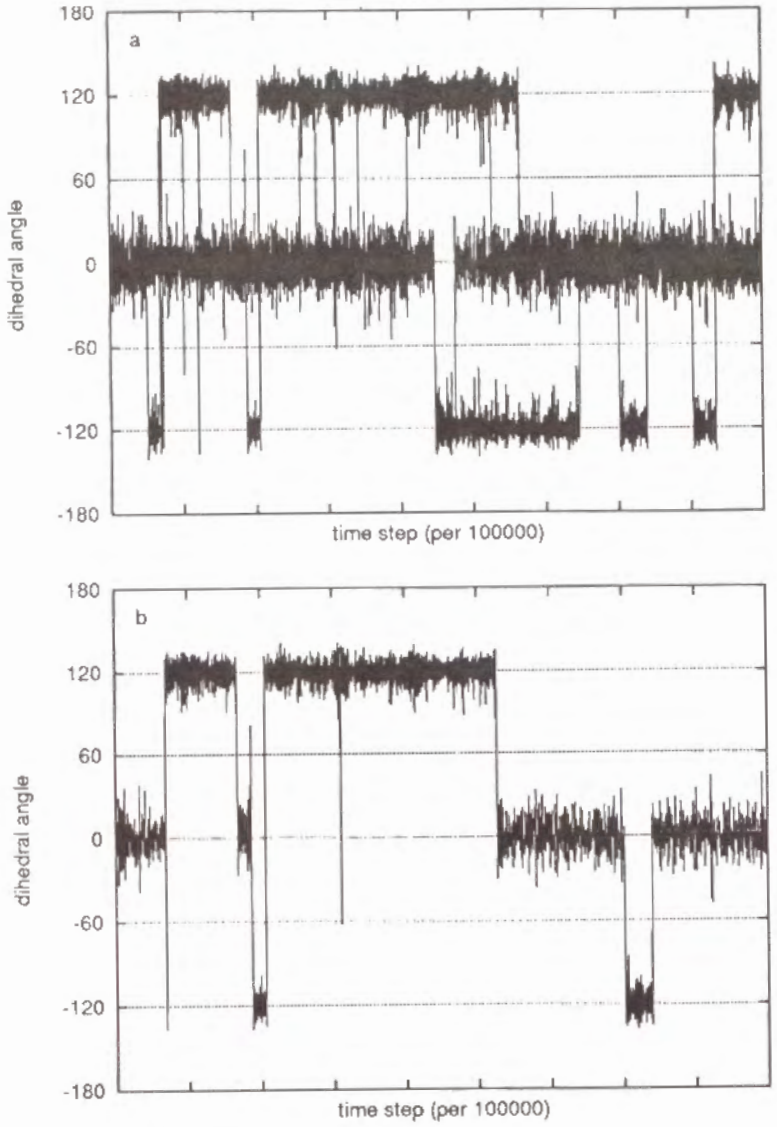

Figure 1 The time evolution of the dihedral angle for system LJ-A (T=192.79K, ρ^*=0.419 and 1737ps) : (a) selected four molecules and (b) selected one molecule.

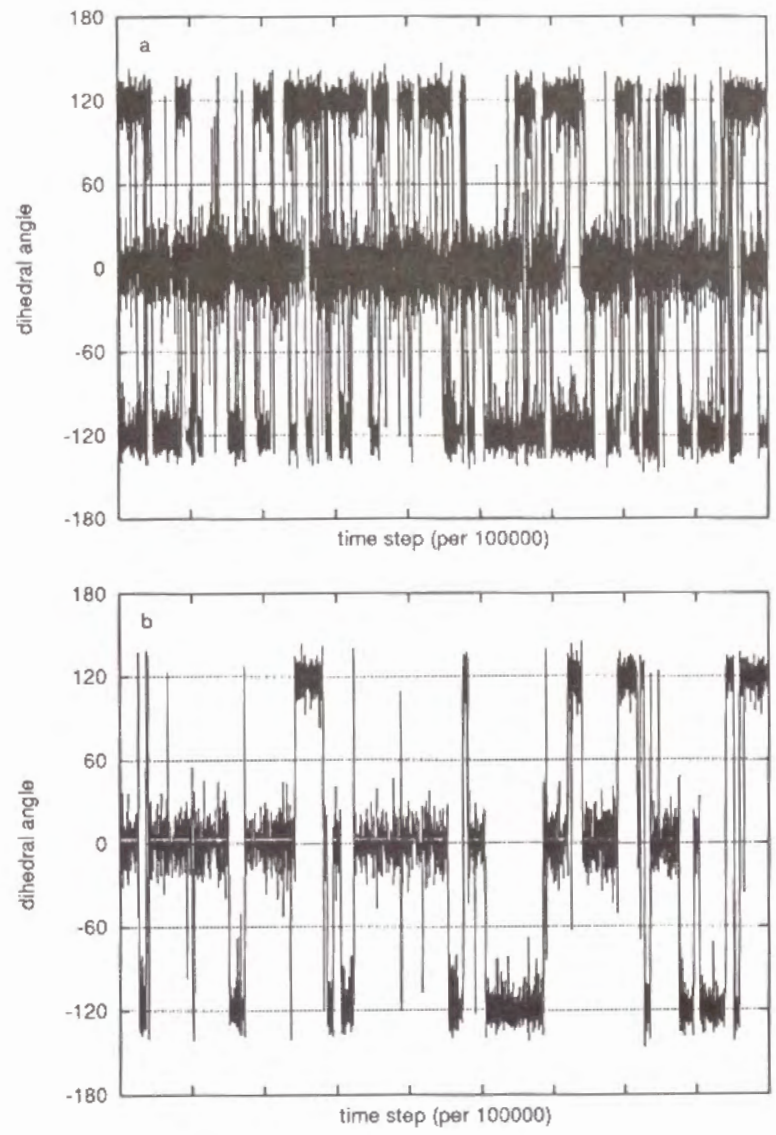

Figure 2 The time evolution of the dihedral angle for system LJ-B (T=279.21K, ρ^*=0.365 and 1737ps) : (a) selected four molecules and (b) selected one molecule.

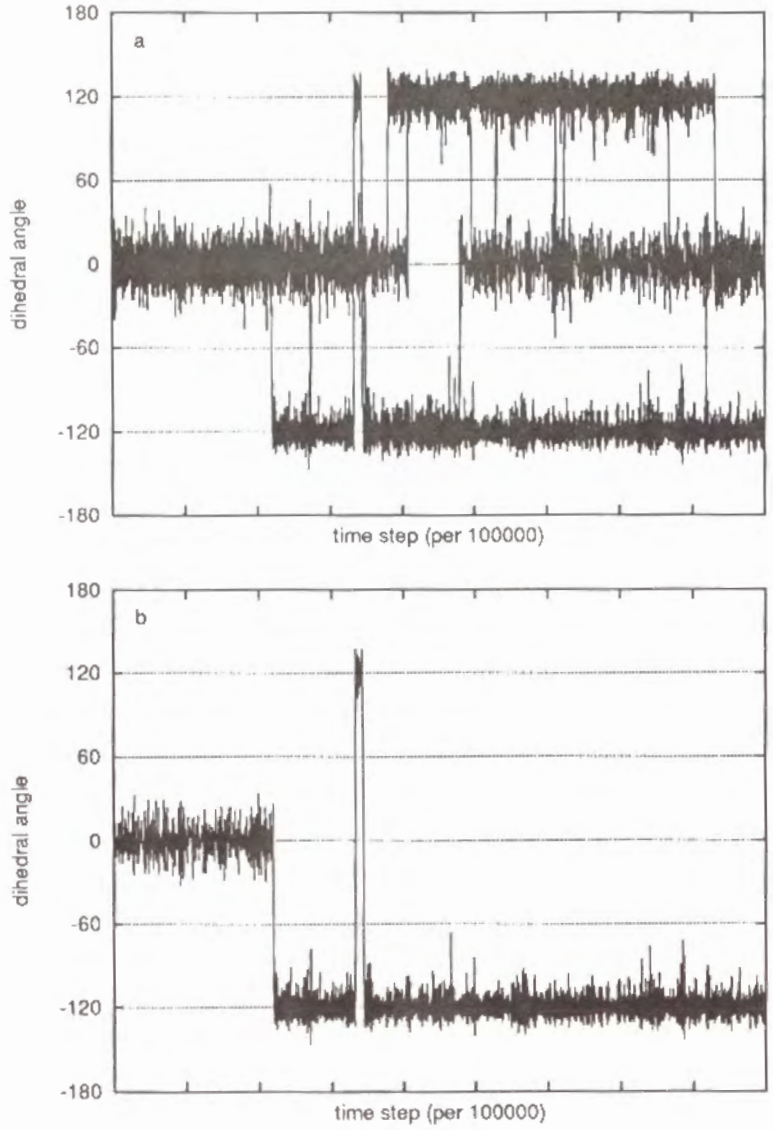

Figure 3 The time evolution of the dihedral angle for system RLJ-A (T=194.89K, ρ^*=0.419 and 1737ps) : (a) selected four molecules and (b) selected one molecule.

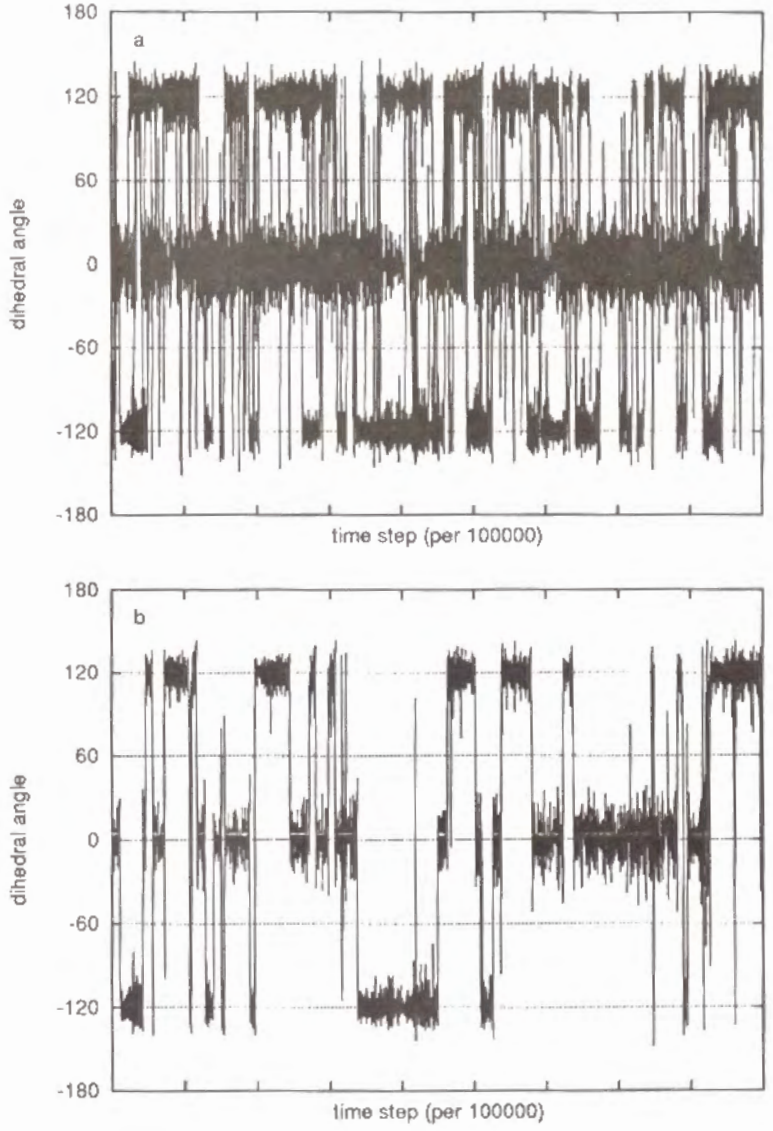

Figure 4 The time evolution of the dihedral angle for system RLJ-B (T=286.23K, ρ^*=0.365 and 1737ps) : (a) selected four molecules and (b) selected one molecule.

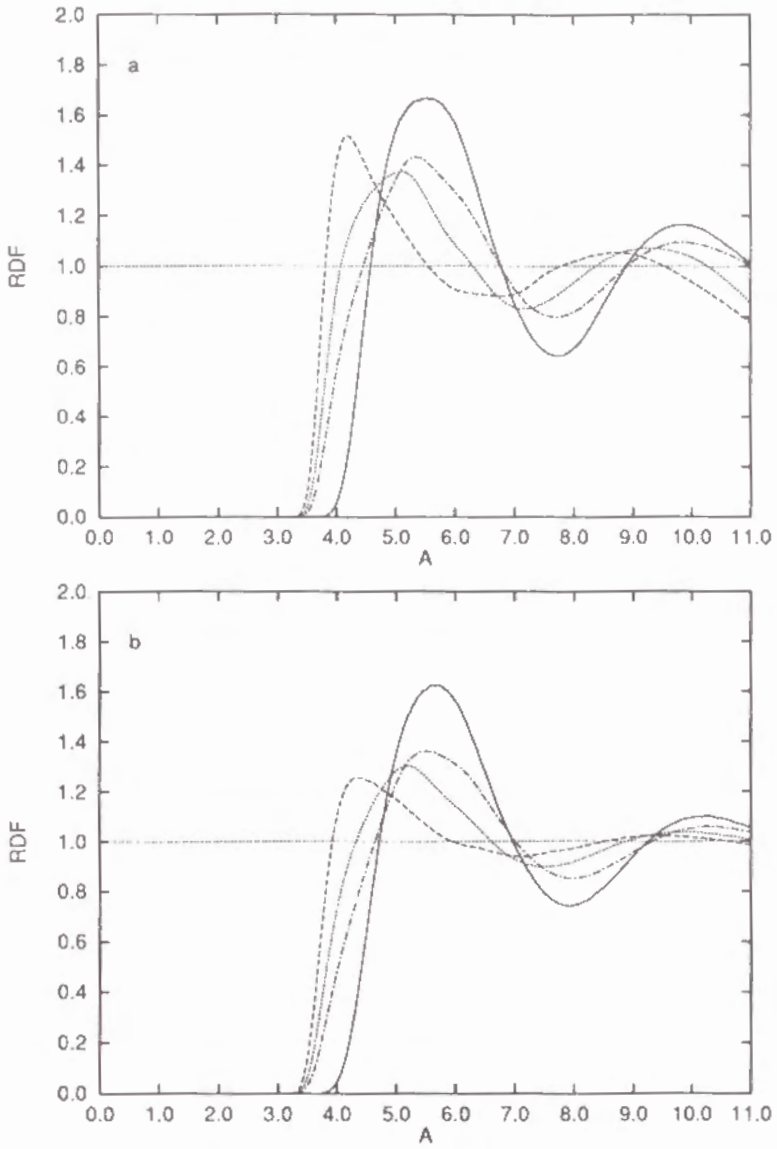

Figure 5 Site-site radial distribution functions for the LJ model n-butane. The dashed line, dash-dot line, dotted line and solid line show the End-End (E-E), Inner-Inner (I-I), End-Inner (E-I) and centers of mass (G-G) RDF, respectively. (a) System LJ-A and (b) LJ-B.

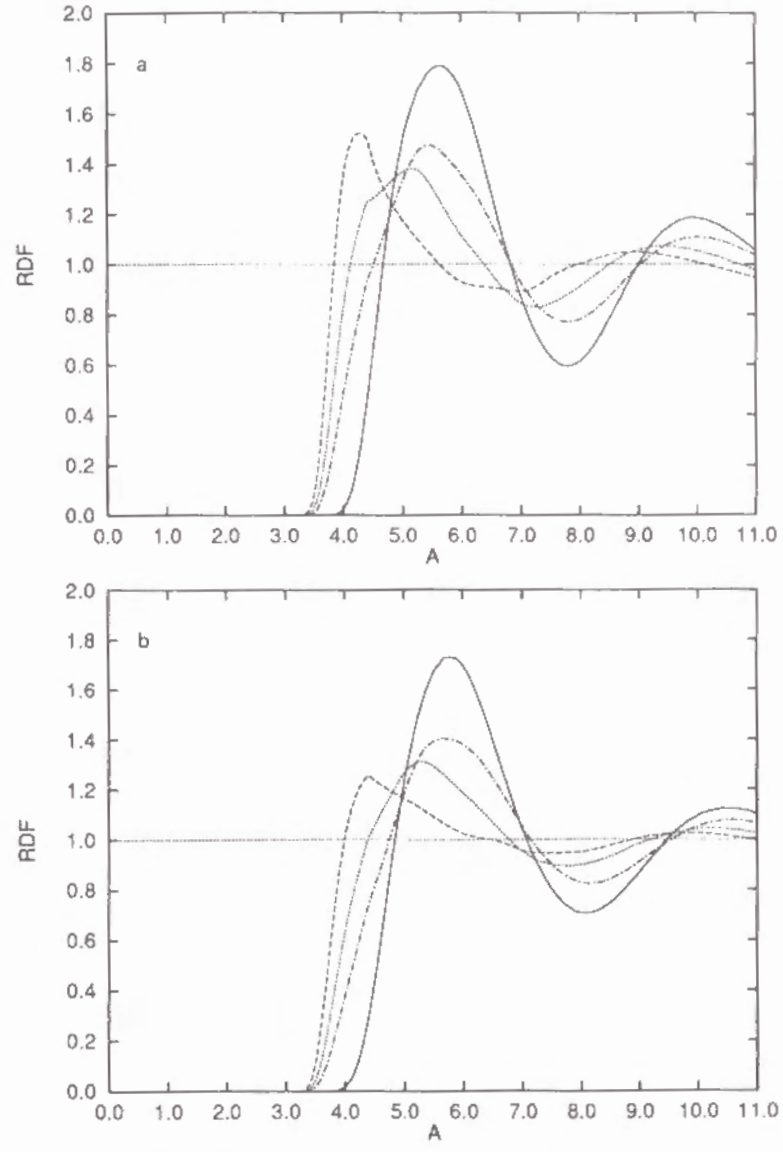

Figure 6 Site-site radial distribution functions for the RLJ model n-butane. End-End (E-E; dashed line), Inner-Inner (I-I; dash-dotted line), End-Inner (E-I; dotted line), centers of mass (G-G; solid line) RDF for (a) System RLJ-A and (b) RLJ-B.

with the site-site RDF's. This is in contrast to the case of small diatomic molecule such as nitrogen. This is caused by the relatively large center of mass motions of individual molecules. Those are, in turn, due partly to the large change of dihedral angles.

Comparing the RLJ model with the LJ model, only a small difference is seen in RDF. The peak positions for the RLJ model shift slightly to long distance direction over all distance ranges. This is explained simply by the fact that there is no attractive interaction in RLJ model. It is found that, except for a small shift in RDF's, there is no significant difference in the short range structures of system between both models (Almarza *et al.*, 1990; Elliott Jr *et al.*, 1990).

Distribution of the dihedral angle

The distribution of the dihedral angle calculated from the MD simulations is shown in Figures 7 (LJ model) and 8 (RLJ model) and also in Table 2. It is found that X^G_{liquid} $(= 1.0 - X^T_{liquid})$ in the liquid state increases from that in the ideal gas state $(X^G_{ideal\ gas})$. The conformational equilibria shift toward the *gauche* form due to the presence of other molecules. This shift ΔX,

$$\Delta X = X^G_{liquid} - X^G_{ideal\ gas} = -(X^T_{liquid} - X^T_{ideal\ gas}) \qquad (6)$$

depends on the simulation conditions and is between 3 and 5% in the case of the LJ model.

For the RLJ model, the increase in ΔX is almost 10%, which should be compared with that obtained from theoretical calculation using a fused hard-sphere system (Pratt *et al.*, 1978). Then, we try to separate the origin of the distribution into two contributions as

$$\mathcal{V}^{DIH}_{liquid}(\alpha) = \mathcal{V}^{DIH}_{ideal\ gas}(\alpha) + \mathcal{W}^{DIH}(\alpha)\ , \qquad (7)$$

where $\mathcal{V}^{DIH}_{liquid}(\alpha)$ is calculated from the dihedral angle distribution as

$$\mathcal{V}^{DIH}_{liquid}(\alpha) = -k_B T \ln(X_{liquid}(\alpha)). \qquad (8)$$

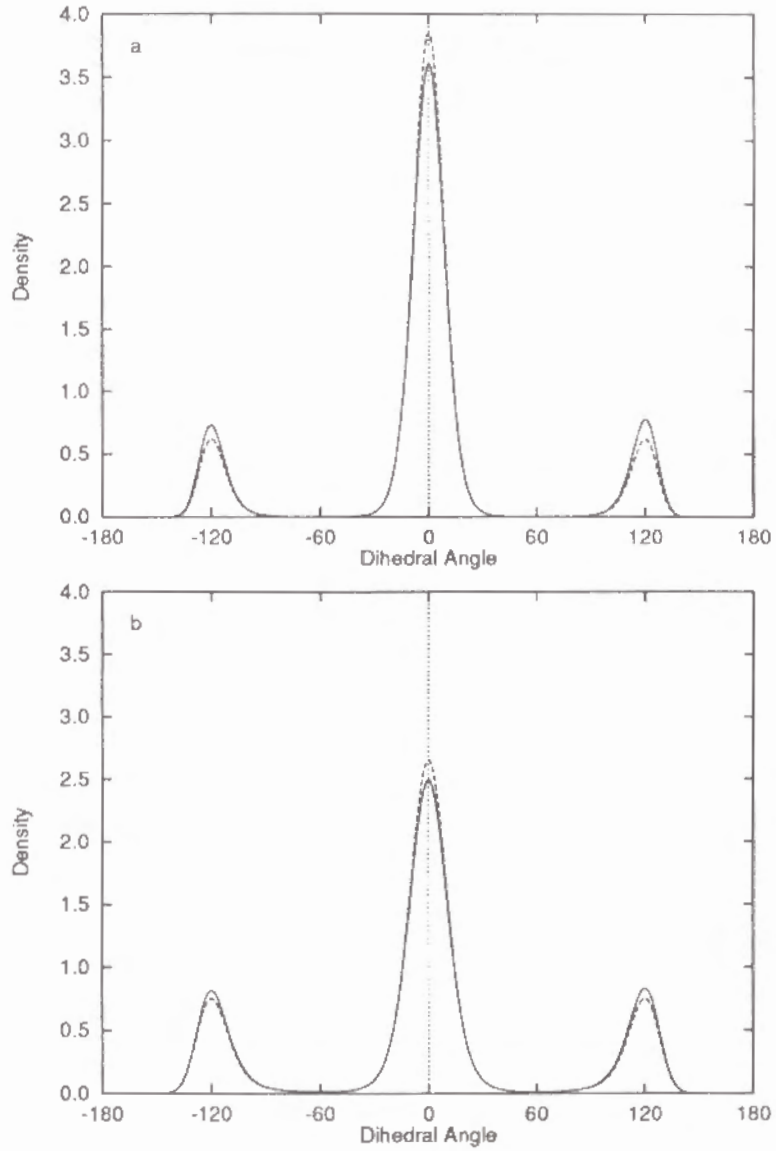

Figure 7 The distribution of the dihedral angle in the LJ model, in liquid phase (solid line) and in the ideal gas state at the same temperature (dashed line). (a) System LJ-A and (b) LJ-B.

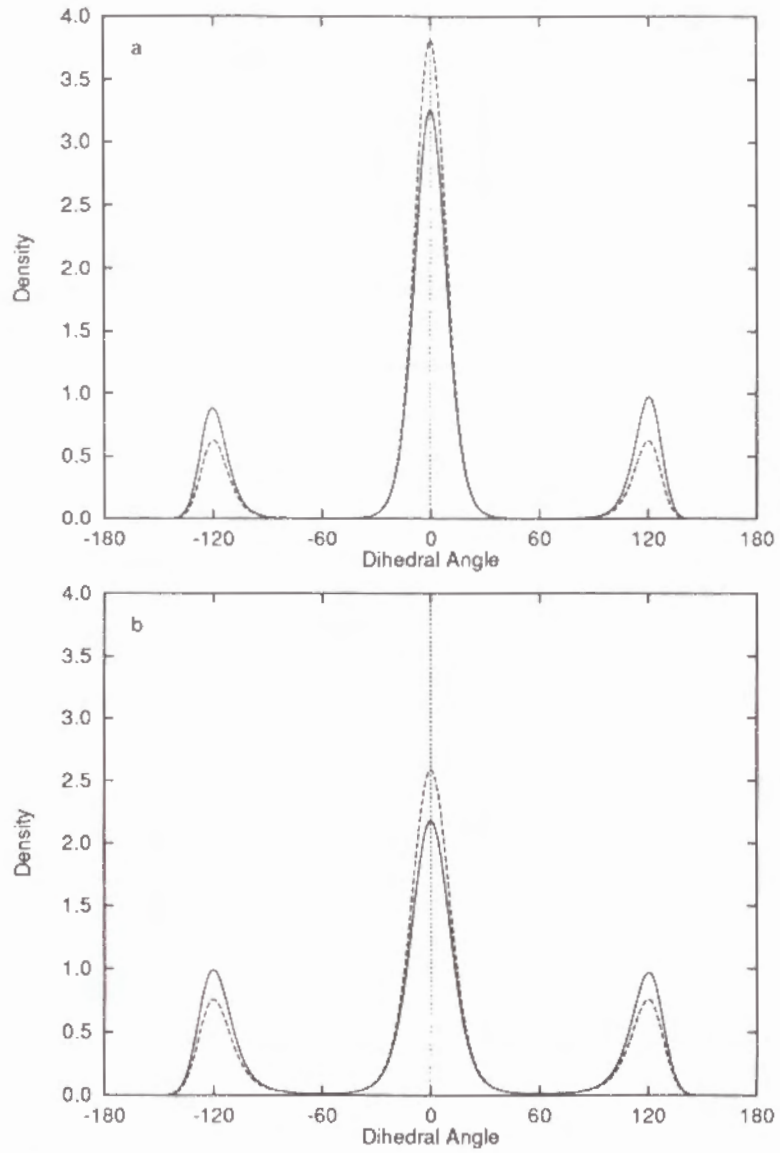

Figure 8 The distribution of the dihedral angle in the RLJ model, in liquid phase (solid line) and in the ideal gas state at the same temperature (dashed line). (a) System RLJ-A and (b) RLJ-B.

Table 2. Dihedral angle distributions for both models. The temperature T, the density ρ^* are in Kelvin, LJ reduced unit, respectively. X^T and X^G $(= 1.0 - X^T)$ are the ratios of *trans* state and *gauche* state population, respectively. ΔX stands for the conformational equilibrium shifts toward the *gauche* form $(\Delta X = X^G_{liquid} - X^G_{ideal\ gas} = -(X^T_{liquid} - X^T_{ideal\ gas}))$. The unit is percent (%).

LJ model		system LJ-A (T = 192.79K, ρ^* = 0.419)			system LJ-B (T = 279.21K, ρ^* = 0.365)		
		X^T	:	X^G	X^T	:	X^G
Ideal gas	(dotted line)	78.321	:	21.679	67.028	:	32.972
Liquid state	(solid line)	73.995	:	26.005	63.842	:	36.158
ΔX				4.326			3.186

RLJ model		system RLJ-A (T = 194.89K, ρ^* = 0.419)			system RLJ-B (T = 286.23K, ρ^* = 0.365)		
		X^T	:	X^G	X^T	:	X^G
Ideal gas	(dotted line)	77.980	:	22.020	66.328	:	33.672
Liquid state	(solid line)	67.581	:	32.419	56.875	:	43.125
ΔX				10.399			9.453

The first term in the right-hand side of eqn (7) is a torsional potential in the ideal gas and the second term is the indirect interaction due to the intermolecular interactions, that is the solvent induced contribution.

In Figure 9 is shown the torsional potential in the liquid state, as a function of the dihedral angle in the LJ and the RLJ models. As seen from this figure, there is a small difference between two systems for which conditions other than the intermolecular potential function are the same. In order to make the discussion clearer when these dihedral angle distributions are compared, we define the relative magnitude of the torsional potential as

$$\mathcal{V}'^{DIH}_{liquid}(\alpha) = -k_B T \ln(X_{liquid}(\alpha)/X_{liquid}(0)). \tag{9}$$

The solvent induced contribution term $\mathcal{W}'^{DIH}(\alpha)$ is shown as

$$\mathcal{W}'^{DIH}(\alpha) = \mathcal{V}'^{DIH}_{liquid}(\alpha) - \mathcal{V}^{DIH}_{ideal\ gas}(\alpha)\ . \tag{10}$$

In Figures 10 and 11 are shown two contributions to the dihedral angle distribution ($\mathcal{V}'^{DIH}_{liquid}(\alpha)$ and $\mathcal{W}'^{DIH}(\alpha)$) in the LJ and the RLJ models, respectively. The induced term ($\mathcal{W}'^{DIH}(\alpha)$) is also shown in Figure 12. On account of intermolecular interactions, the *gauche* conformation in the liquid state is more stabilized than that in the gas phase, relatively. This tendency for the molecule to become 'fold' or small in size is fairly dependent upon the attractive part of the potential.

CONCLUSIONS

Conformational equilibria for n-butane have been investigated by MD simulations. Intermolecular interactions give rise to the shift of the equilibrium toward the *gauche* conformation. This is explained in terms of a simple packing effect in the condensed phase. Our results for the LJ

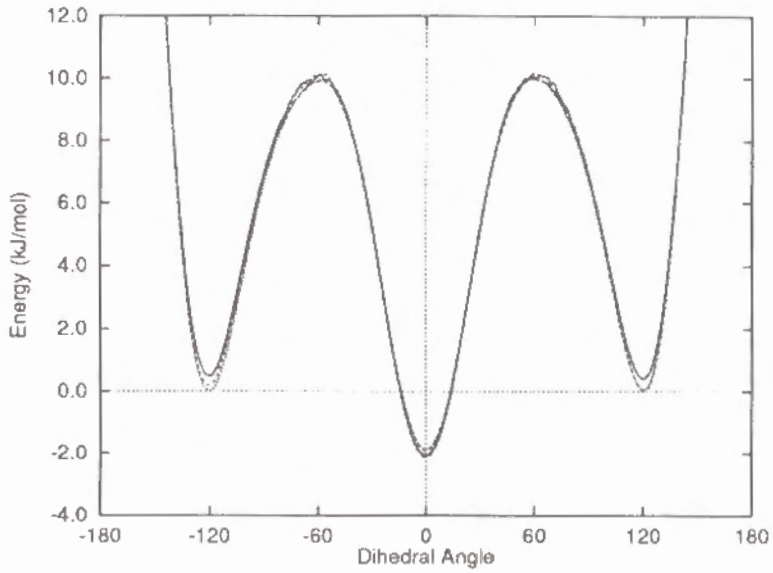

Figure 9 The effective potential in the liquid phase for the System LJ-A (solid line), LJ-B (dashed line), RLJ-A (dash-dot line) and RLJ-B (dotted line) n-butane.

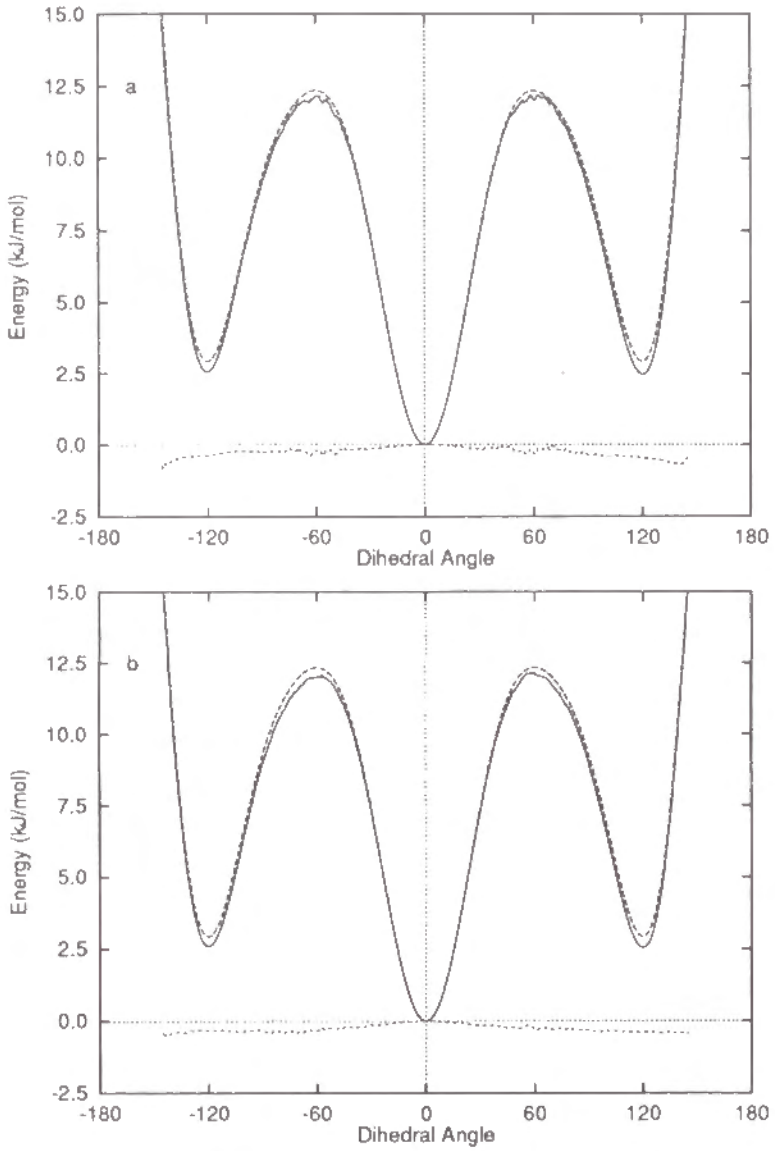

Figure 10 The dihedral angle potential for the LJ model of n-butane in (a) System LJ-A and (b) LJ-B. The solid line shows the relative potential in the liquid phase. The dashed line represents Scott-Scheraga's potential. The dotted line is the solvent induced contribution.

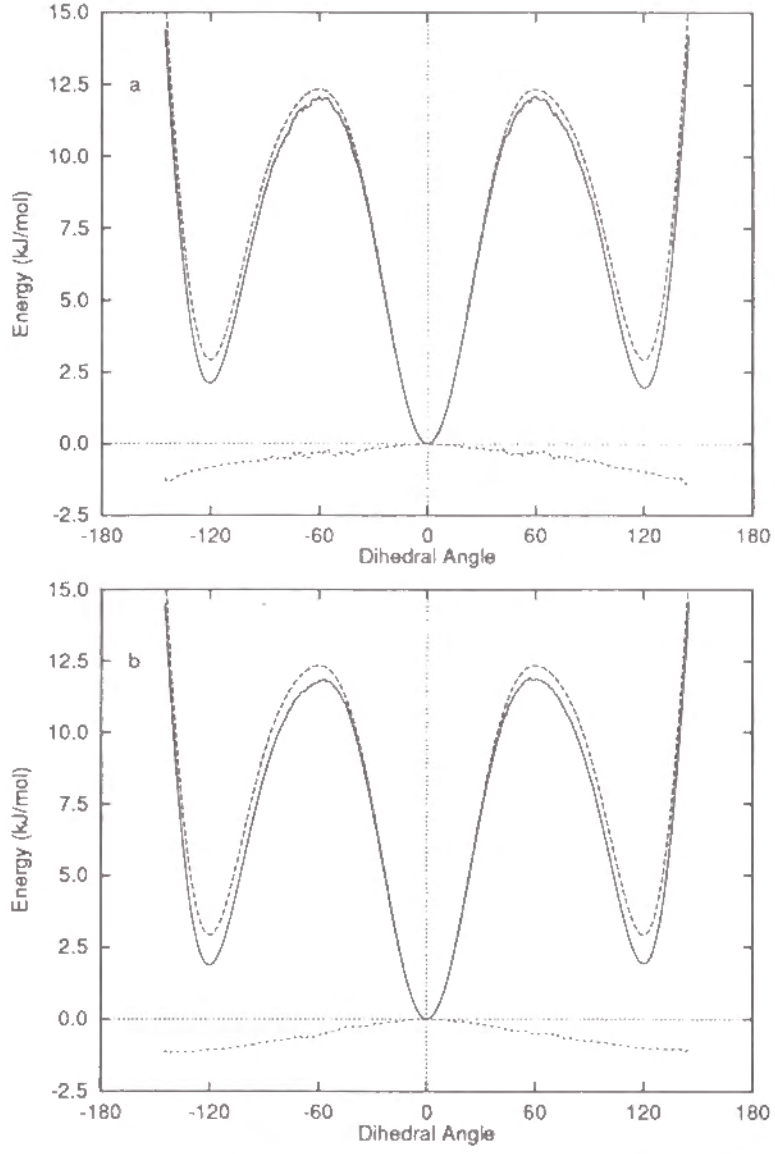

Figure 11 The dihedral angle potential for the RLJ model of n-butane in (a) System RLJ-A and (b) RLJ-B. The solid line is the relative potential in the liquid phase. The dashed line represents Scott-Scheraga's potential. The dotted line shows the solvent induced contribution.

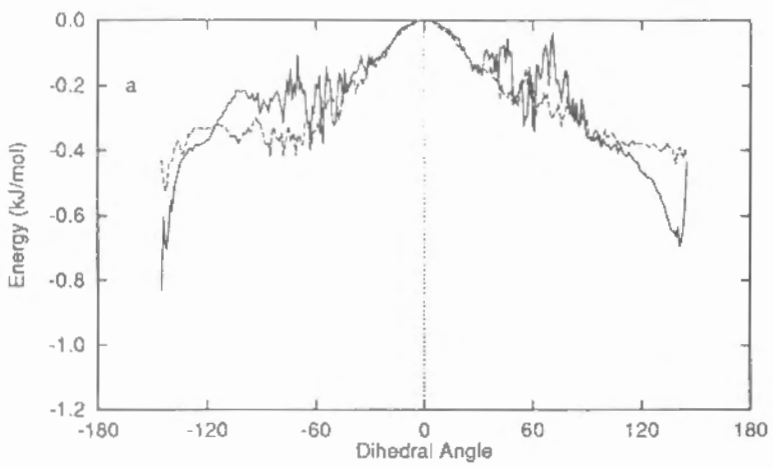

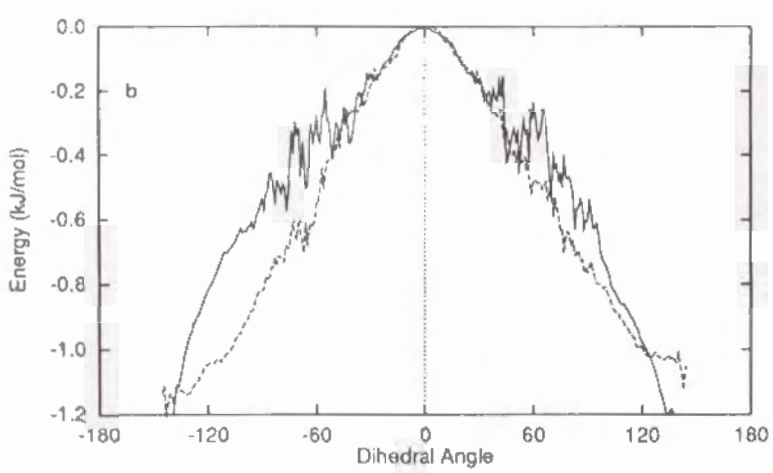

Figure 12 The solvent induced potential $W^{'DIH}(\alpha)$ for (a) LJ model and (b) RLJ model: System A (solid line) and B (dashed line)

model agree qualitatively with those from recent computer simulations (Edberg *et al.*, 1986, 1987; Wielopolski and Smith, 1986; Enciso *et al.*, 1989; Brown and Clarke, 1990). However, the magnitude of the shift in the dihedral angle distribution depends on the models used and the conditions of simulation.

The following results are obtained from the repulsive LJ model calculation. From the result of RDF's, the structure of liquid n-butane can be to great extent represented only by the repulsion part of the potential. However, comparing the dihedral angle distribution of the RLJ model with that of the LJ model, the shift is more enhanced in the system of molecules interacting via a repulsive interaction only in place of the LJ interaction. The shift was 7% in the RISM calculation, where n-butane was approximated to a fused hard-sphere (Pratt *et al.*, 1978). This value is in good correspondence with that obtained from our simulations for the RLJ systems. Therefore, the whole liquid structures including the dihedral distribution are sensitive to the attractive part of the intermolecular interaction as well as the repulsive part.

CHAPTER III

TORSIONAL MOTIONS OF n-BUTANE

Molecular dynamics simulations for n-butane in non-polar solvent Xe have been performed in order to understand a barrier-crossing mechanism of the dihedral angle for n-butane in the presence of solvent molecules. Each n-butane molecule consists of four sites interacting with LJ potential and only one dihedral angle is taken into account as the internal degree of freedom. It is found that the solvent effect is large even in nonpolar solvent. There are various kinds of involvement of solvent molecules in the intramolecular rearrangement of n-butane. The mutual relation among translational, rotational and torsional motions is examined. It sometimes happen that the solvents shift the potential energy of the reactant butane upward and this induces a facile transition.

MODEL AND POTENTIAL

Both intra- and inter-molecular interactions are taken into account. All the hydrogen atoms directly bonded to carbon atoms are neglected. A carbon atom with two or three hydrogen atoms is treated as a single 'united' atom with totalled mass. The interaction site is thereby placed on the carbon atom. It is known that use of this type of simpler model gives reasonable static and dynamic properties in the liquid state. Therefore, we adopt a simpler united-atom model: the present n-butane molecule model has four interaction sites and one dihedral angle with fixed bond lengths and bond angles; all bond stretching and bending vibration are frozen. The bond length vibrational frequencies are well separated from the torsional frequencies of flexible molecules and therefore decoupled with the torsional motions. The effect of the

constraints by freezing the bond lengths of the chain molecule is remarkably insensitive. In contrast, the constraints on the bond angles, however, may change somewhat the fluctuation of the chain molecule (van Gunsteren, 1980; Toxvaerd, 1987). It is not practical that this high frequency vibration is taken into account in the framework of classical mechanics. Therefore, we used the simpler fixed bond angle model. The bond lengths are kept constant at 1.53Å, and the bond angles are fixed to 109.46° by a next-nearest-neighbor constraint (Ryckaert and Bellemans, 1978).

The torsional potential energy of each conformation is given by the sum of various contributions: conjugated effects, non-bonded interaction and so on. The intramolecular conformation of n-butane is defined by the dihedral angle, α ($-180° < \alpha \leq +180°$), and the torsional potential is given as a function of Fourier series,

$$\mathcal{V}^{DIH}(\alpha)/k_B \equiv \sum_{n=0}^{5} V_{\alpha n} \cos^n \alpha \qquad (1)$$

(k_B = Boltzmann's constant), which has three minima corresponding to the $-$*gauche*, *trans* , $+$*gauche* states.

To clarify the torsional motions in terms of intramolecular interaction, two models of n-butane molecule have been used. One is that each n-butane molecule has four beans with the same mass ($m = 2.408 \times 10^{-23}$ g). This model is identical to RB-model (Ryckaert and Bellemans, 1978) (model-A). Another is that each n-butane molecule has four beans with two -CH_3 and two -CH_2- groups which have different masses (model-B) (Padilla and Toxvaerd, 1991). The parameter values in eqn (1) for model-A are the same as employed by Scott and Scheraga (1966), for model-B are proposed by Padilla and Toxvaerd (1991), are given in Table 1. The potential curves are shown in Figure 1. The difference between these two potential functions is the height of potential barrier. This affects sensitively to the behavior

Table 1. Interaction parameters for intramolecular torsional potential functions of n-butane. The unit for V_{xi}'s are 10^3K.

model	V_{x0}	V_{x1}	V_{x2}	V_{x3}	V_{x4}	V_{x5}
A	+1.116	+1.462	−1.578	0.368	+3.156	−3.788
B	+1.03776	+2.42607	+0.08164	−3.12946	−0.16328	0.25273

Table 2. Interaction parameters for intermolecular LJ potential functions of n-butane. The unit for σ is Å, for ϵ/k_B is Kelvin (k_B is the Boltzmann's constant).

model	σ	ϵ_1/k_B	ϵ_2/k_B
A	3.923	72.00	
B	3.905	88.06	59.38
	σ	ϵ/k_B	
Xe	4.1	216.87	
Ar	3.405	119.8	
CCl_4	5.947	322.7	

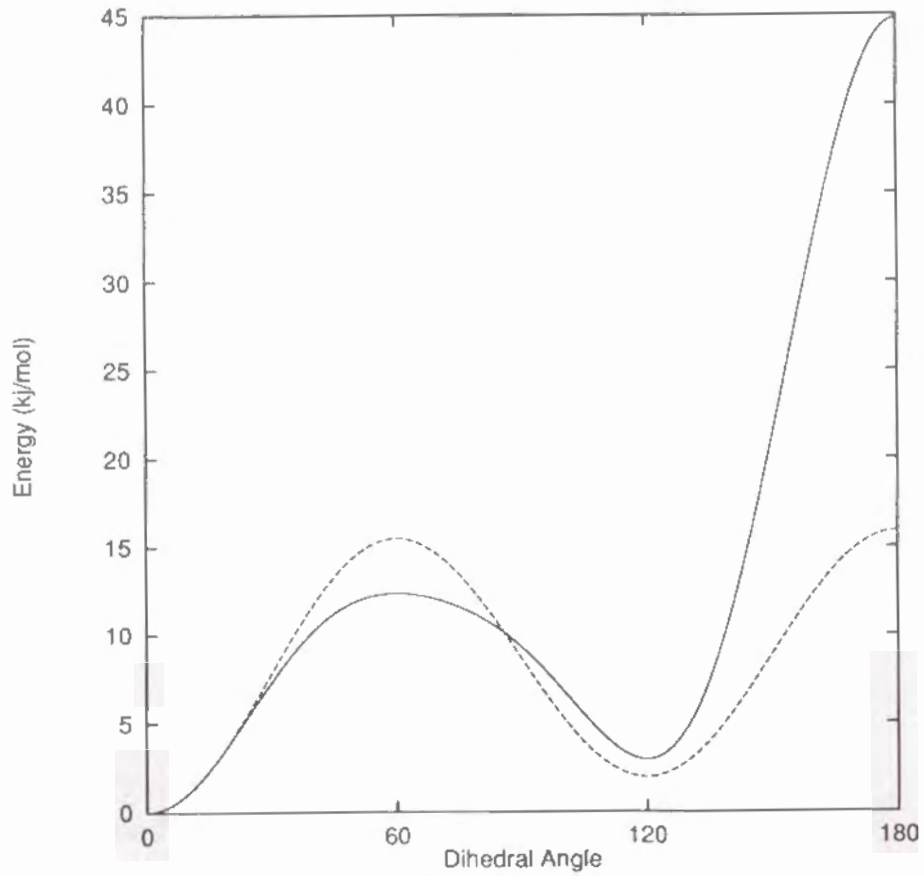

Figure 1. Torsional potential energy around -C-C- for model-A (solid line) and model-B (dashed line)

of the internal rotation. Therefore, we have performed MD simulations with different two dihedral potentials. In model-B, the potential barrier of $\pm gauche \rightarrow \mp gauche$ is much lower than that in model-A. Therefore, the intramolecular rearrangements of $\pm gauche \rightarrow \mp gauche$ take place as frequently as that of $\pm gauche \rightarrow trans$.

The site-site intermolecular potential is described by the Lennard-Jones 12-6 potential with truncated long-tail correction at cut-off distance by multiplying the switching-function (Ohmine *et al.*, 1988).

$$\mathcal{V}^{\mathcal{SF}-\mathrm{LJ}}(r_{ij}) = \mathcal{SF}(r_{ij}) \cdot \mathcal{V}^{\mathrm{LJ}}(r_{ij}) \tag{2}$$

$$\mathcal{SF}(r_{ij}) = \begin{cases} 1, & (\ r_{ij} < r_d\ ) \\ \frac{(r_{ij}-r_c)^3}{(r_d-r_c)^5}\{10(r_{ij}-r_d)^2 + (r_{ij}-r_c)^2 - 5(r_{ij}-r_c)(r_{ij}-r_d)\}, & (\ r_d \le r_{ij} < r_c\ ) \\ 0, & (\ r_c \le r_{ij}\ ) \end{cases} \tag{3}$$

$$\mathcal{V}(r_{ij}) = 4\epsilon_{ij}[(\sigma_{ij}/r_{ij})^{12} - (\sigma_{ij}/r_{ij})^{6}], \tag{4}$$

where r_{ij} stands for the distance between sites i and j in different molecules. Size parameter σ and energy parameter ε/k_B are listed in Table 2. Standard values are used for Xe, Ar and CCl_4. For all unlike site-site pairs, we adopted the Lorentz-Berthelot (LB) combining rule, in which size parameter is give by the arithmetic mean, energy parameter by the geometric mean.

One of the intriguing features of the flexible molecules is to examine the solvent effect on the barrier-crossing dynamics of the individual solute molecule. In the present study, the solute-solute interaction is completely eliminated assuming infinite dilution of n-butane in solvent Xe: It contains a n-butane molecule and 107 solvent molecules. The temperature is set to 200.00K and density ρ is set to 2.36g/cm^3 (reduced density, ρ^*= 0.75).

Newton's equations of motion are solved by the ordinary Verlet method (e.g., Allen and Tildesley, 1987) and the constraints of bond angles and length are treated by the iterative algorithm, named 'Shake' (Ryckaert *et al.*, 1977). A time step Δt, for the integration of equations of motion, is 2.00×10^{-15} sec. The centers of mass of molecules are placed on an f.c.c. crystalline lattice as an initial configuration. Initially, the n-butane molecule has the *trans* conformation ($\alpha = 0°$) with a random orientation of n-butane.

The systems correspond to an NEV-ensemble in the MD simulation. The molecules are confined in a cubic cell box imposing the periodic boundary condition and the cubic minimum image convention. An initial 100 ps of simulation is used for the relaxation of the unrealistic initial conditions to achieve both the structural and conformational equilibria of internal dihedral angles. The MD simulation is extended to 500,000 $\sim$ 1,100,000 time steps (1.0 $\sim$ 2.2ns) in order to calculate thermodynamic properties accurately, to 2,500 $\sim$ 10,000 time steps (5 $\sim$ 20ps) in order to analyze the torsional motion in more detail.

In addition, other intramolecular potential models are also examine how the intramolecular potential affect to the torsional motions. We adopted other four potential models: using three quarters, half and quarter of the real intramolecular potential as well as a model of free torsional potential. We call these 'p'-, 'h'-, 'q'- and 'n'-type intramolecular potential function model, respectively. All of these potential models are examined under the same conditions as the case of 'full' potential model ('o'-type model).

RESULTS AND DISCUSSION

The temperatures and the potential energies calculated from the present MD simulations are given in Table 3. Standard deviations are also given

Table 3. Thermodynamic properties for mixtures of n-butane and solvent. The temperature is in Kelvin. The unit of energy is kJ/mol. Standard deviations are also given in the parentheses of this table. The deviations are calculated by dividing whole simulation run into several blocks comprising consecutive 10000 steps (20.0ps).

System (model)		Average Temp.	Total Energy	n-butane Energy	Solvent Energy	n-butane Intra-pot.
Model A (200.00K)	o ×1.00	201.14 (2.36)	-675.97 (4.74)	-16.51 (2.36)	-6.25 (0.050)	3.33 (1.30)
	p ×0.75	197.85 (7.18)	-683.82 (14.36)	8.40 (2.15)	-6.31 (0.142)	2.25 (1.11)
	h ×0.50	202.94 (2.87)	-673.62 (6.07)	-9.00 (1.78)	-6.21 (0.064)	1.76 (0.67)
	q ×0.25	202.67 (1.98)	-674.16 (3.75)	-9.20 (1.47)	-6.21 (0.040)	1.40 (0.24)
	n ×0.00	206.82 (4.08)	-666.66 (8.02)	10.28 (1.38)	-6.13 (0.080)	0.00
Model B (200.00K)	o ×1.00	199.63 (8.95)	-678.77 (18.50)	-7.85 (1.79)	-6.27 (0.175)	2.87 (0.55)
	p ×0.75	195.94 (3.80)	-688.42 (7.60)	-9.40 (1.80)	-6.35 (0.073)	1.53 (0.82)
	h ×0.50	207.05 (5.76)	-664.69 (11.77)	-9.14 (1.67)	-6.13 (0.111)	1.58 (0.53)
	q ×0.25	199.49 (8.90)	-681.13 (18.71)	-10.65 (1.53)	-6.12 (0.110)	1.32 (0.18)
	n ×0.00	200.57 (3.65)	-680.18 (7.10)	-10.76 (1.23)	-6.26 (0.072)	0.00

in the parentheses of this table. The deviations are calculated by dividing the whole simulation run into several blocks comprising consecutive 10,000 steps (20.0ps). We will pay attention to the intramolecular conformation of n-butane which is defined by the dihedral angles. The *trans* conformation (T) is defined by the region of the dihedral angle α , $-60° < \alpha < +60°$, and the *gauche* conformation by that of $-180° < \alpha \leq -60°(G^-)$ and $+60° \leq \alpha \leq +180°(G^+)$.

Time evolution of the dihedral angle

Figures 2 and 3 show the time evolution of the dihedral angles by the n-butane simulation for each system of 'o'-type model (×1.0) and 'h'-type model ('o'-type ×0.5). The lower the height of potential barrier for torsional motion is, the more frequently the rotation of the dihedral angle in n-butane molecule takes place. Moreover, various patterns of rotation are observed; *trans* → ±*gauche* and ±*gauche* →*trans* rearrangements. Remarkably, in the case of B-model, we can obtain ±*gauche* → ∓ *gauche* transformation frequently since the intramolecular potential of B-model has a lower potential barrier than that of A-model for $G^{\pm} \rightarrow G^{\mp}$ direct transformation.

Solvent induced contribution

This simulation time proves to be long enough to obtain reliable distributions of dihedral angle in the case of dense n-butane liquids. Since we treat only one n-butane molecule as a solute in this work, the dihedral angle distribution has a tendency to take either positive or negative values for a long time. We calculated the distribution only for 'n'-type intramolecular potential ('o'-type ×0.0) of model-A. The 'n'-type intramolecular potential is defined as a model of free torsional potential. For this type model, the dihedral angle of n-butane rotates freely.

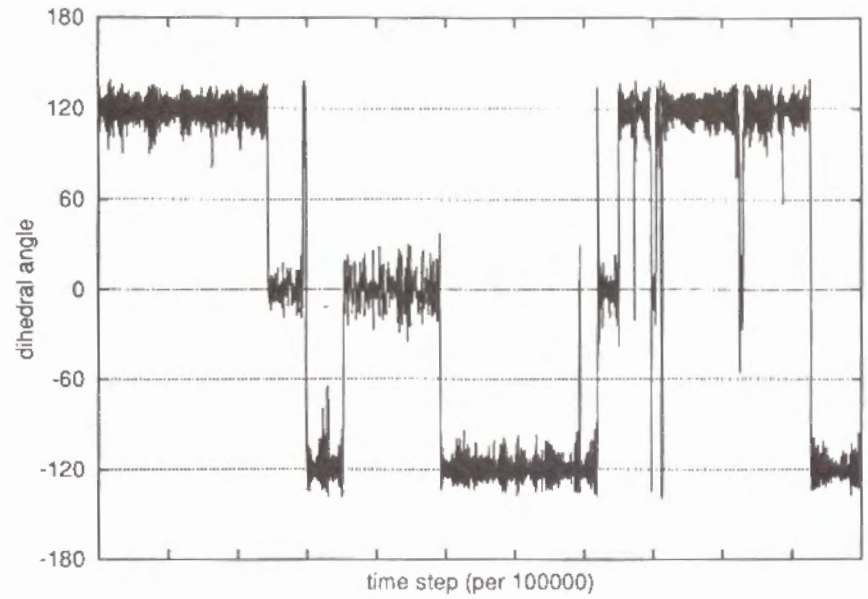

Figure 2. The time evolution of the dihedral angle of n-butane for 2.2ns (1,100,000steps): 'o'-type (×1.0) of model-A (TOP) and model-B (BOTTOM).

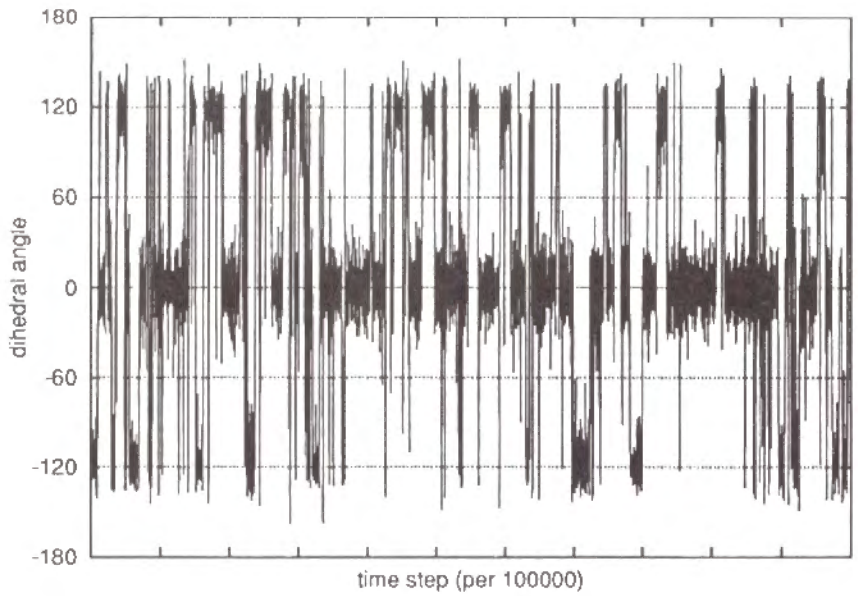

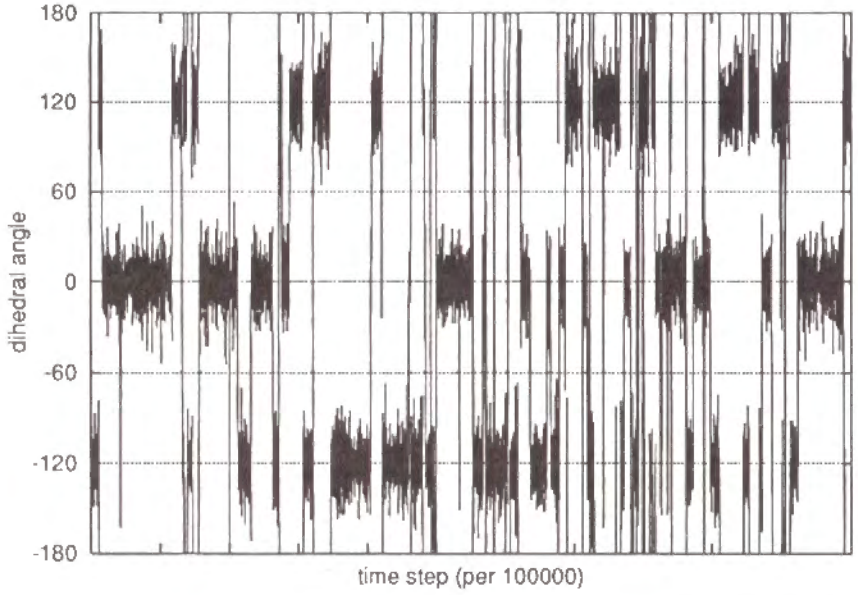

Figure 3. The time evolution of the dihedral angle of n-butane for 2.2ns (1,100,000steps): 'h'-type (×0.5) of model-A (TOP) and model-B (BOTTOM).

Table 4. The distributions of the dihedral angle α. The *trans* form is defined by the region of $-60° < \alpha < +60°$, and the *gauche* form by $-180° < \alpha \leq -60°$ and $+60° \leq \alpha \leq +180°$.

	Model	G^-	T	G^+
	o (×1.00)	32.31 %	21.37 %	46.32%
	p (×0.75)	23.87 %	47.57 %	28.56%
A	h (×0.50)	17.09 %	57.86 %	25.05%
	q (×0.25)	25.13 %	43.92 %	30.95%
	n (×0.00)	34.98 %	29.88 %	35.14%
	o (×1.00)	8.78 %	1.80 %	89.42%
	p (×0.75)	27.38 %	58.68 %	13.94%
B	h (×0.50)	45.76 %	30.70 %	23.54%
	q (×0.25)	36.72 %	29.33 %	33.95%
	n (×0.00)	36.19 %	29.63 %	34.18%

	Model	$G^- \to T$	$G^- \leftarrow T$	$T \to G^+$	$T \leftarrow G^+$	$G^- \to G^+$	$G^- \leftarrow G^+$
	o (×1.00)	5	6	10	11	0	0
	p (×0.75)	21	21	25	23	0	0
A	h (×0.50)	101	101	113	112	0	0
	q (×0.25)	322	320	350	349	5	3
	n (×0.00)	644	641	650	647	1006	1002
	o (×1.00)	0	1	1	1	1	1
	p (×0.75)	8	7	5	4	5	4
B	h (×0.50)	26	28	22	23	27	29
	q (×0.25)	191	197	158	165	258	266
	n (×0.00)	682	699	604	620	965	981

Therefore, the dihedral angle distribution of this model is dominated only by the intermolecular interaction, obviously.

The distribution for a positive angle value after symmetrizing the obtained distributions is given in Figures 4. In order to clarify the solvent induced contribution, we define the relative magnitude of the torsional potential as

$$\mathcal{V}'^{DIH}_{liquid}(\alpha) = -k_B T \ln(X_{liquid}(\alpha)/X_{liquid}(0)), \qquad (5)$$

(where $X_{liquid}(\alpha)$ is the dihedral angle distribution at dihedral angle α) and this contribution shows also in Figures 4.

As seen from these figures, the *cis* conformation in the liquid state is more stabilized than the *trans* conformation (*ca.* –0.5kJ/mol), relatively. On account of intermolecular interactions, the molecule become 'fold' or small in size in the liquid state.

Structure of solvent molecules

Although the temperatures for all systems and models are different slightly with each other, the difference in the radial distribution function (RDF) arising from the temperature difference is expected to be small. No correction due to the difference is made for RDF's, when they are compared.

Figures 5 and 6 show the End(CH_3)-Xe, Inner(CH_2)-Xe RDF's. In both Xe-Xe RDF's and center of mass G-Xe RDF's, which are not shown here, there are difference slightly among each potential model. Comparing both n-butane models with various strengths of torsional potentials, only a small difference is seen in RDF. Therefore, it is found that there is no significant difference in the short range structures of system between A-model and B-model and among all potential models.

As seen from these figures, the End-Xe RDF of 'n'-type model (×0.0) in both n-butane models is rather disordered slightly compared

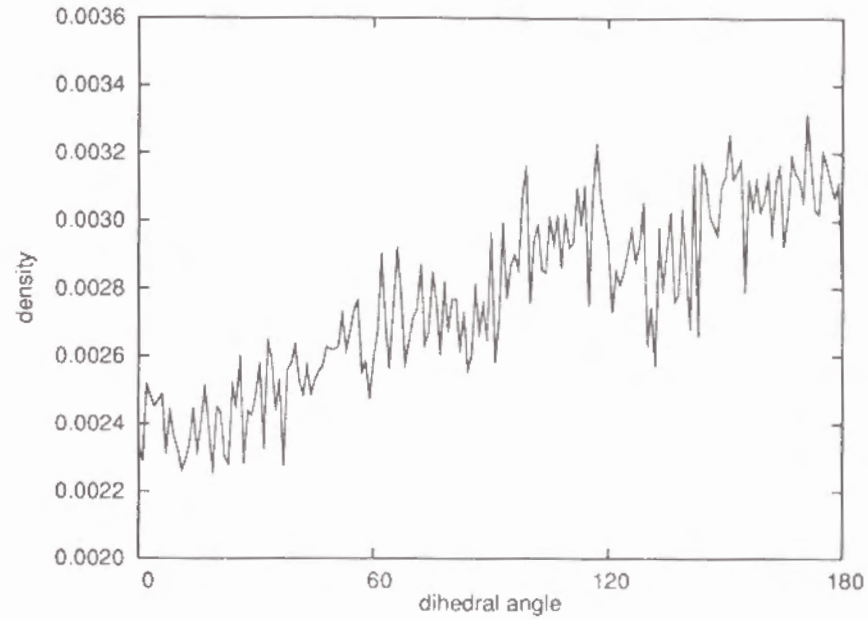

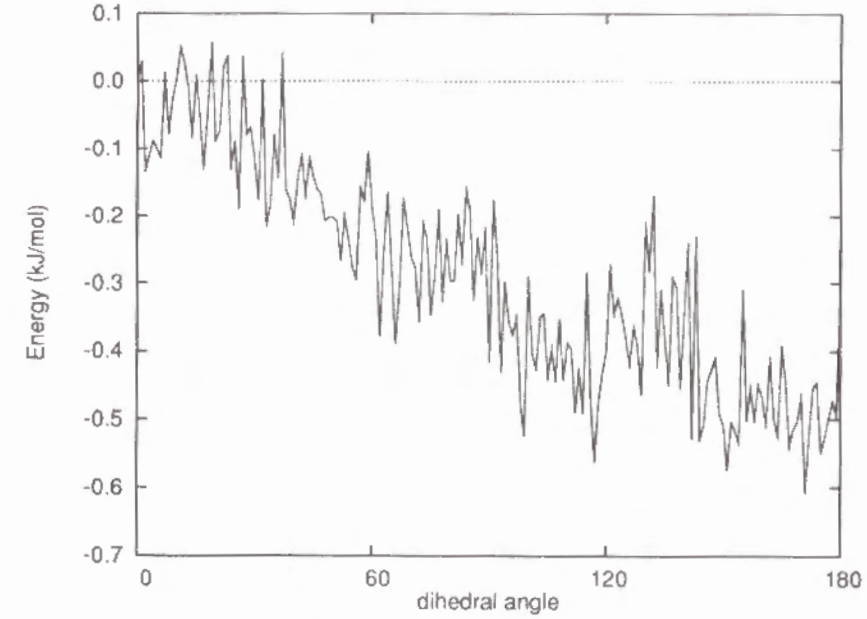

Figure 4. The solvent induced contribution for 'n'-type of model-A: the distribution of the dihedral angle (TOP) and induced torsional potential (BOTTOM) of n-butane.

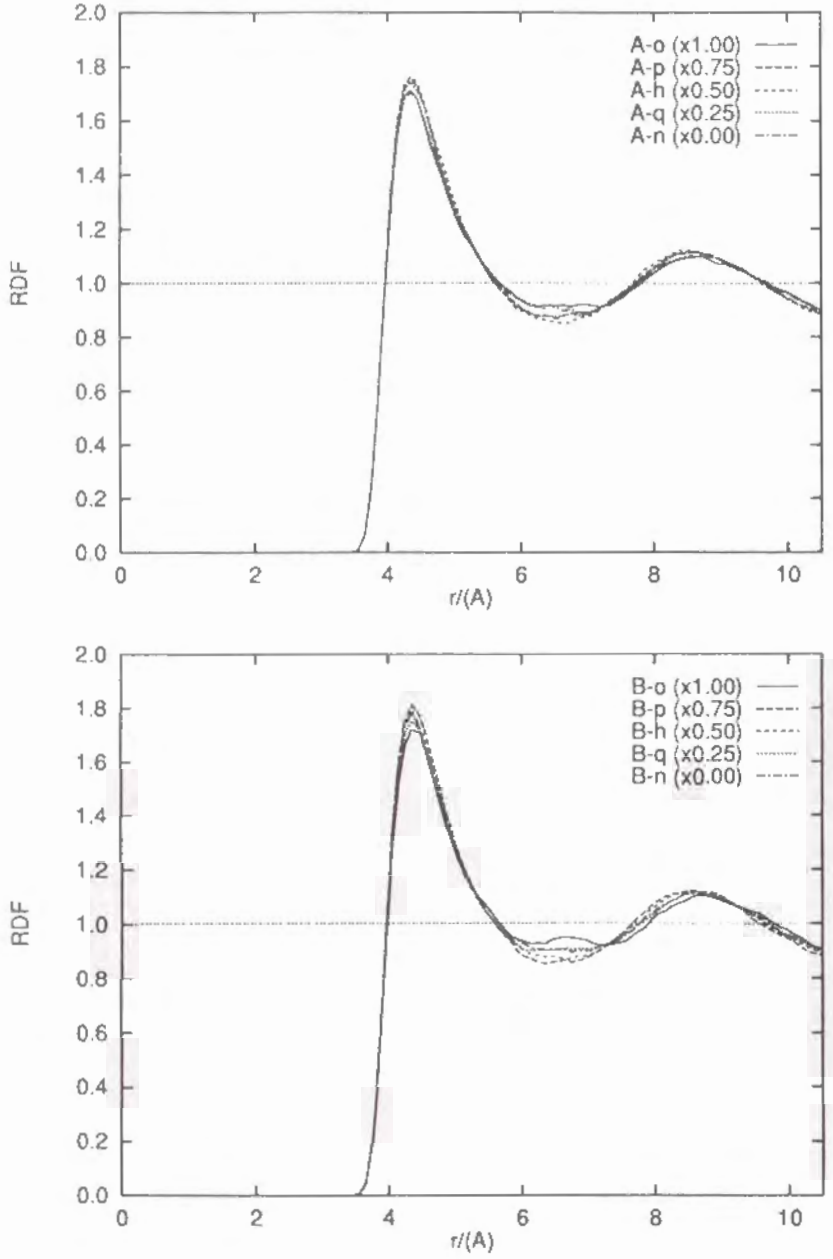

Figure 5. End-Xe radial distribution functions: for model-A (TOP) and model-B (BOTTOM) of n-butane.

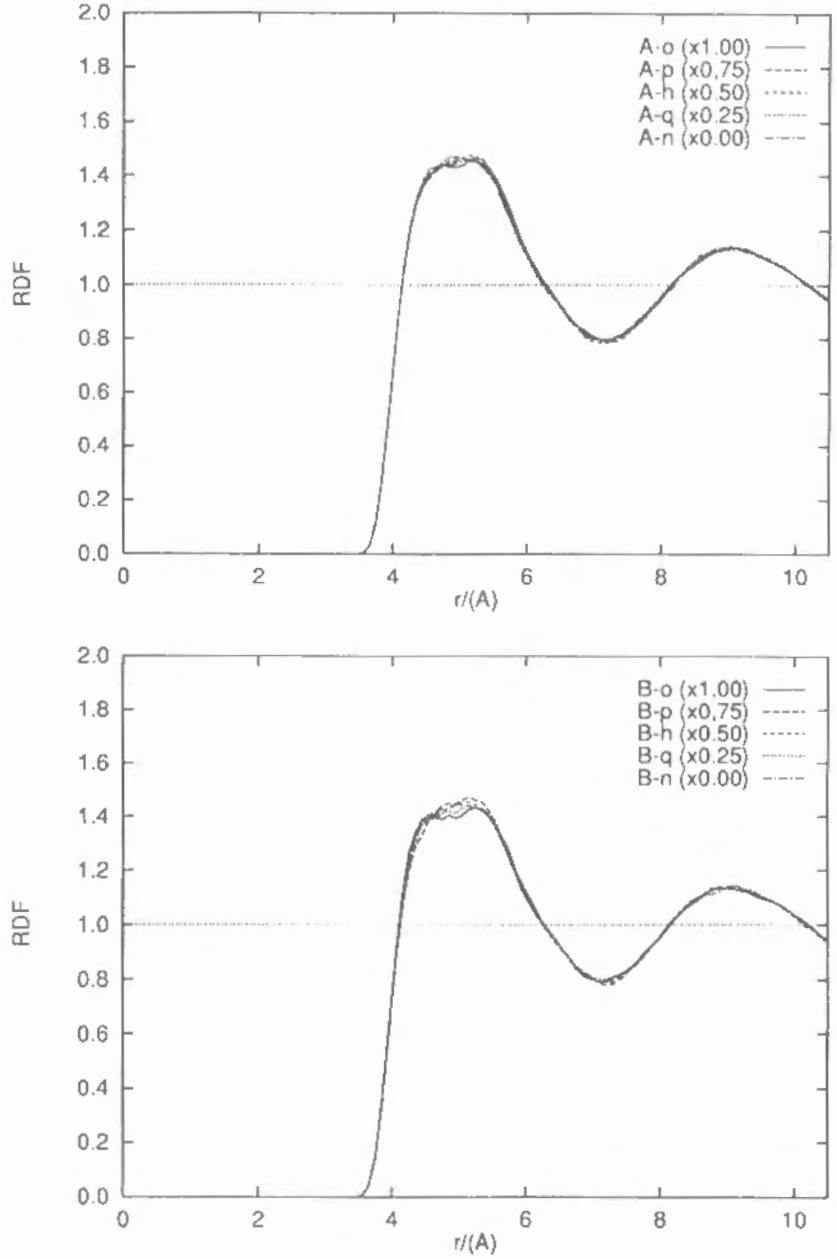

Figure 6. Inner-Xe radial distribution functions: for model-A (TOP) and model-B (BOTTOM) of n-butane.

with that of other potential models. Those are due to the free change of dihedral angles and also to the relatively large center of mass motions of individual molecules.

Figures 7 plot the Fourier transformation of the autocorrelation functions for the velocity of solvent Xe molecules,

$$\mathcal{V}(\omega) = \frac{1}{2\pi} \int \exp(i\omega t) \langle \mathbf{v}_i(t) \cdot \mathbf{v}_i(0) \rangle, \tag{6}$$

where the average $\langle\ \rangle$ is over the initial time $t = 0$ and over all Xe molecules. As seen from these figures, the power spectrum is dependent neither on the potential form nor on the strength of the dihedral potential.

Figures 8 show the normalized autocorrelation functions for the $\dot{\alpha}(t)(= d\alpha(t)/dt)$, where $\alpha(t)$ is dihedral angle of n-butane molecule at time t. The time correlations of $\dot{\alpha}(t)$ of model-B are longer than that of model-A. Figures 9 plot the Fourier transformation of the autocorrelation functions for the $\dot{\alpha}(t)$. The 'q'-type intramolecular potential ($\times 0.25$) n-butane of both models has the power spectrum localized around $\omega \sim 0$. This indicates that the torsional motion is free, because the torsional potential barrier of 'q'-type potential functions is well lower than that of other 'o'-,'p'-,'h'-type potential functions. The existence of two peaks in A-model is characteristic of the torsional potential function while there exists the single peak in B-model.

Torsional Motion Analysis

We can obtain the time evolution of both dihedral angle and the intermolecular potential of n-butane from the surrounding solvents during the intramolecular rearrangement. There are various kinds of the transition patterns involving solvent motions. We show some typical examples: Case I and II are results in n-butane(model-A)-Xe system,

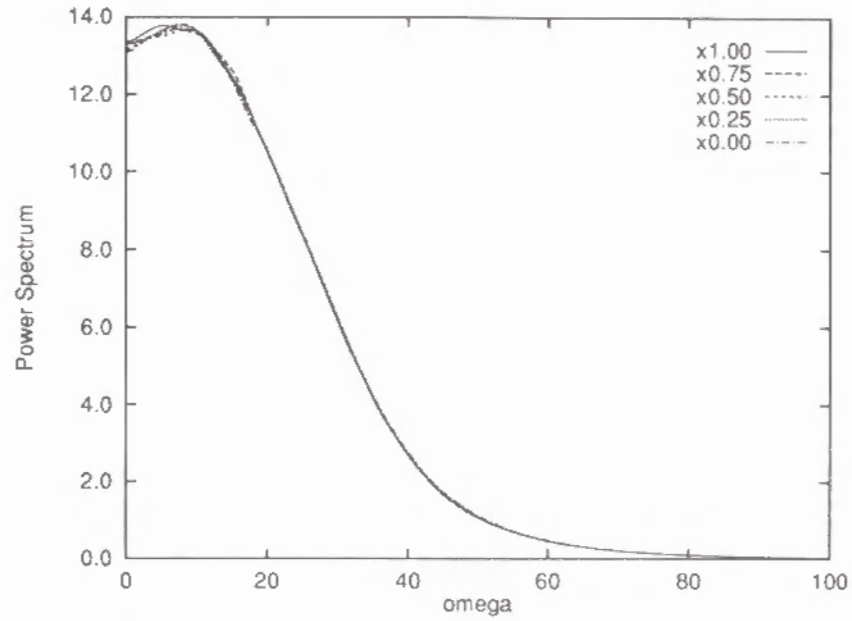

Figure 7. The Fourier transformation of the autocorrelation functions for the velocity of solvent Xe molecules: for model-A (TOP) and model-B (BOTTOM) of n-butane.

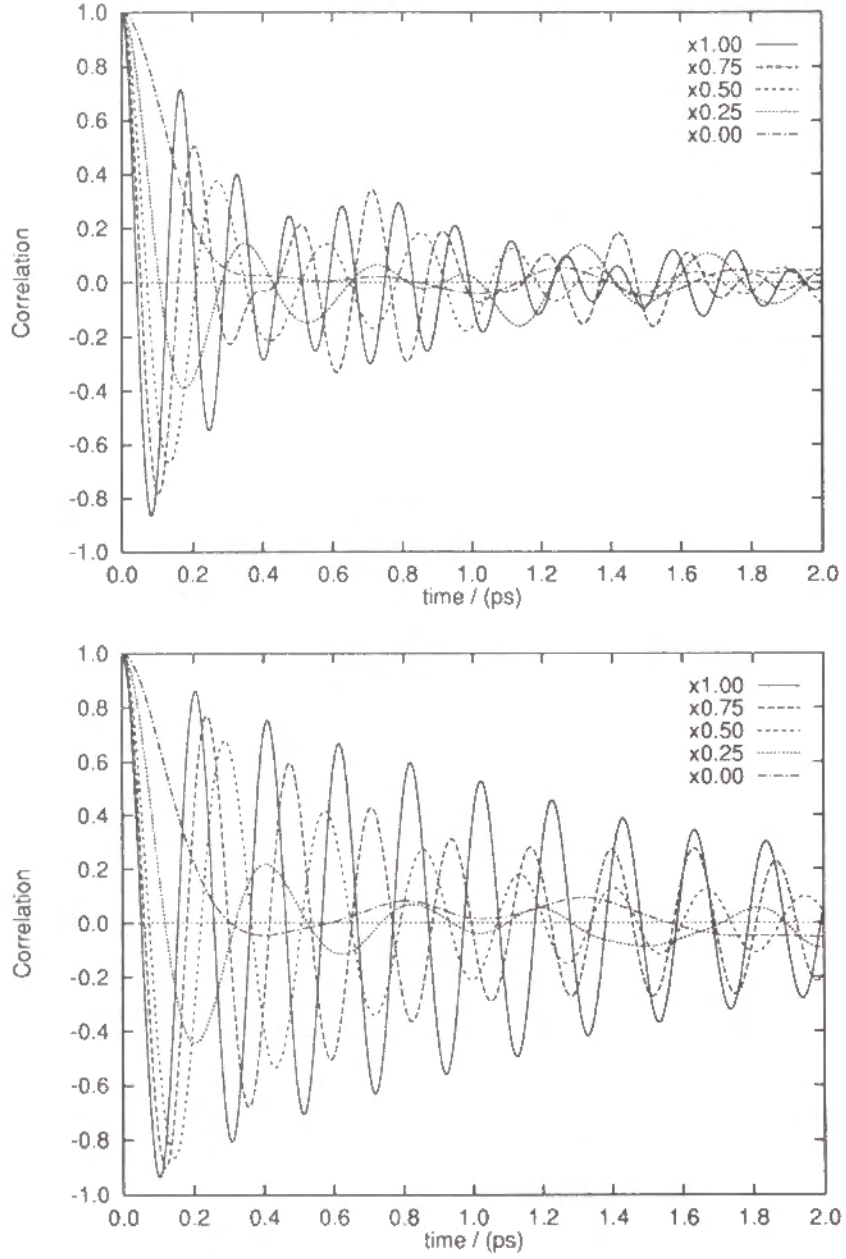

Figure 8. The normalized autocorrelation functions for the $\dot{\alpha}(t)(= d\alpha(t)/dt)$, where $\alpha(t)$ is dihedral angle of n-butane molecule at time t: for model-A (TOP) and model-B (BOTTOM) of n-butane.

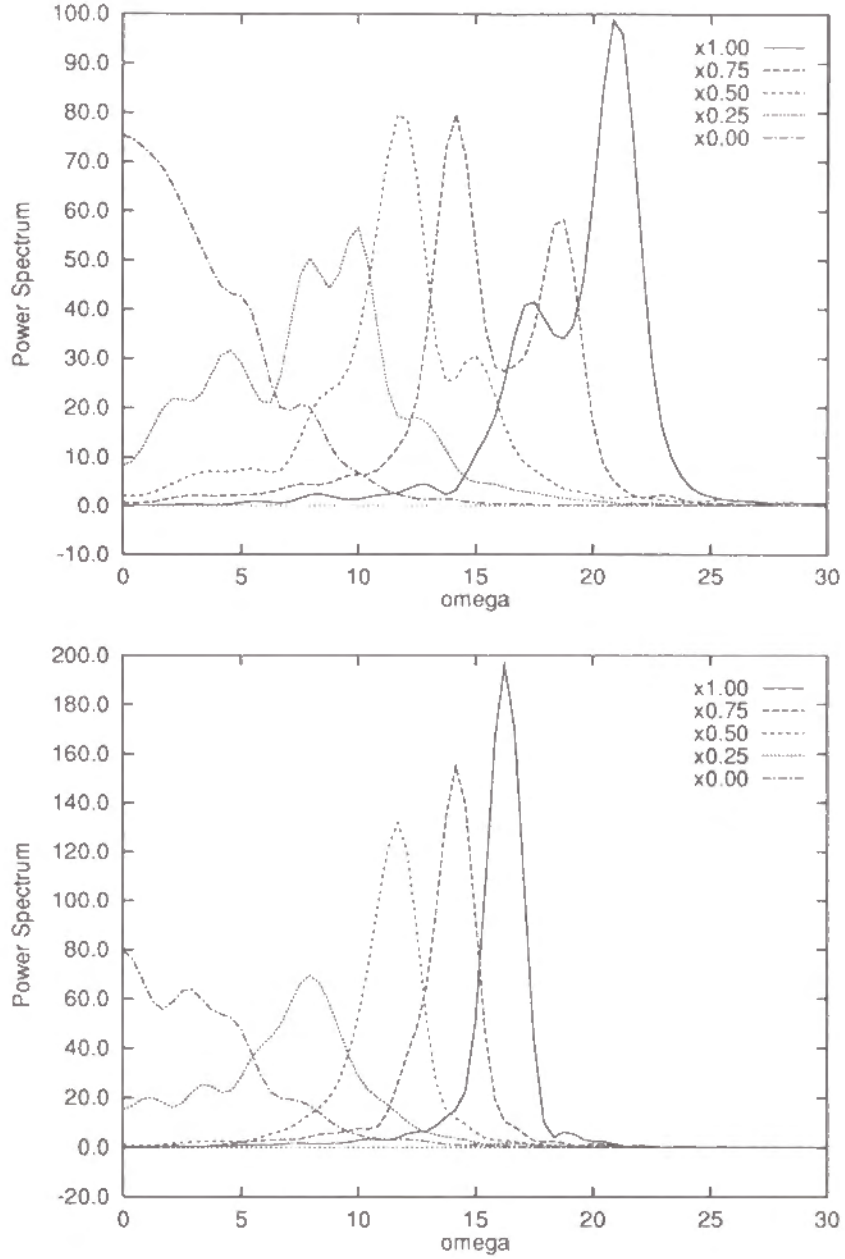

Figure 9. The Fourier transformation of the autocorrelation functions for the $\dot{\alpha}(t)$: for model-A (TOP) and model-B (BOTTOM) of n-butane.

case III and IV are in n-butane(model-B)-Xe system and case V is in n-butane(Model-A)-CCl_4 system.

Kinetic Energy Analysis

To clarify the interference of translation and rotation with torsional motion of dihedral angle, we divide the kinetic energy of n-butane into those three contributions. The movements of center of mass for n-butane occur translational energy. To analyze kinetic energy, we introduced rigid-molecule approximation that the motions of flexible molecule such as n-butane are regarded as instantaneous motions of rigid molecular. We defined that the rotational energy is occurred by rotating the whole molecule, which is treated as a rigid molecule. We noticed bond lengths and bond angles of our model were fixed, so that the internal vibrational term is equivalent for the term of dihedral angle vibration.

For rigid molecules, the relationship between the space fixed system of coordinates and the body fixed system (Goldstein, 1980) is defined by

$$(\mathbf{dG})_{space} = (\mathbf{dG})_{body} + (\mathbf{dG})_{rotation} \qquad (7),$$

where $\mathbf{G}$ is any vector. The velocity $\mathbf{v}$ is

$$\mathbf{v}_{space} = \mathbf{v}_{body} + \vec{\omega} \times \mathbf{r}. \qquad (8)$$

Angular momentum $\mathbf{L}$ is given by

$$\mathbf{L} = \sum_i m_i \, (\mathbf{r}_i \times \mathbf{v}_i) \qquad (9),$$

where $\mathbf{r}_i$ is the body fixed coordinate and $\mathbf{v}_i$ is the body fixed velocity to the center of mass of n-butane.

Obviously, $\mathbf{v}$ is not composed of only the rotational motion. The

moment of inertia for the rotational motion, $\mathbf{I}$, is,

$$\mathbf{I} = \begin{pmatrix} \sum_i m_i(r_i^2 - x_i^2) & -\sum_i m_i x_i y_i & -\sum_i m_i z_i x_i \\ -\sum_i m_i x_i y_i & \sum_i m_i(r_i^2 - y_i^2) & -\sum_i m_i y_i z_i \\ -\sum_i m_i z_i x_i & -\sum_i m_i y_i z_i & \sum_i m_i(r_i^2 - z_i^2) \end{pmatrix} \qquad (10).$$

We can write

$$\mathbf{L} = \mathbf{I}\,\vec{\omega} \qquad (11),$$

and therefore we can obtain $\vec{\omega}$ by $\mathbf{L}$ and $\mathbf{I}^{-1}$. ω is angular velocity of n-butane can be defined at any instance.

We then write each energy term of n-butane,

$$\mathcal{E}_k = \mathcal{E}_{k(translation)} + \mathcal{E}_{k(rotation)} + \mathcal{E}_{k(dihed.vibration)}, \qquad (12)$$

$$\mathcal{E}_k = \frac{1}{2}\sum_i \, m_i \, v_i^2, \qquad (13)$$

$$\mathcal{E}_{k(translation)} = \frac{1}{2}\sum_j \, m_j \, {v_{Gj}}^2, \qquad (14)$$

$$\mathcal{E}_{k(rotation)} = \frac{1}{2}\sum_n \, L_n \, \omega_n, \qquad (15)$$

respectively, where $\mathcal{E}_k$ is the total kinetic energy of n-butane, $\mathcal{E}_{k(translation)}$ is the translational energy, $\mathcal{E}_{k(rotation)}$ is the rotational energy of whole n-butane fixed to the temporal geometry, $\mathcal{E}_{k(dihed.vibration)}$ is the internal vibrational energy, which is equal to the torsional kinetic energy of dihedral angle, α, can be defined by

$$\mathcal{E}_{k(dihed.vibration)} = \mathcal{E}_k - \left(\mathcal{E}_{k(translation)} + \mathcal{E}_{k(rotation)}\right). \qquad (16)$$

Potential Energy Analysis

In order to understand how the LJ interaction from other molecules affects the torsional motion, we examine the contribution of both the attractive part ($\mathcal{E}_p^A$) and the repulsive part ($\mathcal{E}_p^R$) of the intermolecular potential that are evaluated by adopting the Weeks-Chandler-Andersen (W.C.A.) type separation (Weeks *et al.*, 1971).

$$\begin{aligned} \mathcal{E}_p &= \mathcal{E}_{p(inter.)} + \mathcal{E}_{p(intra.)} \\ &= \mathcal{E}^A_{p(inter.)} + \mathcal{E}^R_{p(inter.)} + \mathcal{E}_{p(intra.)}. \end{aligned} \tag{17}$$

$$\mathcal{E}^R_{p(inter.)}(r) = \begin{cases} \mathcal{E}_{p(inter.)}(r) + \varepsilon & , \quad (\text{ for } r < r_{min}) \\ 0 & , \quad (\text{ for } r \geq r_{min}) \end{cases} \tag{18}$$

$$\mathcal{E}^A_{p(inter.)}(r) = \begin{cases} -\varepsilon & , \quad (\text{ for } r < r_{min}) \\ \mathcal{E}_{p(inter.)}(r) & , \quad (\text{ for } r \geq r_{min}) \end{cases} \tag{19}$$

where r_{min} is $2^{1/6}\sigma$.

Torsional Motion Analysis

For the intramolecular rearrangement, that is, the transition of the potential barrier in the dihedral angle, the total potential energy of n-butane molecule is evaluated. In the gas phase, the profile of the total intramolecular potential energy is the same to the torsional potential energy, is given in eqn (1). However, in the liquid, the solvent induced contribution alters the topography of the potential energy hypersurface. The location of the top of the barrier in liquid may be difference from the that in gas phase, which are at 0°, ±60°, 180°. In Table 5, the dihedral angle of the top of the barrier, $\alpha^{barrier}$, the difference of the dihedral angle, $\Delta\alpha^{barrier}(= |\alpha^{barrier} - \alpha^{barrier}_{(gas)}|)$, the height of potential barrier, $E_p^{barrier}$, and the energy difference, $\Delta E_p^{barrier}(= E_p^{barrier} - E_{p(gas)}^{barrier})$ are listed.

Examples

Case I

One of the typical examples is plotted in Figures 10, in which the $G^+ \rightarrow T \rightarrow G^-$ transition is occurred. Figure 10a shows the time evolution of the dihedral angles during the intramolecular rearrangements

Table 5. The dihedral angle of the top of potential barrier and the hight of potential barrier for the intramolecular rearrangement of n-butane.

Case	System	Model	Rearrangement	$\alpha^{barrier}$ $\Delta\alpha^{barrier}$	$E_p^{barrier}$ $\Delta E_p^{barrier}$
I	Bu-Xe	A-o	$G^+ \rightarrow T$	55.45 (+4.55)	8.75 (0.67)
			$T \rightarrow G^-$	68.76 (+8.76)	8.75 (+2.02)
II	Bu-Xe	A-o	$T \rightarrow G^+$	52.93 (7.07)	11.04 (–1.31)
			$G^+ \rightarrow T$	60.78 (0.78)	11.97 (+2.55)
III	Bu-Xe	B-o	$G^+ \rightarrow T$	62.52 (+2.52)	11.75 (1.78)
IV	Bu-Xe	B-o	$T \rightarrow G^+$	62.78 (+2.87)	15.13 (–0.35)
			$G^+ \rightarrow G^-$	178.08 (+1.92)	13.79 (0.16)
V	Bu-CCl_4	A-o	$T \rightarrow G^-$	–63.70 (+3.70)	10.01 (–2.34)
			$G^- \rightarrow T$	–59.31 (+0.69)	10.19 (+0.77)
			$T \rightarrow G^+$	48.38 (+11.62)	13.74 (+1.39)

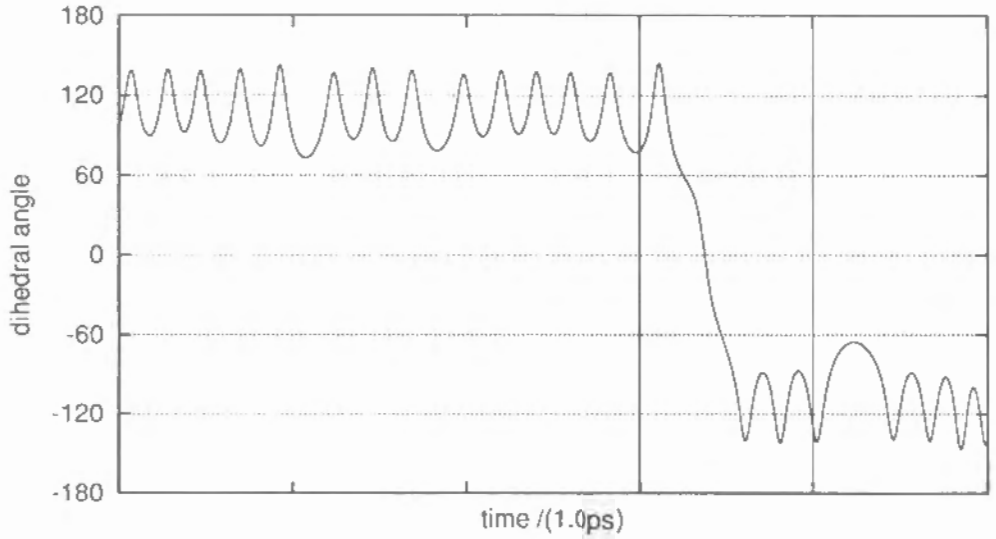

Figure 10. One of the typical examples is plotted during the intramolecular rearrangements (Case I): (**a**) the time evolution of the dihedral angle of n-butane for 5.0ps (2,500steps)

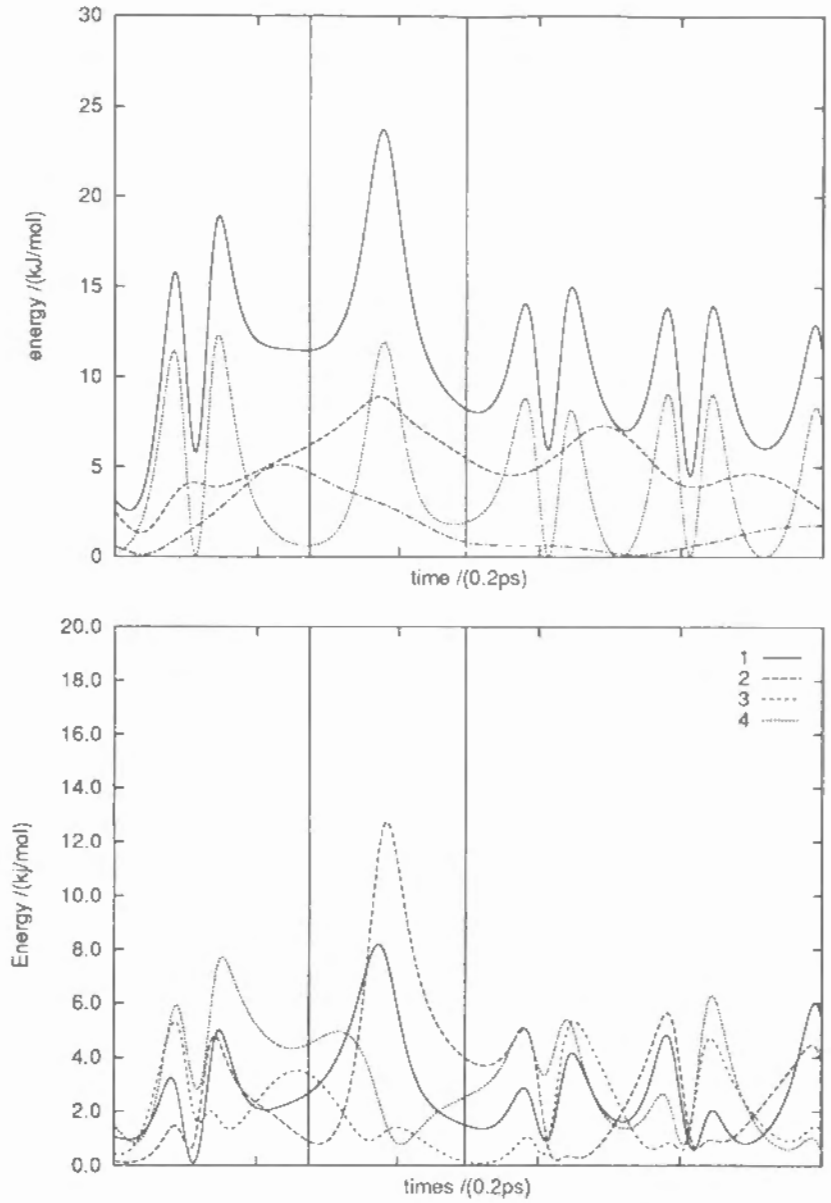

Figure 10. One of the typical examples is plotted during the intramolecular rearrangements (Case I): the time evolution of (**b**) each kinetic energy term (TOP) for total (solid line), rotate (dashed line), translate (dash-dot line) and dihedral vibrational energy (dotted line); (**c**) the kinetic energy of each CH_n group (BOTTOM) for $\mathbf{C}^1$ (solid line), $\mathbf{C}^2$ (dashed line), $\mathbf{C}^3$ (dash-dot line) and $\mathbf{C}^4$ (dotted line) within 1.0ps.

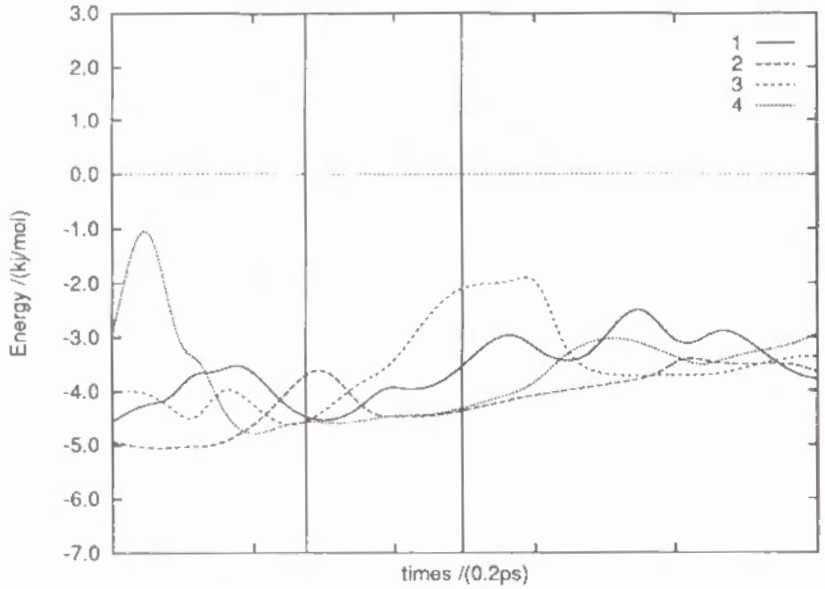

Figure 10. One of the typical examples (Case I): (**d**) each intermolecular potential energy term (TOP) for $\mathbf{C}^1$ (solid line), $\mathbf{C}^2$ (dashed line), $\mathbf{C}^3$ (dash-dot line) and $\mathbf{C}^4$ (dotted line); (**e**) each potential energy term of n-butane molecule as a function of the dihedral angle (BOTTOM), for total (solid line), intramolecular (dashed line), intermolecular-attractive (dash-dot line) and intermolecular repulsive potential energy (dotted line) within 1.0ps.

(2500steps, 5.0ps). The transition event is completed within 1.0 ps (500steps) which is shown by two vertical lines in Figure 10a. A more detailed analysis is made to examine the dynamics of torsional motions. In Figures 10b, 10c, 10d and 10e, the time evolution of each kinetic energy term, the kinetic energy of each CH_n group and each intermolecular potential energy term, and each potential energy term of n-butane molecule as a function of the dihedral angle are shown, respectively. The motion of each CH_n group is not independent of each other since these groups are constrained by fixed angles and bonds. In order to investigate how the motions of each group affect torsional motion, the kinetic energy of each CH_n group are, however, calculated treating each group with independent atoms.

The maximum values of the barrier are shown in Figure 10e by two vertical lines. Two vertical lines in Figures 10b, 10c, 10d are corresponding to the time of these intramolecular rearrangement events.

We defined each group of n-butane, CH_3-, -CH_2-, -CH_2- and -CH_3 as $\mathbf{C}^1$, $\mathbf{C}^2$, $\mathbf{C}^3$and $\mathbf{C}^4$, respectively. As seen from Figure 10c, these continual rearrangements ($G^+ \rightarrow T \rightarrow G^-$) are dominated mainly by the motion of $\mathbf{C}^1$ and $\mathbf{C}^2$. The motion of $\mathbf{C}^4$is not very large, however, plays a significant role in these rearrangements since this group moves the opposite direction of $\mathbf{C}^1$ and $\mathbf{C}^2$. The kinetic energy of $\mathbf{C}^4$which leads to the torsional motion is transformed mainly to that of $\mathbf{C}^1$ and $\mathbf{C}^2$. In the forward transition ($G^+ \rightarrow T$), in the term of the rotational energy of whole n-butane ($\mathcal{E}_{k(rotation)}$), the rearrangement occurs accompanying a large rotational motion of whole n-butane. The backward transition ($T \rightarrow G^-$) is occurred continually after the forward transition. In this transition, the height of potential barrier is not lowered by relaxation of the surrounding solvents. Therefore, this arrangement is caused dominantly by the kinetic energy.

Case II

Another example is plotted in Figures 11, in which the $T \rightarrow G^+ \rightarrow T$ transition occurs. As seen from Figure 11b, the rotational energy of whole n-butane, $\mathcal{E}_{k(rotation)}$, is transformed to the translational energy and the torsional energy. The motion of each group of n-butane is closely related to the intermolecular interaction from the solvent. In the case of $\mathbf{C}^1$ and $\mathbf{C}^3$, the direct energy transfer from kinetic to potential part occurs.

Case III

The other example is plotted in Figures 12, in which the $G^+ \rightarrow T$ transition occurs. As seen from Figure 12b, the dihedral angle α stays in a small region, is closed to the very limit of intramolecular transition before the real rearrangement is occurred. While this motion, most of the kinetic energy of $\mathbf{C}^2$, $\mathbf{C}^3$ and $\mathbf{C}^4$is transferred to that of $\mathbf{C}^1$. These motions lead the intermolecular interaction to less stable conformation(-1.78kJ/mol). The real height of potential barrier is slightly lowered by the intermolecular interaction. Therefore, this rearrangement is caused by both the kinetic energy and potential energy.

Case IV

The other example is shown in Figures 13, in which the $T \rightarrow G^+ \rightarrow G^-$ transition is occurred, Two intramolecular rearrangements occur continually. The motions of $\mathbf{C}^2$ and $\mathbf{C}^4$which are contributed to the former intramolecular transitions to the excitation of the motions of $\mathbf{C}^1$, $\mathbf{C}^3$ and $\mathbf{C}^4$which contributes to the later rearrangement. Then, most of the kinetic energy is transformed to that of $\mathbf{C}^2$. Finally, the extra energy is transformed dominantly to the rotational energy $\mathcal{E}_{k(rotation)}$.

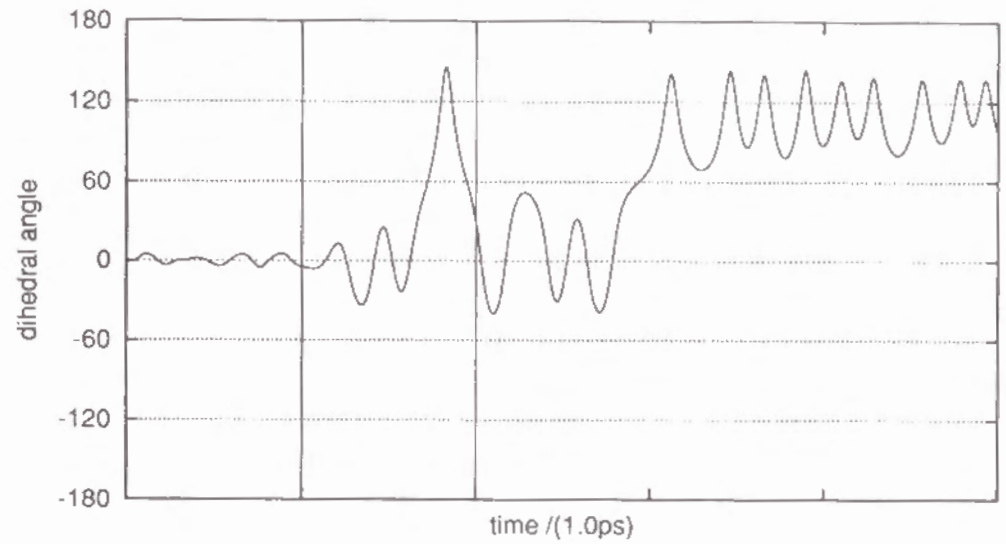

Figure 11. One of the typical examples is plotted during the intramolecular rearrangements (Case II): (**a**) the time evolution of the dihedral angle of n-butane for 5.0ps (2,500steps)

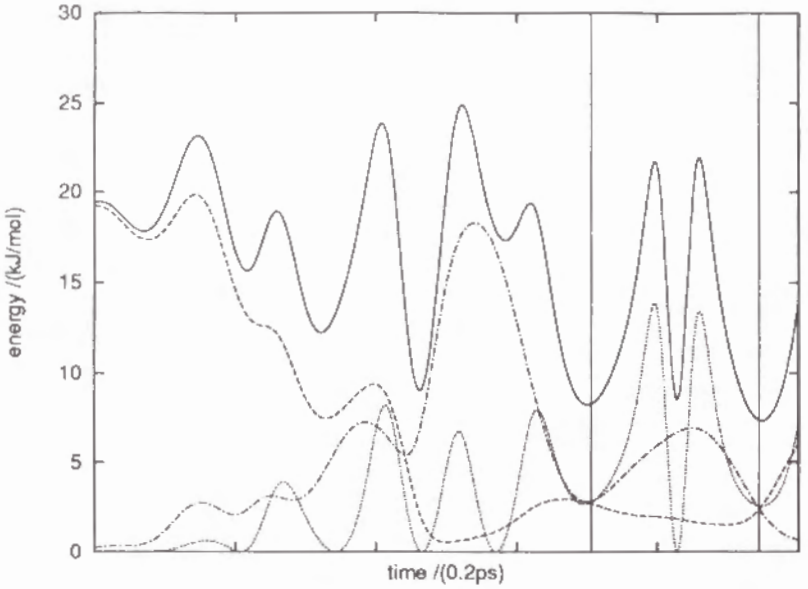

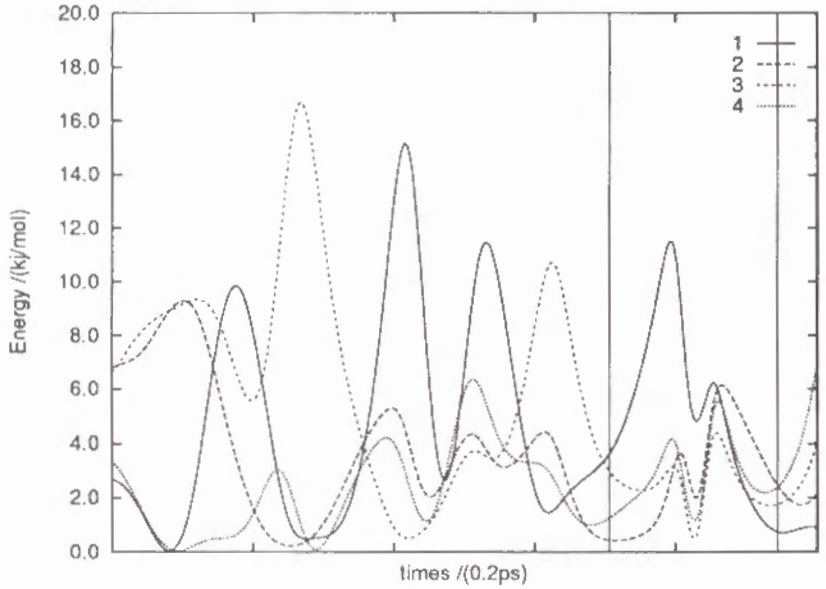

Figure 11. One of the typical examples is plotted during the intramolecular rearrangements (Case II): the time evolution of (**b**) each kinetic energy term (TOP) for total (solid line), rotate (dashed line), translate (dash-dot line) and dihedral vibrational energy (dotted line); (**c**) the kinetic energy of each CH_n group (BOTTOM) for $\mathbf{C}^1$ (solid line), $\mathbf{C}^2$ (dashed line), $\mathbf{C}^3$ (dash-dot line) and $\mathbf{C}^4$ (dotted line) within 1.0ps.

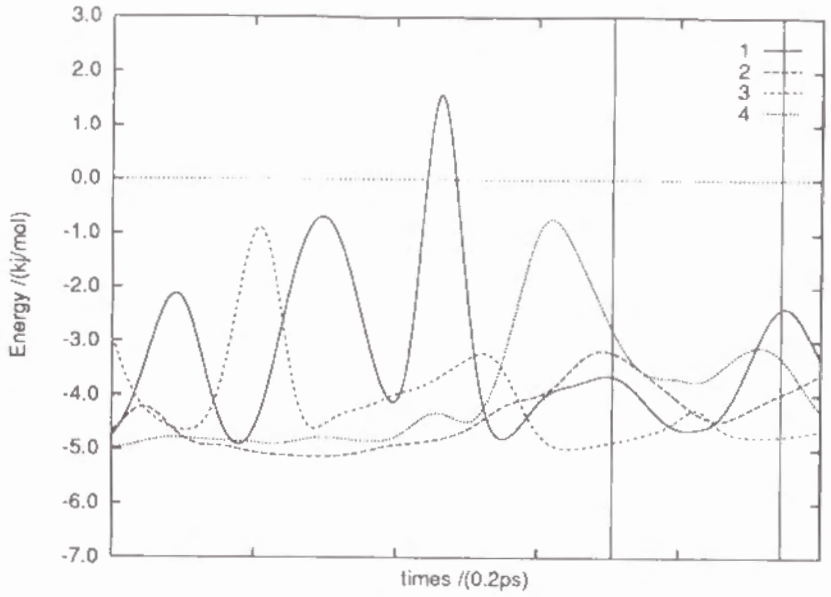

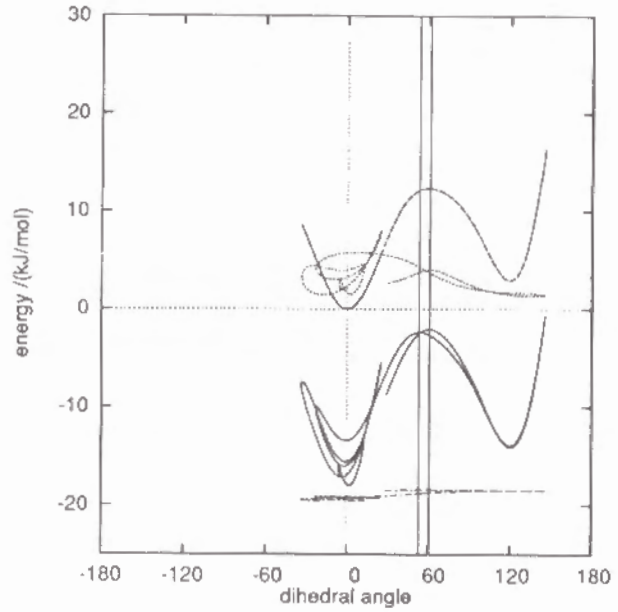

Figure 11. One of the typical examples (Case II): (**d**) each intermolecular potential energy term (TOP) for $\mathbf{C}^1$ (solid line), $\mathbf{C}^2$ (dashed line), $\mathbf{C}^3$ (dash-dot line) and $\mathbf{C}^4$ (dotted line); (**e**) each potential energy term of n-butane molecule as a function of the dihedral angle (BOTTOM), for total (solid line), intramolecular (dashed line), intermolecular-attractive (dash-dot line) and intermolecular repulsive potential energy (dotted line) within 1.0ps.

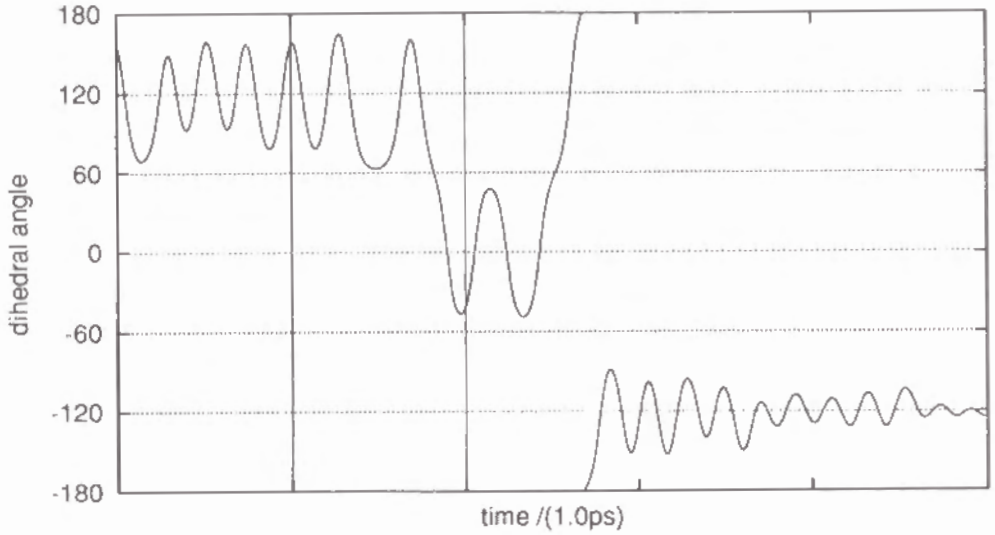

Figure 12. One of the typical examples is plotted during the intramolecular rearrangements (Case III): (**a**) the time evolution of the dihedral angle of n-butane for 5.0ps (2,500steps)

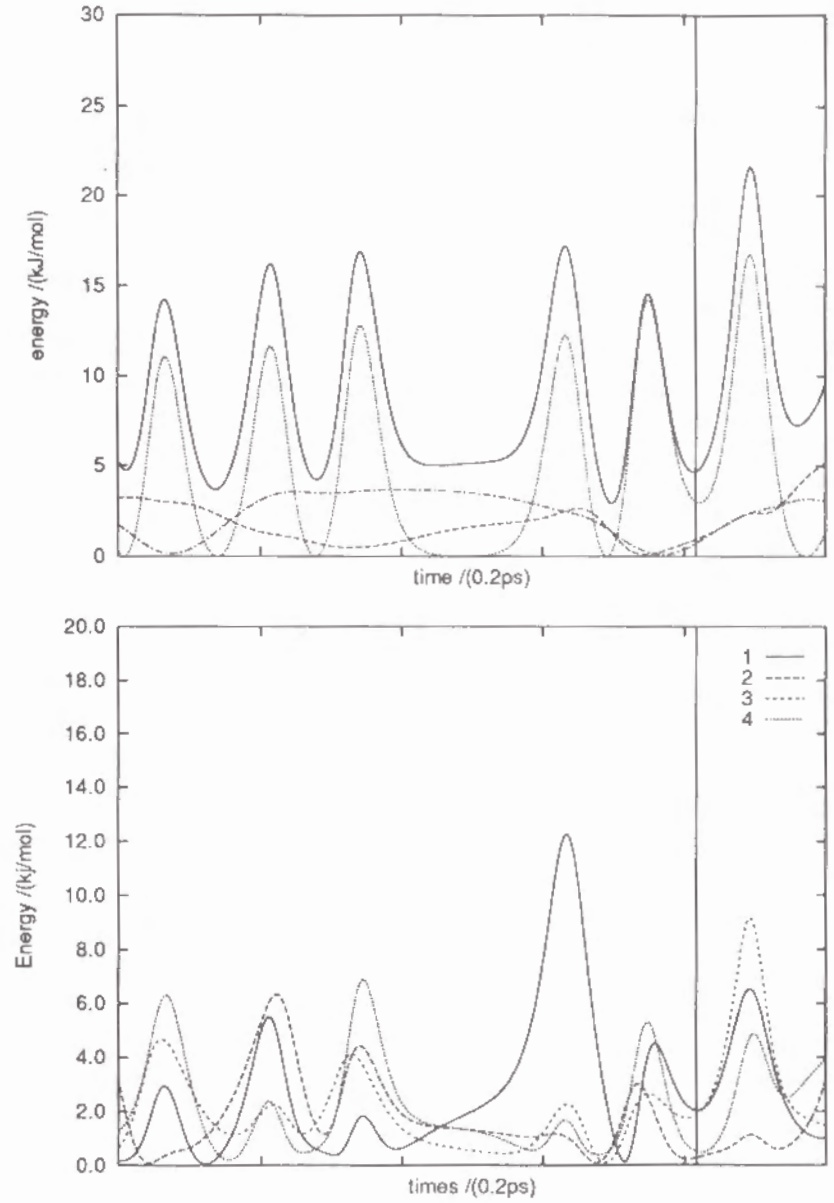

Figure 12. One of the typical examples is plotted during the intramolecular rearrangements (Case III): the time evolution of (**b**) each kinetic energy term (TOP) for total (solid line), rotate (dashed line), translate (dash-dot line) and dihedral vibrational energy (dotted line); (**c**) the kinetic energy of each CH_n group (BOTTOM) for $\mathbf{C}^1$ (solid line), $\mathbf{C}^2$ (dashed line), $\mathbf{C}^3$ (dash-dot line) and $\mathbf{C}^4$ (dotted line) within 1.0ps.

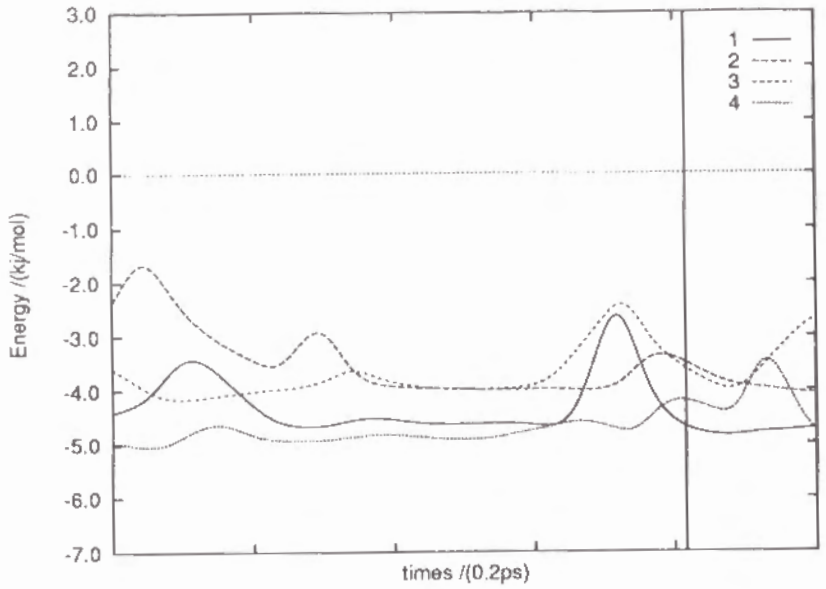

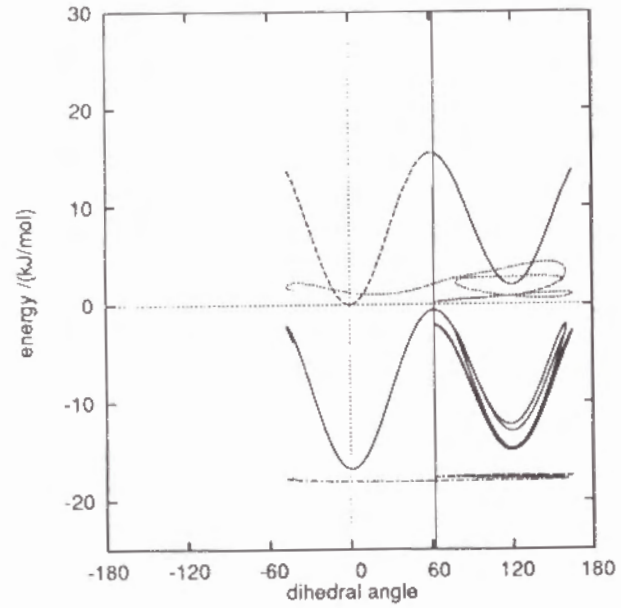

Figure 12. One of the typical examples (Case III): (**d**) each intermolecular potential energy term (TOP) for $\mathbf{C}^1$ (solid line), $\mathbf{C}^2$ (dashed line), $\mathbf{C}^3$ (dash-dot line) and $\mathbf{C}^4$ (dotted line); (**e**) each potential energy term of n-butane molecule as a function of the dihedral angle (BOTTOM), for total (solid line), intramolecular (dashed line), intermolecular-attractive (dash-dot line) and intermolecular repulsive potential energy (dotted line) within 1.0ps.

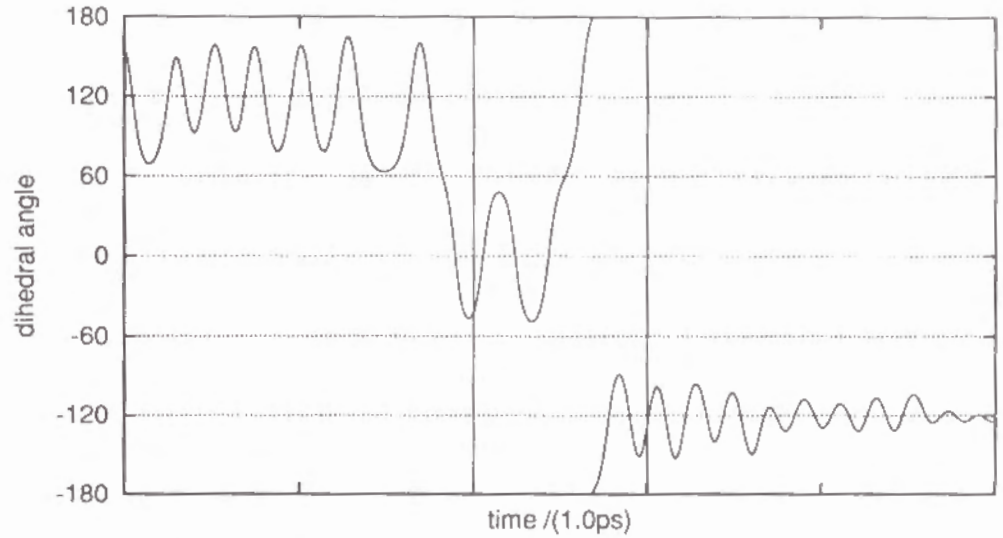

Figure 13. One of the typical examples is plotted during the intramolecular rearrangements (Case IV): (**a**) the time evolution of the dihedral angle of n-butane for 5.0ps (2,500steps)

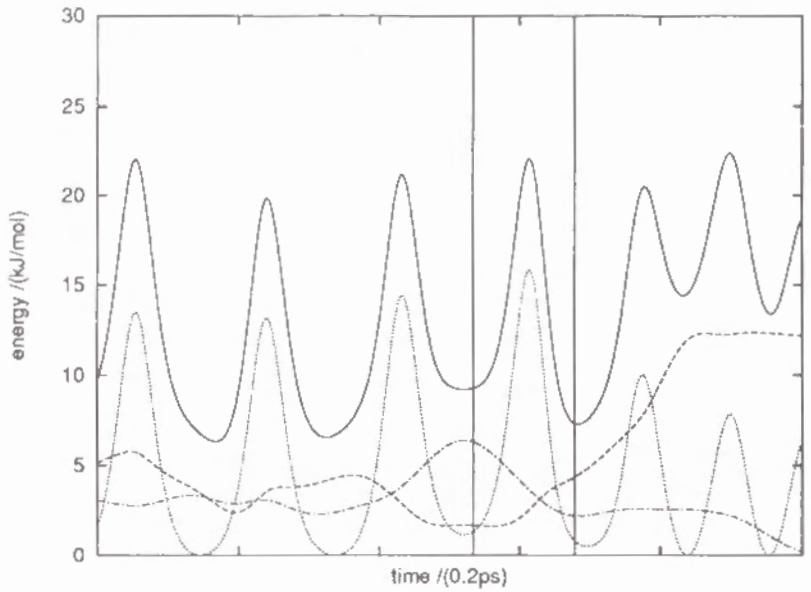

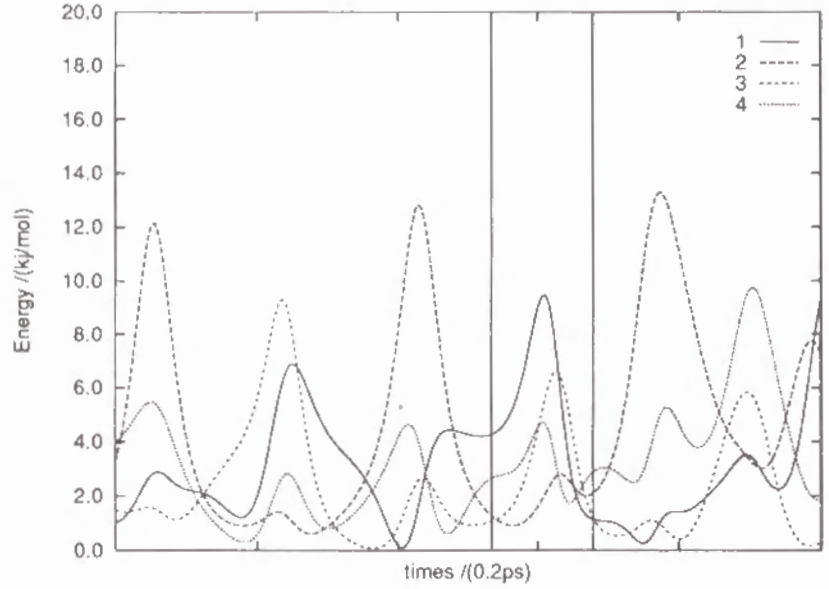

Figure 13. One of the typical examples is plotted during the intramolecular rearrangements (Case IV): the time evolution of (**b**) each kinetic energy term (TOP) for total (solid line), rotate (dashed line), translate (dash-dot line) and dihedral vibrational energy (dotted line); (**c**) the kinetic energy of each CH_n group (BOTTOM) for $\mathbf{C}^1$ (solid line), $\mathbf{C}^2$ (dashed line), $\mathbf{C}^3$ (dash-dot line) and $\mathbf{C}^4$ (dotted line) within 1.0ps.

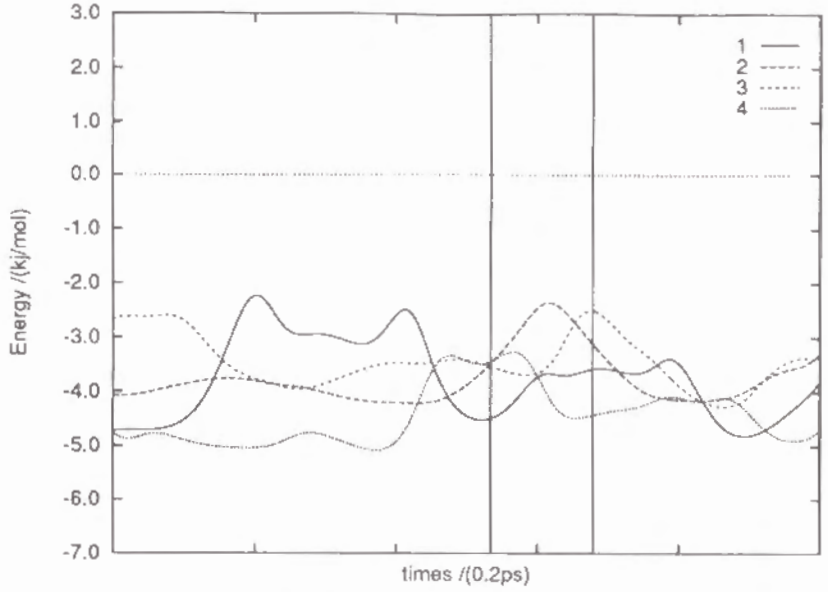

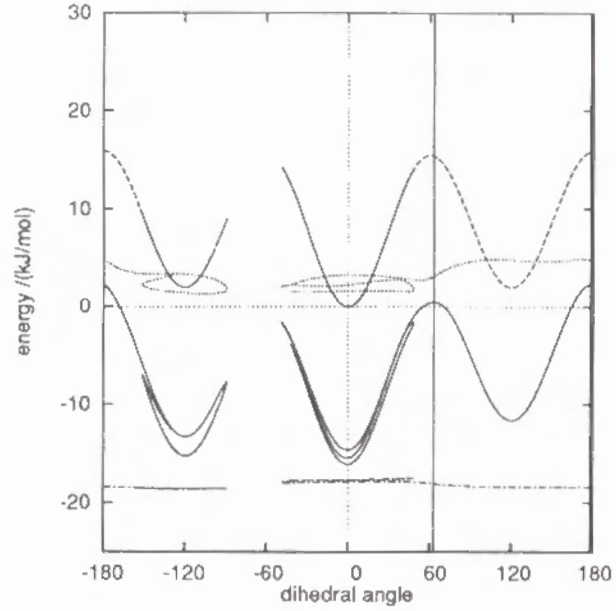

Figure 13. One of the typical examples (Case IV): (**d**) each intermolecular potential energy term (TOP) for $\mathbf{C}^1$ (solid line), $\mathbf{C}^2$ (dashed line), $\mathbf{C}^3$ (dash-dot line) and $\mathbf{C}^4$ (dotted line); (**e**) each potential energy term of n-butane molecule as a function of the dihedral angle (BOTTOM), for total (solid line), intramolecular (dashed line), intermolecular-attractive (dash-dot line) and intermolecular repulsive potential energy (dotted line) within 1.0ps.

Case V

The last example is given in Figure 14, in which the $T \rightarrow G^- \rightarrow T \rightarrow G^+$ transition occurs. As seen from Figure 14d, before the first transition ($T \rightarrow G^-$), strong repulsive force is exerted from some of Xe molecule affects on $\mathbf{C}^1$. This rearrangement is caused by both the kinetic energy and potential energy.

CONCLUSIONS

Torsional motions for n-butane have been analyzed by MD simulations. Various kinds of the transition patterns involving solvent motions are observed. The motion of each CH_n group is not independent of each other.

From the results of RDF between n-butane and solvent molecules and velocity autocorrelation function of solvent molecules, there is no significant difference between different dihedral potential models in the short range structures. However, these results show the time averaged structure. During the intramolecular rearrangement, some solvent molecules may be closed instantaneously to the solute molecule.

In the liquid state, the profile of the total intramolecular potential energy of n-butane is altered by the solvent induced contribution. In one case of intramolecular rearrangement, the intermolecular interaction led solute molecule to be less stable conformation. Therefore, the height of potential barrier is lowered by relaxation of the surrounding solvents. This effect caused dominantly to a facile rearrangement. In another case, the torsional kinetic energy of dihedral angle is caused dominantly to the rearrangement.

From the results of energy analysis, the surplus energy caused by the internal transition is transformed rapidly to other energy term: the

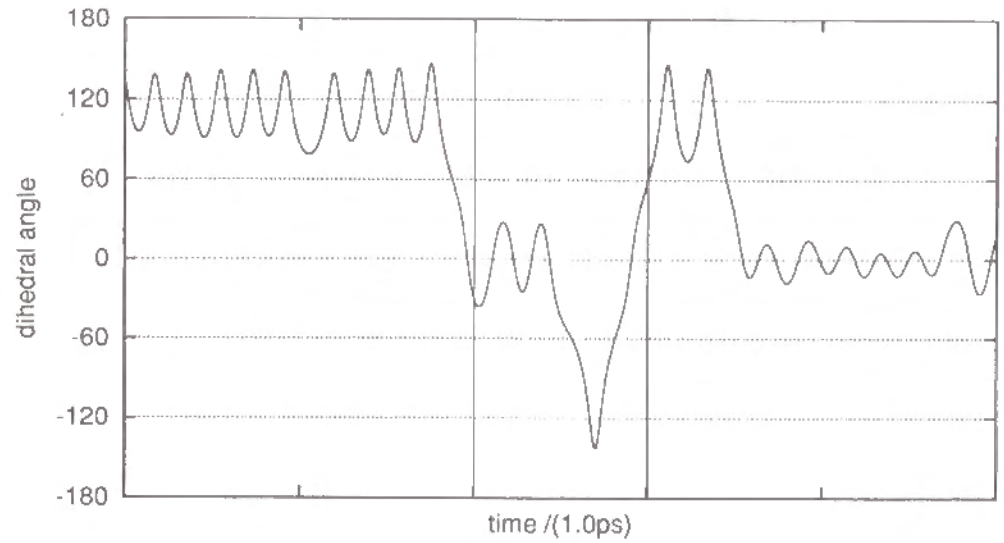

Figure 14. One of the typical examples is plotted during the intramolecular rearrangements (Case V): (**a**) the time evolution of the dihedral angle of n-butane for 5.0ps (2,500steps)

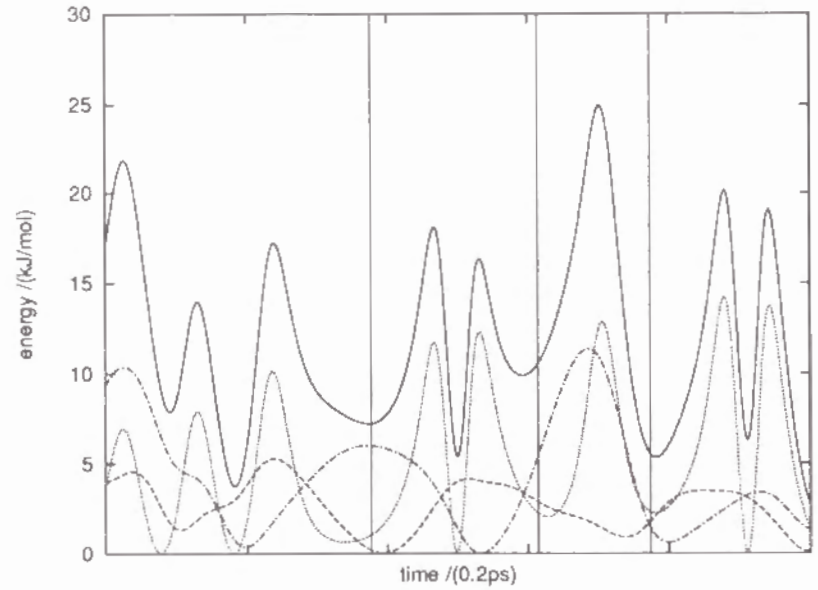

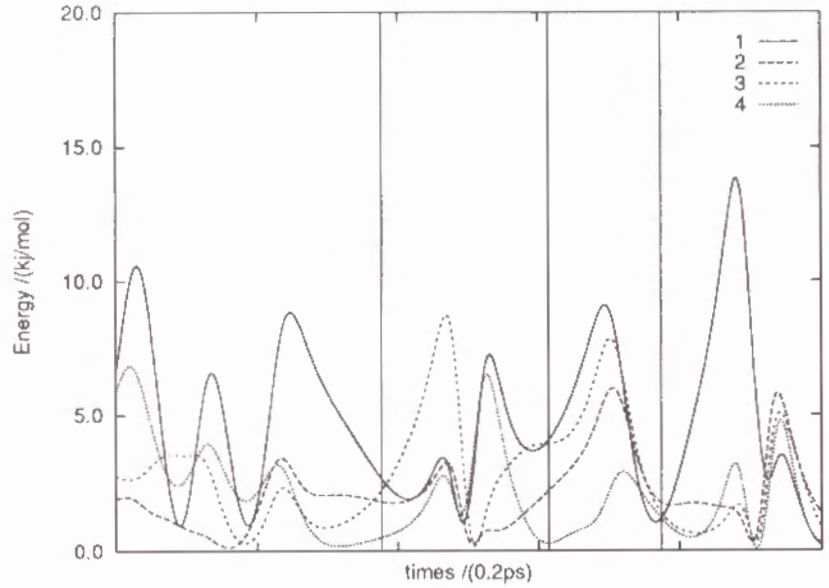

Figure 14. One of the typical examples is plotted during the intramolecular rearrangements (Case V): the time evolution of (**b**) each kinetic energy term (TOP) for total (solid line), rotate (dashed line), translate (dash-dot line) and dihedral vibrational energy (dotted line); (**c**) the kinetic energy of each CH_n group (BOTTOM) for $\mathbf{C}^1$ (solid line), $\mathbf{C}^2$ (dashed line), $\mathbf{C}^3$ (dash-dot line) and $\mathbf{C}^4$ (dotted line) within 1.0ps.

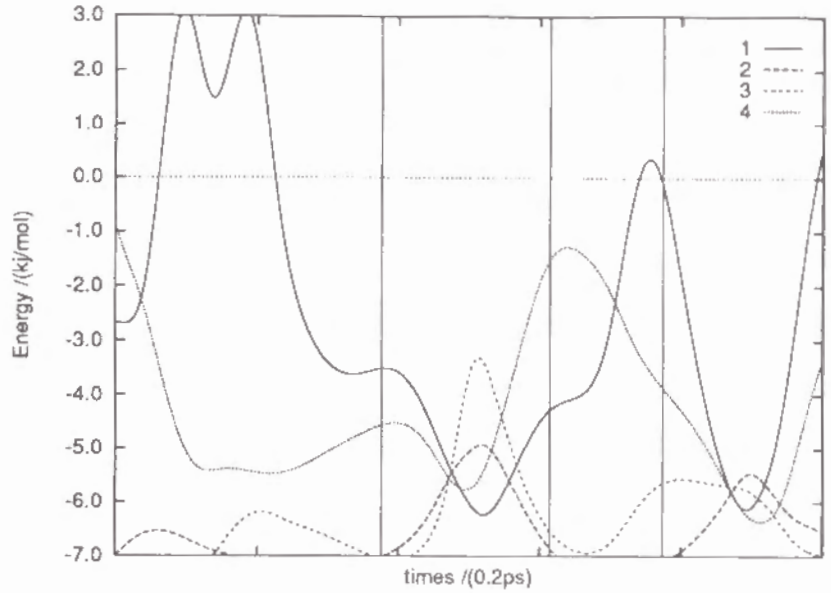

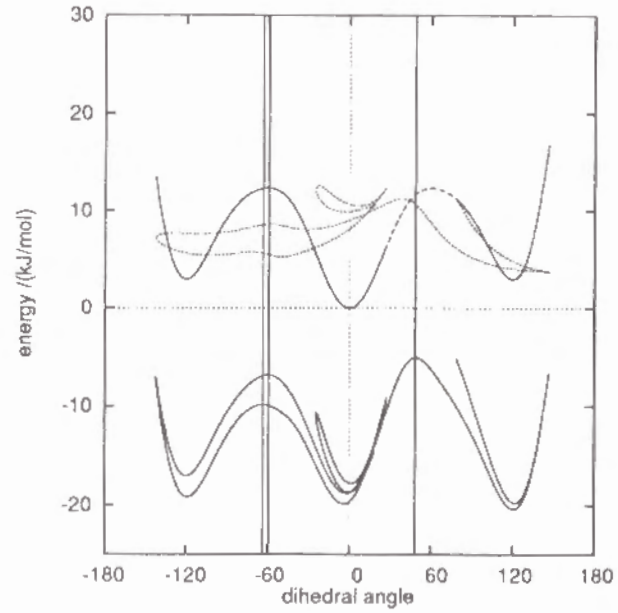

Figure 14. One of the typical examples (Case V): (**d**) each intermolecular potential energy term (TOP) for $\mathbf{C}^1$ (solid line), $\mathbf{C}^2$ (dashed line), $\mathbf{C}^3$ (dash-dot line) and $\mathbf{C}^4$ (dotted line); (**e**) each potential energy term of n-butane molecule as a function of the dihedral angle (BOTTOM), for total (solid line), intramolecular (dashed line), intermolecular-attractive (dash-dot line) and intermolecular repulsive potential energy (dotted line) within 1.0ps.

energy of solvent molecule and the energy of solute molecule except the torsional kinetic term of dihedral angle.

CHAPTER IV

AQUEOUS SOLUTION OF ETHYLENE GLYCOL

Molecular dynamics simulations have been performed for ethylene glycol (ethane-1,2-diol, EG) in water. Each EG molecule consists of six sites interacting through LJ and coulomb potentials together with three dihedral angle potentials. A comparison of EG molecules in water and in Xe shows that EG molecules in the Xe solvent tend to fold unlike those in water. In order to investigate how the intramolecular interaction affects intermolecular hydrogen bonds, some rigid-EG models are also examined.

MODEL AND MD SIMULATIONS

Ethylene glycol (EG) is a fairly flexible molecule in which both intra- and inter-molecular interactions should be taken into account. One carbon atom and two hydrogen atoms directly bonded to the carbon atom, namely, a methylene group, is treated as a single 'united' atom. The total mass and the interaction site is thereby placed on the carbon atom. The simulations using the full atomic model are found to be more accurate such as the distribution of the dihedral angle, than those using the united-atom model (Ryckaert, 1985). Recently, the use of an anisotropic united atom model, whose structural parameters are improved and are in good correspondence with the experimentally observed values such as the self-diffusion coefficient, was advocated (van Gunsteren, 1980; Toxvaerd, 1990). These models may be too complicated for studying the role of the torsional motions and structural properties of EG solutions in which electrostatic interactions dominate. Moreover, it is known that use of this simple type of model gives

reasonable static and dynamic properties in the liquid state. Therefore, we adopt a simpler united-atom model. The present EG molecule model has six interaction sites and three dihedral angles with fixed bond lengths and bond angles; neither bond stretching nor bending vibrations are taken into consideration. In general, the bending frequencies are different from the torsional frequencies of flexible molecules and therefore do not couple with the torsional motions. The constraints on the bond angles, however, may change somewhat the flexibility of the chain molecule (Toxvaerd, 1987). This is in contrast to keeping the bond lengths of the chain molecule constraint, which has a negligible effect. It is not practical to take into account this high-frequency vibration in the framework of classical mechanics. Therefore, we used the simpler fixed-bond-angle model. The bond angles are realized by next-nearest-neighbor constraints. Standard values are adopted for the fixed bond lengths (Bowen and Sutton, 1958): C-C = 1.54Å, C-O = 1.43Å and O-H = 0.97Å. The bonds are assumed to be fixed in a tetrahedral geometry: ∠ C-O-H = ∠ C-C-O = 109.5°. The minimal-energy conformers of the EG molecule in the gas phase are calculated by the MO method (van Alsenoy *et al.*, 1984). However, in the pure liquid and in solution, it is not easy to estimate directly the intramolecular structure of each EG.

The intramolecular interaction potential is defined by two contributions: a torsional potential term and the long-range LJ and coulomb terms. This type of interaction acts on pairs of groups of atoms in the same molecule which are separated by more than three bonds. Since no reliable torsional potential function of EG is available, we performed *ab initio* MO single-point calculations with the 4-31G basis set for 100 conformations of EG. The torsional potential energy of each conformation is given by the sum of various contributions: dipole-dipole interactions, conjugated effects, non-bonded interactions, intramolecular

OH-O hydrogen-bonded interactions, and so on. Since the intramolecular conformation of EG is defined by three dihedral angles, β_1, α and β_2, (the values of the ∠H-O-C-C-, ∠-O-C-C-O- and ∠-C-C-O-H angles are respectively, $-180° < \beta_1,\ \alpha,\ \beta_2 \leq +180°$; all the *trans* conformation have the same angle, 0°), we assumed that the torsional potential energy is given by a function of these dihedral angles. The torsional potential may be divided into two contributions: the non-bonded interactions due to the fractional charge and the purely torsional potential when there is no electrostatic interaction. Therefore, using the electrostatic charges on H, O and C as parameters, we fitted the MO results to the following function of Fourier series,

$$\mathcal{V} \equiv \sum_{n=0}^{5} V_{\beta n} \cos^n \beta_1 + \sum_{n=0}^{5} V_{\alpha n} \cos^n \alpha + \sum_{n=0}^{5} V_{\beta n} \cos^n \beta_2 + \sum_i \sum_{j>i} (q_i q_j / r_{ij}), \tag{1}$$

where q_i is the charge on site i and r_{ij} is the distance between sites i and j which depends directly on these three dihedral angles. The standard deviation is 3.62 kJ mol^{-1}. The parameters in eqn (1) are given in Table 1. The potential energies from MO calculations and our parameters are also listed in Table 2 and the potential curves are shown in Figure 1. Because of the three internal degrees of freedom around one C-C and two C-O bonds, there must be many stable torsional isomers of EG: the *gauche*$^{(-)}$, *trans*, *gauche*$^{(+)}$ conformations around C-C, and the *gauche*$^{(-)}$, *eclipsed*$^{(-)}$, *trans*, *eclipsed*$^{(+)}$, *gauche*$^{(+)}$ conformations around O-C. These correspond to the three and five minima of the torsional potential, respectively.

The intermolecular site-site potential is described by the Lennard-Jones (LJ) 12-6 interaction potential and coulomb-coulomb interaction potential,

$$\mathcal{V}(r_{ij}) = 4\epsilon_{ij}[(\sigma_{ij}/r_{ij})^{12} - (\sigma_{ij}/r_{ij})^6] + (q_i q_j / r_{ij}), \tag{2}$$

where the charge q_i on the site i is determined in the fitting of the

Table 1. Electrostatic charges on individual interaction sites and interaction parameters for intramolecular torsional potential functions of EG. Units of q is electron, of V_{xi}'s are kJ/mol.

group	H	O	$C(CH_2)$
q	+0.523	−0.587	+0.064

x	V_{x0}	V_{x1}	V_{x2}	V_{x3}	V_{x4}	V_{x5}
α (-O-C-C-O-)	−1.026	−19.466	+14.370	+89.701	−9.605	−73.974
β (H-O-C-C-)	+9.269	+2.341	−19.157	+60.418	+21.824	−74.695

Table 2. Total energies (E_{MO}, in hartree), relative energies (ΔE_{MO}, in kJ mol^{-1}), relative energies using our parameters (ΔE_{fit}, in kJ mol^{-1}) for 8 important conformers of the EG molecule; standard deviation of all 100 conformations is 3.62 kJ mol^{-1}.

conformation	$-E_{MO}$	ΔE_{MO}	ΔE_{fit}
trans-gauche$^{\pm}$-*gauche*$^{\mp}$	228.9215504	0.000	0.000
eclipsed$^{\pm}$-*gauche*$^{\pm}$-*gauche*$^{\pm}$	228.9196660	4.947	2.031
gauche$^{\pm}$-*gauche*$^{\pm}$-*gauche*$^{\mp}$	228.9194512	5.511	12.293
trans-trans-trans	228.9184191	8.221	8.754
trans-trans-gauche^{+}	228.9179094	9.559	13.694
gauche$^{\pm}$-*trans-gauche*$^{\mp}$	228.9169470	12.086	11.004
trans-gauche$^{\pm}$-*gauche*$^{\pm}$	228.9144598	18.616	21.281
cis-cis-cis	228.8544483	176.176	163.876

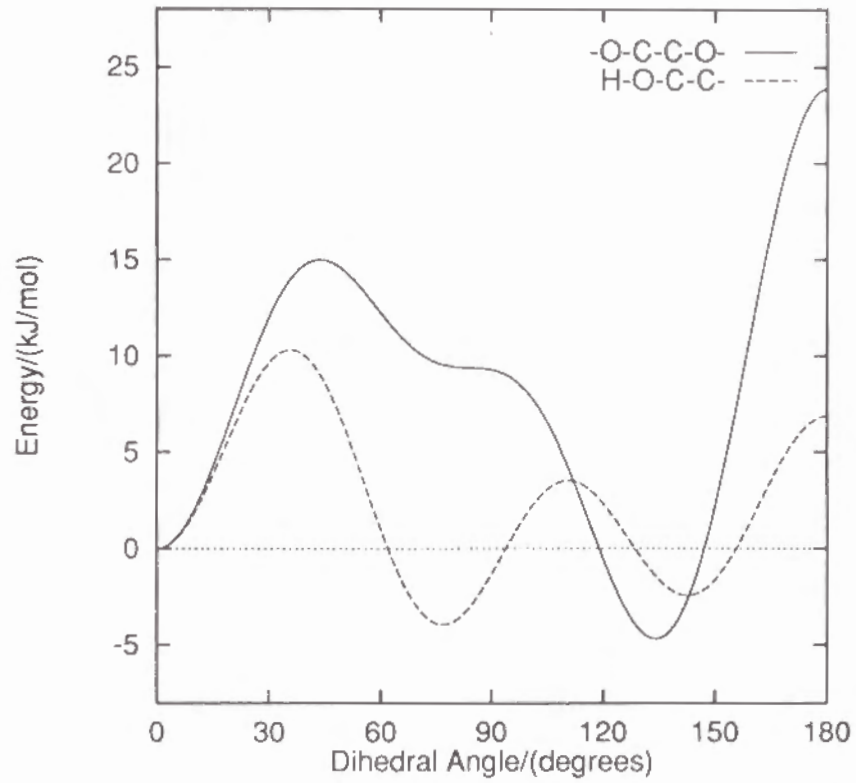

Figure 1. Torsional potential energy around -C-C- (solid line) and -O-C- (dashed line) bonds of Ethylene Glycol

intramolecular interaction and r_{ij} is the distance between sites i and j in different molecules. In order to truncate the interaction smoothly at 9Å, the intermolecular site-site potential is multiplied by a switching-function (Ohmine *et al.*,1988). Standard values of the optimized potentials for liquid simulations (OPLS) (Jorgensen, 1986) are used for the size parameter σ and the energy parameter ϵ for EG. The water molecules are modelled by the TIP4P potential function (Jorgensen *et al.*, 1983), which is well known to reproduce both the static and dynamic properties of pure water. For all unlike site-site pairs, we adopted the Lorentz-Berthelot (LB) combination rule.

In the present MD simulation, the temperatures are set to (a) 298.15, (b) 278.15, (c) 253.15 and (d) 233.15K, and the densities ρ are set to experimentally observed values for aqueous solutions of EG (Hout *et al.*, 1988; Douheret *et al.*, 1991) and pure water (Franks, 1982) by applying an interpolation method.

One of the interesting features of flexible molecules is conformational equilibria. To examine this, an EG-water mixture has been adopted (system A), a 25 mol% aqueous solution which contains 54 EG molecules and 162 water molecules.

Newton's equations of motion are solved by the ordinary Verlet method (e.g., Allen and Tildesley, 1987) and the constraints of bond angles and lengths are handled by the iterative algorithm 'Shake' (Ryckaert *et al.*, 1977). A time step Δt for the integration of the equations of motion is 2.00×10^{-15} sec. At the initial stage of the MD simulation, the centers of mass of the molecule are placed on an fcc crystal lattice as an initial configuration. Initially, all the EG molecules have *trans-trans-trans* (*t-t-t*) conformations ($\beta_1 = \alpha = \beta_2 = 0°$) and the orientations of the EG and water molecules are random. The systems correspond to an NEV-ensemble in the MD simulation. The molecules are confined to a cube imposing a periodic boundary condition and the

cubic minimum image convention. The length of cell box is 21.38Å at 298.15K and 21.84Å at 233.15K. An initial 100 ps of simulation is used for the relaxation of the unrealistic initial conditions to achieve both the structural and conformational equilibria of internal dihedral angles. The MD simulation is extended up to 1,000,000∼1,500,000 time steps (2000∼3000ps) in order to calculate thermodynamic properties accurately. This simulation time proves to be long enough to obtain a reliable distribution of dihedral angles. A CPU time of about two weeks by an HP9000-730 workstation is required for one MD simulation.

The conformational equilibria depend on the nature of the intermolecular interactions of both solvents and EG molecules. The EG molecule can be hydrogen bonded with water. This causes large shifts in the dihedral angle distributions. In order to compare the distribution in water and to examine the solvent effect, a similar MD simulation is also carried out where the solvent species is Xe ($\sigma = 4.1$Å; $\epsilon/k = 216.9$K). This solvent molecule is much simpler and does not take part in any intermolecular hydrogen bonding; this system is system B, a 25 mol% Xe solution of EG which contains 54 EG molecules and 162 Xe molecules.

In addition, rigid-EG models are also examined under the same conditions as system A in order to understand how internal degrees of freedom affect the equilibrium properties. We adopted five rigid-EG models: *cis-cis-cis* (*c-c-c*), *trans-gauche*$^{\pm}$*-gauche*$^{\mp}$ (*t-g*$^{\pm}$*-g*$^{\mp}$), *trans-gauche*$^{\pm}$*-trans* (*t-g*$^{\pm}$*-t*), *eclipsed*$^{\pm}$*-gauche*$^{\pm}$*-gauche*$^{\mp}$ (*e*$^{\pm}$*-g*$^{\pm}$*-g*$^{\mp}$) and *trans-trans-trans* (*t-t-t*) conformations. All of these conformations except *c-c-c* are stable in the gaseous state of EG. In particular, an intramolecular hydrogen bond is expected to be formed in the *e*$^{\pm}$*-g*$^{\pm}$*-g*$^{\mp}$ and *t-g*$^{\pm}$*-g*$^{\mp}$ conformations of EG. The trajectories of individual rigid molecules are obtained by solving the Newton-Eulars equations of mo-

tion numerically.

RESULTS AND DISCUSSION

The temperatures and the potential energies calculated from MD simulations are given in Table 3. Standard deviations are also given in parentheses in this table. The deviations are calculated by dividing the whole simulation run into several blocks comprising 10000 consecutive steps (20.0ps). We will pay attention to the intramolecular conformation of EG which is defined by the dihedral angles. The *trans* conformation is defined by the range of $-36.0° < \theta < +36.0°$, the *eclipsed* conformation by the ranges $-108.0° < \theta \leq -36.0°$ and $+36.0° \leq \theta < +108.0°$, and the *gauche* conformation by the ranges $-180.0° < \theta \leq -108.0°$ and $+108.0° \leq \theta \leq +180.0°$ ($\theta = \beta_1$, α and β_2). X^{trans}, $X^{eclipsed}$ and X^{gauche} stand for the populations of the *trans*, *eclipsed*$^{(\pm)}$ and *gauche*$^{(\pm)}$ conformations. The most stretched conformation of EG is *t-t-t*.

Distribution of the Dihedral Angles

The dihedral angle distributions (DAD) for systems A and B are given in Table 4. As is expected from the intermolecular interactions, the distribution of the dihedral angle β (H-O-C-C-) is wide. Since the motions of the two HO groups in each EG molecule are correlated through intramolecular interactions, the distribution of angle β has a tendency to take either positive or negative values for a long time. We give only the distribution for a positive β (H-O-C-C-) value after symmetrizing the obtained distributions. In the aqueous solution, the *eclipsed* and *gauche* conformations are dominant. The distributions of the population of the dihedral angle α (-O-C-C-O-) show that most EG molecules take the *gauche* conformation in both aqueous and Xe solutions. The

Table 3. Thermodynamic properties for mixtures of EG and solvent. The temperature is in Kelvin. The unit of energy is kJ/mol. Standard deviations are also given in the parentheses of this table. The deviations are calculated by dividing whole simulation run into several blocks comprising 10000 consecutive steps (20.0ps).

System (EG : water)	Init. Temp.	Average Temp.	Total Energy	EG Energy	Water Energy
System A (54 : 162)	a) 298.15	304.60 (3.43)	-7792.96 (49.64)	-51.08 (3.32)	-42.48 (0.91)
	b) 278.15	281.76 (4.87)	-8307.26 (48.62)	-52.44 (3.01)	-44.34 (1.02)
	c) 253.15	249.96 (3.42)	-9007.68 (27.63)	-55.03 (2.26)	-46.61 (0.78)
	d) 233.15	237.08 (4.00)	-9110.48 (19.78)	-54.11 (1.69)	-47.08 (0.54)
System (EG : Xe)	**Init. Temp.**	**Average Temp.**	**Total Energy**	**EG Energy**	**Xe Energy**
System B (54 : 162)	a) 298.15	301.84 (3.76)	-2847.91 (1.54)	-48.70 (0.76)	8.88 (0.16)
	b) 278.15	282.04 (4.13)	-3020.74 (1.39)	-50.38 (0.79)	-8.89 (0.15)
	c) 253.15	248.53 (2.87)	-3198.93 (0.66)	-50.24 (0.63)	-9.20 (0.16)
	d) 233.15	236.89 (2.96)	-3344.53 (0.73)	-51.90 (0.72)	-9.25 (0.14)

Table 4. Distributions of the dihedral angles β (H-O-C-C-) and α (-O-C-C-O-) for both EG-water (system A) and EG-Xe (system B). X^{trans} , $X^{eclipsed}$ and X^{gauche} ($X^{trans} + X^{eclipsed} + X^{gauche} = 100(\%)$) are the populational ratios of *trans*, *eclipsed*$^{(\pm)}$ and *gauche*$^{(\pm)}$ conformations of EG molecules. The unit is percent (%).

	β (H-O-C-C-)			α (-O-C-C-O-)		
EG-water	X_β^{trans}	$X_\beta^{eclipsed}$	X_β^{gauche}	X_α^{trans}	$X_\alpha^{eclipsed}$	X_α^{gauche}
a	6.24	52.58	41.18	2.09	0.86	97.05
b	4.55	58.33	37.12	3.52	0.87	95.61
c	3.97	59.80	36.23	8.19	0.58	91.23
d	3.97	56.13	39.90	7.09	0.31	92.60
EG-Xe	X_β^{trans}	$X_\beta^{eclipsed}$	X_β^{gauche}	X_α^{trans}	$X_\alpha^{eclipsed}$	X_α^{gauche}
a	7.37	43.39	49.24	0.44	0.63	98.93
b	11.10	41.60	47.30	0.00	0.24	99.76
c	9.91	44.24	45.85	0.00	0.16	99.84
d	8.54	47.37	44.09	0.00	0.42	99.58

temperature dependence is not as distinct. A comparison of the Xe solvent environment (system B) with the aqueous media (system A) shows that there is a very small population of the *trans* conformation (X_α^{trans}) in the Xe solution. The predominant peak in the intramolecular O-O distance for gaseous EG, which has been observed using electron diffraction studies (Bastiansen, 1949), corresponds to the *gauche* form with no indication of the O-O distance of the *trans* conformation. Our results for EG in Xe solvent show the same tendency as experimental results in the gaseous state (Buckley and Giguère, 1967). However, there is also a small population of the *trans* conformation in the aqueous solution, due partly to hydrogen bonding with water. These results agree qualitatively with those from recent computer studies (Nagy *et al.*, 1991; Hooft *et al.*, 1992).

In both systems, we observe that the difference in intramolecular structure is not very large at the different temperatures and densities studied. Therefore, the typical cases at (a) 298.15K and (d) 233.15K are shown here.

When both of the two dihedral angles, α and β, are of the *gauche* type, the remaining angle β has a preference for the *trans* or *eclipsed* conformation rather than *gauche* or *cis* , (when the angle for the *cis* conformation is exactly 180°). In order to examine the correlations between the dihedral angles of EG in solution, we choose ten configurations generated from MD simulations, each of which is separated by 2 ps. Marks are plotted in the figure for the pairs of dihedral angles (β_1, β_2) of each EG molecule. The procedure is repeated for ten configurations and we obtain Figures 2a and 2b for the aqueous solution (system A) and the Xe solution (system B), respectively. In addition, the contour map of the torsional potential energy hypersurface for angle α fixed to the *gauche* conformation is superimposed in Figures 2. The positions of the dots from the simulation coincide essentially with

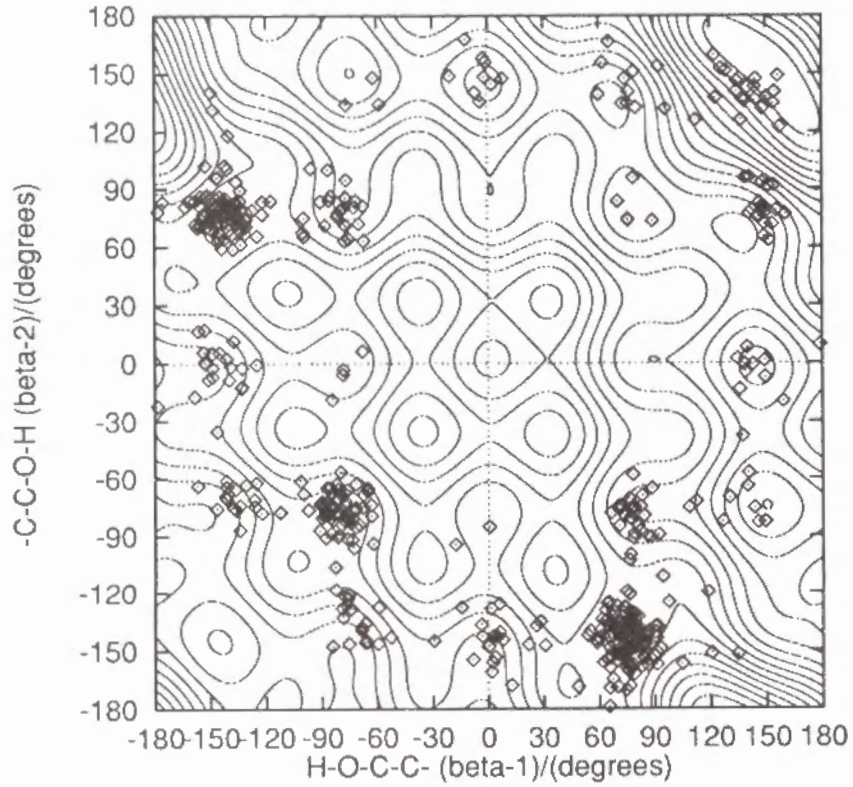

Figure 2a. Probability distribution for the correlation between the two two H-O-C-C- angles (β_1, β_2) of EG in aqueous solution with an initial temperature of 298.15K. In addition, the contour map of intramolecular potential energy (per 5kJ/mol) when -O-C-C-O- dihedral angle is gauche conformation is superimposed. The x-g^--y conformation is transformed to the x^--g-y^-. The contour map of the torsional potential energy hypersurface for angle α fixed to the *gauche* conformation is superimposed.

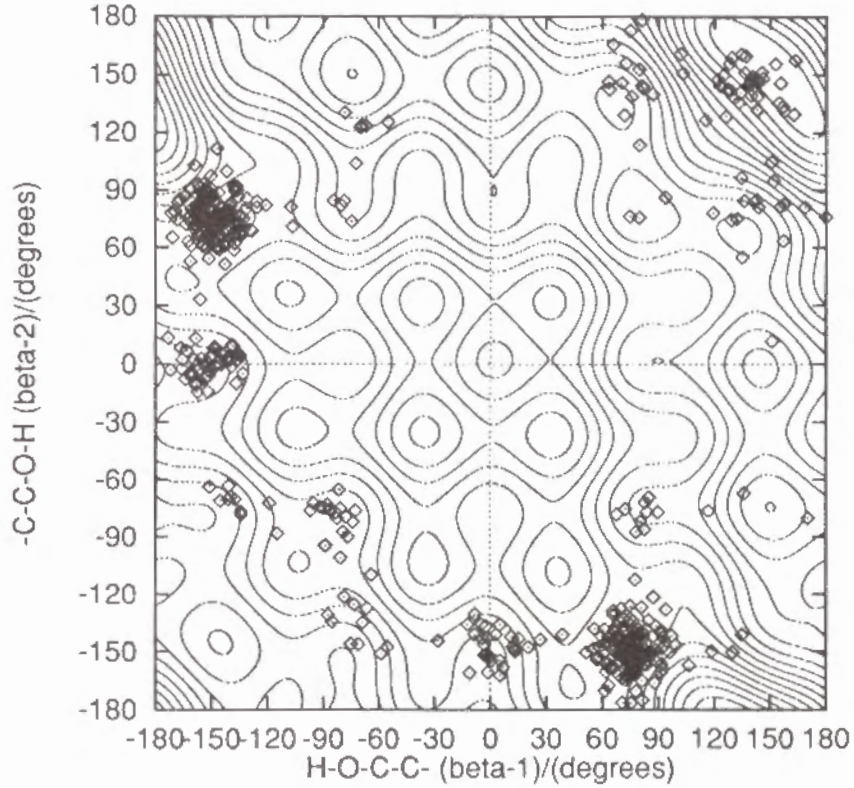

Figure 2b. Probability distribution for the correlation between the two two H-O-C-C- angles (β_1, β_2) of EG in Xe solution with an initial temperature of 298.15K. In addition, the contour map of intramolecular potential energy (per 5kJ/mol) when -O-C-C-O- dihedral angle is gauche conformation is superimposed. The x-g^--y conformation is transformed to the x^--g-y^-. The contour map of the torsional potential energy hypersurface for angle α fixed to the *gauche* conformation is superimposed.

the minima of the potential surface map. As seen from these figures, the most dominant conformation in both systems is $e^{\pm}$-$g^{\pm}$-$g^{\mp}$which provides direct evidence for the formation of intramolecular hydrogen bonds in EG. In contrast to system A (EG-water), there is a small population of the *trans* conformation (X_{α}^{trans}) in the Xe solution. This means that the EG molecule in the Xe solvent has a tendency to become 'folded' or more compact than in water. This compact form of EG indicates that there exists an internal hydrogen bond, because here the EG molecules cannot form any hydrogen bonds with the solvent.

Radial Distribution Functions

Since the calculated temperatures in both systems are only slightly different, the difference in the radial distribution functions (RDF) due to the temperature difference is expected to be small. When they are compared, no correction is made to the RDFs.

The water-water RDFs for system A and pure water at the same temperature as system A are shown in Figures 3. A comparison with pure TIP4P water (Jorgensen *et al.*, 1983) at almost the same temperature, as calculated from a 40 ps simulation, reveals no difference in the RDFs. The peak and minimum positions do not change with temperature. However, the peaks of all RDFs for system A are enhanced. This upward shift, indicating large concentration fluctuations in water, was also seen in methanol-water mixtures (Tanaka and Gubbins, 1992). The centers-of-mass of EG molecules (EG(G)-EG(G)) for the aqueous solution (system A) and the Xe solution (system B) are shown in Figure 4. As far as the first peak is concerned, the EG-EG RDF in system B (Xe solvent) is higher than that in system A. Its first maximum appears at 4.9~5.0 Å, which reveals a closer contact of the EG molecules in Xe than in aqueous solution. The first peak height is greater than 4.0. This is in sharp contrast to the case of the aqueous

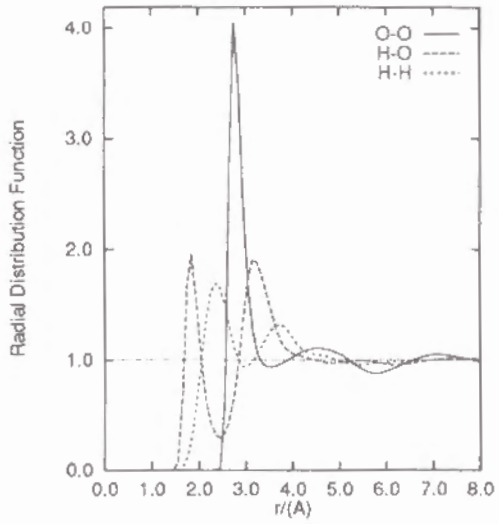

Figure 3a. Water-water RDFs in an aqueous solution of EG (system A) at (a) 298.15K

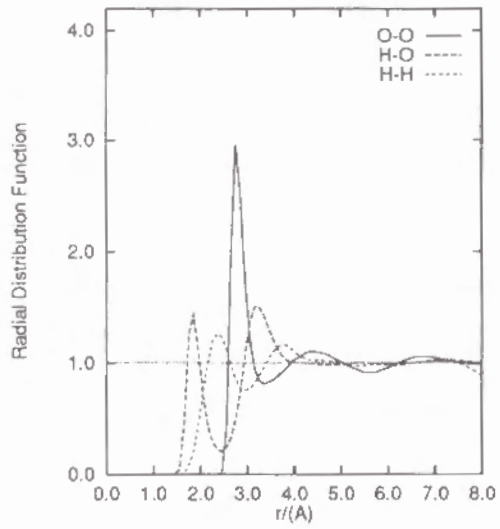

Figure 3b. Water-water RDFs in pure water at (a) 298.15K

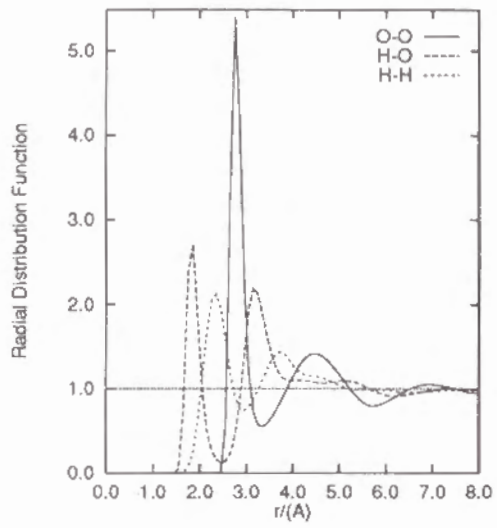

Figure 3c. Water-water RDFs in an aqueous solution of EG (system A) at (d) 233.15K

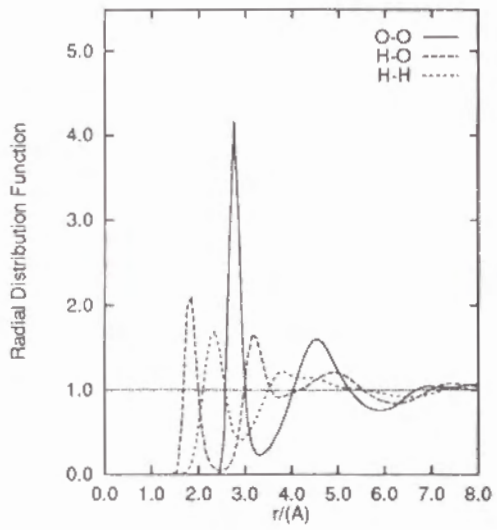

Figure 3d. Water-water RDFs in pure water at (d) 233.15K

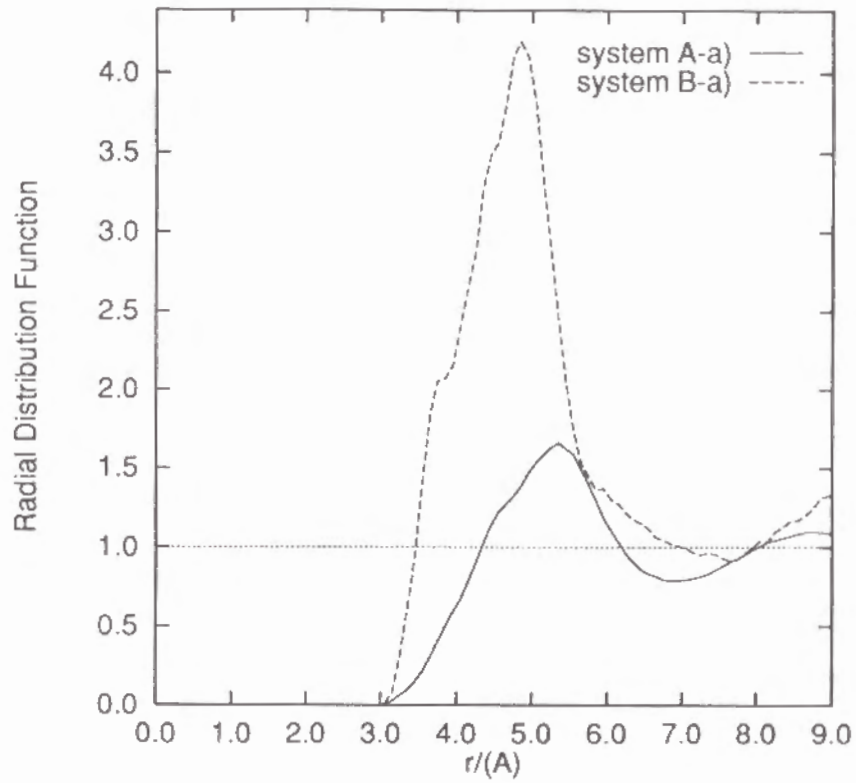

Figure 4. The centers of mass for EG radial distribution functions in an aqueous solution of EG (system A) and in an Xe solution of EG (system B) at (a) 298.15K

solution. Therefore, it is expected that there exist many EG-dimers in the Xe solution (system B). EG molecules possess a high degree of self-association; however, it is not easy to say whether there are EG trimers or highly associated EG species in the Xe solution. The reason for this is that it is difficult to determine the size distribution of the cluster of EG molecules owing to the small size of the simulation cell. This distribution has not been evaluated.

Intramolecular Hydrogen Bonds

An EG molecule has the ability to form hydrogen bonds with water and with other EG molecules. In addition, there exists an intramolecular hydrogen bonding interaction with other EG molecules. Previous investigations (Podo *et al.*, 1974) have suggested that the *gauche* conformation with intramolecular hydrogen bonding is very important. Since each EG molecule has two HO groups, can be expected to form single or double intramolecular hydrogen bonds. An EG molecule doubly connected by intramolecular hydrogen bonds should have either the $g^{\pm}$-$g^{\mp}$-$g^{\pm}$ or $e^{\pm}$-$e^{\mp}$-$e^{\pm}$ conformation. These conformations have a pair of anti-parallel vectors for each HO group. This is indeed observed in IR measurements (Krueger and Mettee, 1965). The formation of a single intramolecular hydrogen bond requires that the two vectors of the HO group of an EG molecule have the same direction, *i.e* an $e^{\pm}$-$g^{\pm}$-$g^{\mp}$ or t-$g^{\pm}$-$g^{\mp}$ conformation. The direction is determined by the inner products of these two HO vectors. The intramolecular interaction energies, which are the sums of the contributions from the H-H, H-O, O-H and O-O pairs excluding the normal torsional potential terms, fall into two groups depended on those directions. These contributions calculated from MD simulations are shown in Figures 5a and 5b.

The hydrogen-bond energy is assumed to be –10 kJ/mol for both types of intramolecular hydrogen bond. In the case of two simultaneous

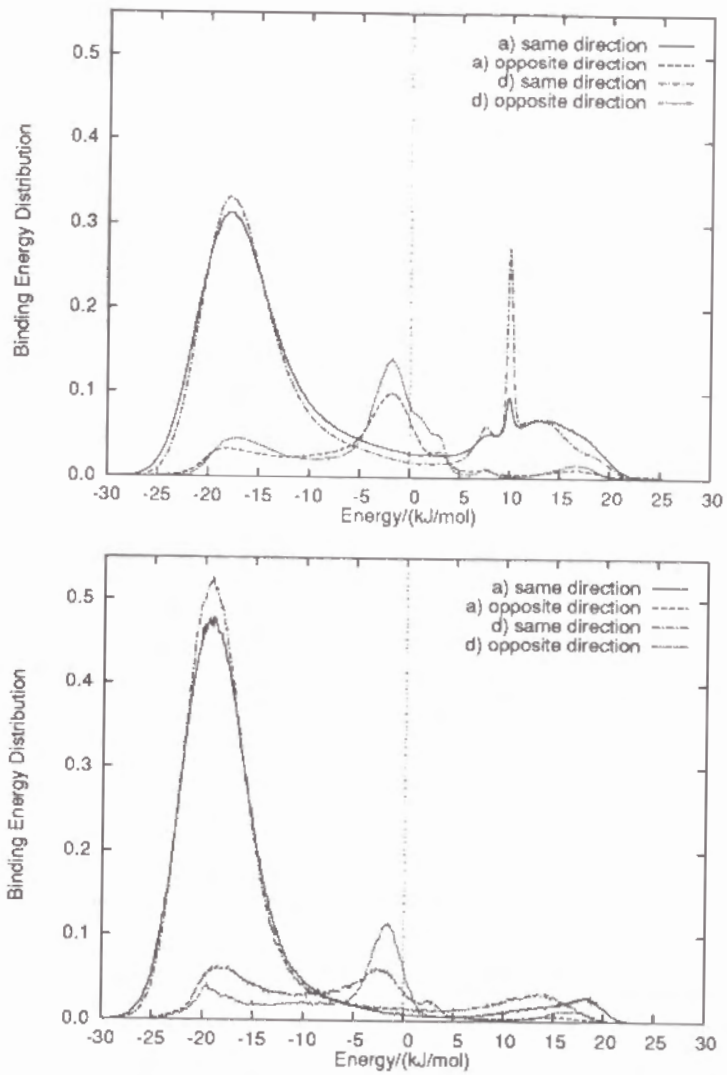

Figure 5. Distributions of individual EG potential energy in aqueous solution (**5a**) TOP) and Xe solution (**5b**) BOTTOM) for HO- vectors with the same and opposite directions.
The system has 54 EG molecules; (a) T=298.15K and (d) 233.15K; energies are in kJ/mol.

hydrogen bonds, the bond angles of the EG molecule are twisted and far from the most favorable angles so that the intramolecular interaction energy is of the same order of magnitude as for the single hydrogen bonds.

The average populations of single and double intermolecular hydrogen bonds, the average lifetime of the hydrogen bonds and the average numbers of intramolecular hydrogen bonds occurring during 1 ps are given in Table 5. The lifetime of a hydrogen bond is defined as the duration of its existence until breakage. The $s(HB)$ and $d(HB)$ are the fraction of the EG population which have single and double intramolecular hydrogen bonds, respectively.

As seen in Figures 5a and 5b (when two vectors of an HO group have the same direction), there are two peaks: a broad peak around –18 kJ/mol and a sharp peak around +10 kJ/mol. The former indicates a single intramolecular hydrogen bond. It is found from a comparison of systems A (aqueous) and B (solvent Xe) that the latter peak is due to the *trans* conformation of the dihedral angle α (-O-C-C-O-). This is because there is indeed only a small population of the *trans* conformation (X_α^{trans}) in the Xe solvent (system B). As seen in these figures, the small broad peak around –18 kJ/mol is assigned to the formation of double intramolecular hydrogen bonds. There is a small population of doubly intramolecular hydrogen-bonded EG molecules, which compares *ca.* 4$\sim$ 9 % of the EG molecules in the both systems.

The existence of intramolecular hydrogen-bonding interactions does not necessarily imply the presence of constraints on the HO groups in each EG molecule. The time autocorrelation functions of H-O- and -O-C- bond vectors in EG for both systems A and B exhibit nearly exponential decay. The relaxation times (τ_{HO} and τ_{OC}) of these vectors are given in Table 6. The values for system B (solvent Xe) show much shorter relaxation times than those for system A (aqueous solution).

Table 5. Results for intramolecular hydrogen bonds in systems, A and B (EG:solution = 54:162); average population of single and double intramolecular hydrogen bonds in EG, average lifetime, and average number of intramolecular hydrogen bonds formed during 1 picoseconds.

A) EG-water	$s(HB)$	$d(HB)$	Lifetime	Num (per 1ps)
a	52.06	5.62	0.12	211.90
b	44.65	5.19	0.13	207.13
c	40.16	6.14	0.13	160.58
d	50.53	6.50	0.16	156.90
B) EG-Xe	$s(HB)$	$d(HB)$	Lifetime	Num (per 1ps)
a	71.17	9.33	0.32	125.33
b	76.27	4.67	0.37	110.73
c	75.92	5.17	0.36	106.20
d	72.20	5.10	0.35	116.55

Table 6. Relaxation time of the HO vector (τ_{HO}) and the OC vector (τ_{OC}) of EG in EG-water (system A) and EG-Xe (system B). The unit is picoseconds.

	Relaxation Time			
	System A		System B	
	τ_{HO}	τ_{OC}	τ_{HO}	τ_{OC}
a	15.90	15.85	13.82	11.48
b	20.36	21.19	15.82	11.22
c	29.19	31.76	18.29	13.52
d	30.87	30.31	21.61	16.62

We define the time-dependent autocorrelation function of intramolecular hydrogen bonds (Rapaport, 1983) as

$$C(t) = \langle \sum_i s_i(t+t_0) \cdot s_i(t_0) \rangle / \langle \sum_i s_i^2(t_0) \rangle \qquad (3)$$

where the value of $s_i(t)$ is unity if an intramolecular hydrogen bond exists for the ith EG molecule and is zero if the bond is absent at time t. Since the $C(t)$s show nearly exponential decay, the relaxation time constants, τ_{hb}, which represent the longer term rearrangements of intramolecular hydrogen bonds are obtained by the same method as the rotational relaxation time constants and are listed in Table 7.

This relaxation time is different from the hydrogen-bond lifetime discussed above; a hydrogen bond which is once broken and later reforms contributes to the correlation function, $C(t)$ (enq (3)). Clearly, the existence of a coulomb interaction between EG and solvent molecules causes a shift in hydrogen-bond lifetime. The autocorrelation functions in system B (solvent Xe) show longer correlation times than those in system A (aqueous solution). This means that an EG molecule in aqueous solution is associated strongly both with water and with other EGs by intermolecular hydrogen bonds.

The dynamics of intramolecular hydrogen bonding over a short time range (0.1ps) can be seen in Figures 6a and 6b. Both figures illustrate two probability distributions, the lifetime distribution and the interval time distribution of intramolecular hydrogen-bonded EG. The lifetime of a hydrogen bond is defined as the continuous time until the first breakage of that hydrogen bond, while the interval time of a hydrogen bond is the time until the first formation of hydrogen bond. In other words, these probability densities show how long an intramolecular hydrogen bond remained in continuous existence. In terms of queueing theory (e.g., Saaty, 1961), the short time range of the interval-time distributions in both system A and B is almost the same as 2-Erlang's distribution, which is the same as the gamma function.

Table 7. Relaxation time constant (τ_{hb}) of the autocorrelation function for intramolecular hydrogen bonds $C(t)$ in EG-water (system A) and EG-Xe (system B). The unit is picoseconds.

	Relaxation Time	
	System A	System B
a	2.80	7.10
b	3.00	13.32
c	3.62	9.10
d	4.52	10.19

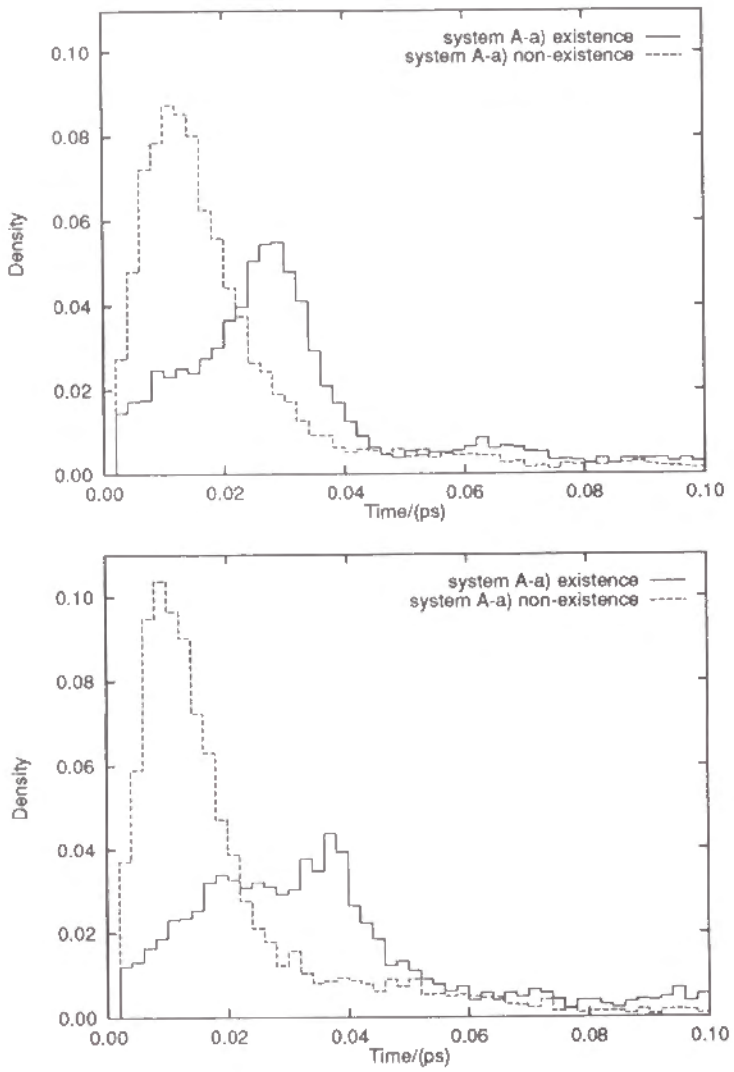

Figure 6. Time distribution of intramolecular hydrogen bonds in EG for the existence of hydrogen bonds (on: solid line); for the non-existence of hydrogen bonds (off: dashed line). The system has 54 EG molecules and 162 water molecules; T=298.15K. **6a)** TOP: system A-a (in aqueous solution), **6b)** BOTTOM: system B-a (in Xe solution).

This means that formation of hydrogen bonds over a short time period occurs nearly at random.

The averaged lifetime is *ca.* 0.13 ps in aqueous solution (system A) and > 0.3 ps in Xe solution (system B). Comparison of the aqueous solution with the Xe solution, in spite of the different lifetimes, indicates that there is only a small difference in these distributions. That is, the short-time behaviors of the intramolecular hydrogen bonds is almost the same in each system. In the lifetime distributions, the peak positions for the Xe solution shift to slightly longer times than those for the aqueous solution. This is due partly to the slow rotational relaxation of HO groups in Xe solution. The interval-time distributions are almost the same in both systems.

Intermolecular Hydrogen Bonds

Hydrogen bonds between EG and water molecules are formed in competition with intramolecular hydrogen bonds within EG molecules. In order to understand how the internal degrees of freedom affect various properties, different EG models, which are all rigid rotors, are also examined under the same conditions as system A. We adopted five rigid-EG models: the *c*-*c*-*c*, *t*-$g^{\pm}$-$g^{\mp}$, $e^{\pm}$-$g^{\pm}$-$g^{\mp}$, *t*-$g^{\pm}$-*t* and *t*-*t*-*t* conformations. The *t*-$g^{\pm}$-$g^{\mp}$ and $e^{\pm}$-$g^{\pm}$-$g^{\mp}$ conformations may be important components in the conformational equilibria of EG since an intramolecular hydrogen bond is expected to be formed in both conformations. From our results, the $e^{\pm}$-$g^{\pm}$-$g^{\mp}$ conformation corresponds to the dominant conformation of flexible EG in both water and Xe solvents. The parameters of intermolecular interaction for these rigid models are the same as those used in our flexible-EG model.

The distributions of the potential energy of individual EG molecules are shown in Figure 7 for an initial temperature of (a) 298.15K. The average values and standard deviations of the potential energies of indi-

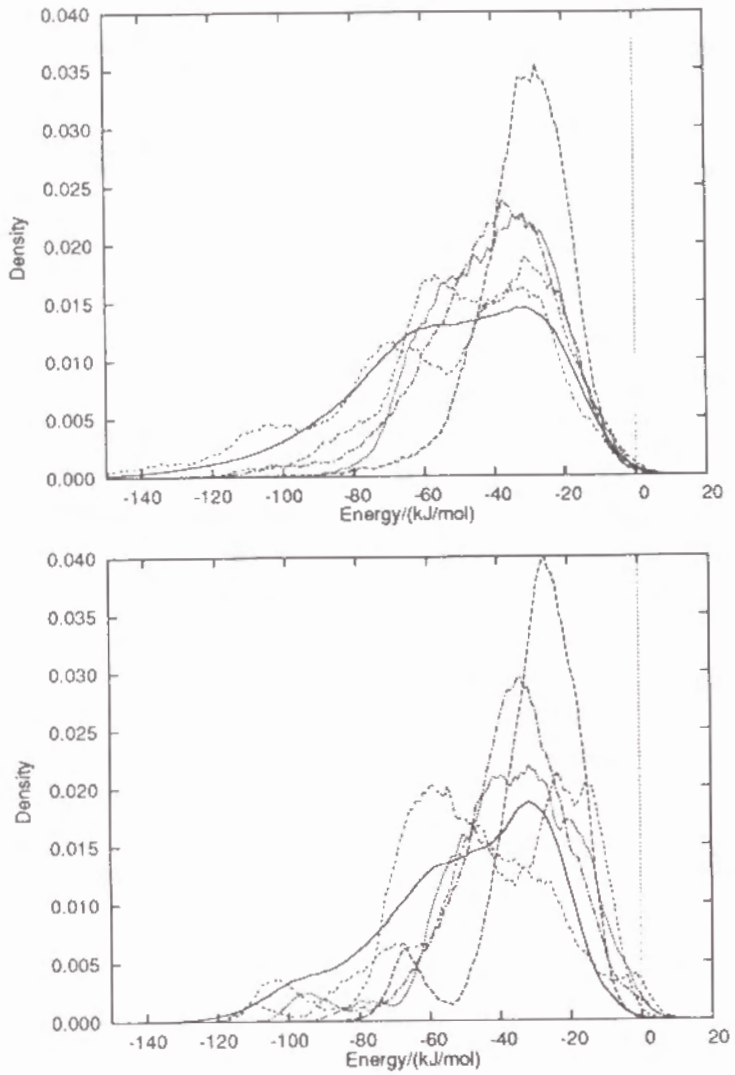

Figure 7. Distribution of the binding energies of EG in an aqueous solution for the following models: flexible (solid line), *c*-*c*-*c* (ccc; dashed line), $e^{\pm}$-$g^{\pm}$-$g^{\mp}$ (egg'; dash-dotted line), *t*-$g^{\pm}$-$g^{\mp}$ (tgg'; dotted line), *t*-$g^{\pm}$-*t* (tgt; double-dashed line), *t*-*t*-*t* (ttt; triple-dashed line). The system has 54 EG molecules and 162 water molecules; **7a)** TOP: T=298.15K (system A-a), **7b)** BOTTOM: T=233.15K (system A-d).

vidual EG and water molecules are listed in Table 8. From these results of the potential energy for water molecules, the pair interaction energy distributions for water-water and the water-water RDF (not shown), we see that there is no significant difference between the structures of water in the flexible model and in the five rigid models.

The pair interaction energy distributions for EG-water in each system are illustrated in Figure 8. In both flexible and rigid models, we observe a similar tendency at different temperatures and densities, so only the results from an initial temperature of (a) 298.15K. In the case of *c*-*c*-*c* model, there is a small peak around –60 kJ/mol, which is quite different from any other model. As seen in this figure, the results for the flexible model are rather similar to those for the rigid $e^{\pm}$-$g^{\pm}$-$g^{\mp}$ or *t*-$g^{\pm}$-$g^{\mp}$ models.

Integration of these curves up to the threshold value gives the estimated number of EG hydrogen bonds. The threshold value for the hydrogen-bond energy is assumed to be either –12 or –14 kJ/mol. The average numbers of intermolecular hydrogen bonds between EG and water molecules for each model are given in Table 9. These values increase in the order *c*-*c*-*c*, flexible, $e^{\pm}$-$g^{\pm}$-$g^{\mp}$, *t*-$g^{\pm}$-$g^{\mp}$and *t*-*t*-*t*. As seen from the energy contour map and also from our results for the dihedral angle distributions, the *c*-*c*-*c* conformation is hardly observed. The average number for the flexible model is smaller than for any other reasonable rigid model. This is, of course, caused by the presence of intramolecular hydrogen bonds.

The diffusion coefficient (D) and rotational relaxation time (τ_s) of water molecules for all models are calculated from the results of MD simulations and are listed in Table 10. These show that at 298.15K (a) and 278.15K (b) the diffusion coefficients of water molecules for the flexible EG model are larger than those for the rigid EG models. In contrast, at 253.15K (c) and 233.15K (d), the diffusion coefficients for

Table 8. Average potential energies of EG and water molecules for both the flexible-EG model and rigid EG models in EG-water (system A); standard deviations of the potential energy of individual molecules are given in parentheses. Energies are given in kJ/mol.

		EG				
	Flexible	*c-c-c*	$e^{\pm}$-$g^{\pm}$-$g^{\mp}$	*t*-$g^{\pm}$-$g^{\mp}$	*t*-$g^{\pm}$-*t*	*t-t-t*
a	–52.52	–31.41	–41.18	–39.67	–56.26	–44.80
	(27.17)	(13.05)	(19.06)	(16.68)	(30.25)	(21.60)
b	–52.51	–30.89	–37.96	–34.71	–58.28	–45.84
	(26.91)	(12.96)	(20.53)	(17.86)	(29.16)	(22.24)
c	–57.63	–32.59	–34.69	–37.47	–57.26	–42.65
	(33.10)	(15.81)	(16.45)	(20.31)	(29.90)	(19.24)
d	–49.73	–30.22	–35.78	–37.10	–49.27	–38.60
	(23.90)	(13.69)	(15.39)	(19.52)	(23.03)	(23.24)
		Water				
	Flexible	*c-c-c*	$e^{\pm}$-$g^{\pm}$-$g^{\mp}$	*t*-$g^{\pm}$-$g^{\mp}$	*t*-$g^{\pm}$-*t*	*t-t-t*
a	–54.77	–53.24	–54.08	–53.38	–50.17	–50.03
	(20.23)	(19.90)	(19.04)	(18.51)	(19.58)	(18.45)
b	–57.05	–55.20	–54.70	–54.09	–52.00	–52.08
	(20.36)	(19.87)	(18.56)	(17.67)	(18.83)	(18.53)
c	–60.69	–56.04	–55.31	–56.90	–54.70	–53.97
	(20.36)	(18.27)	(18.52)	(18.62)	(18.18)	(16.98)
d	–61.55	–58.08	–56.87	–57.60	–54.92	–53.60
	(20.31)	(18.54)	(17.48)	(18.37)	(18.92)	(17.26)

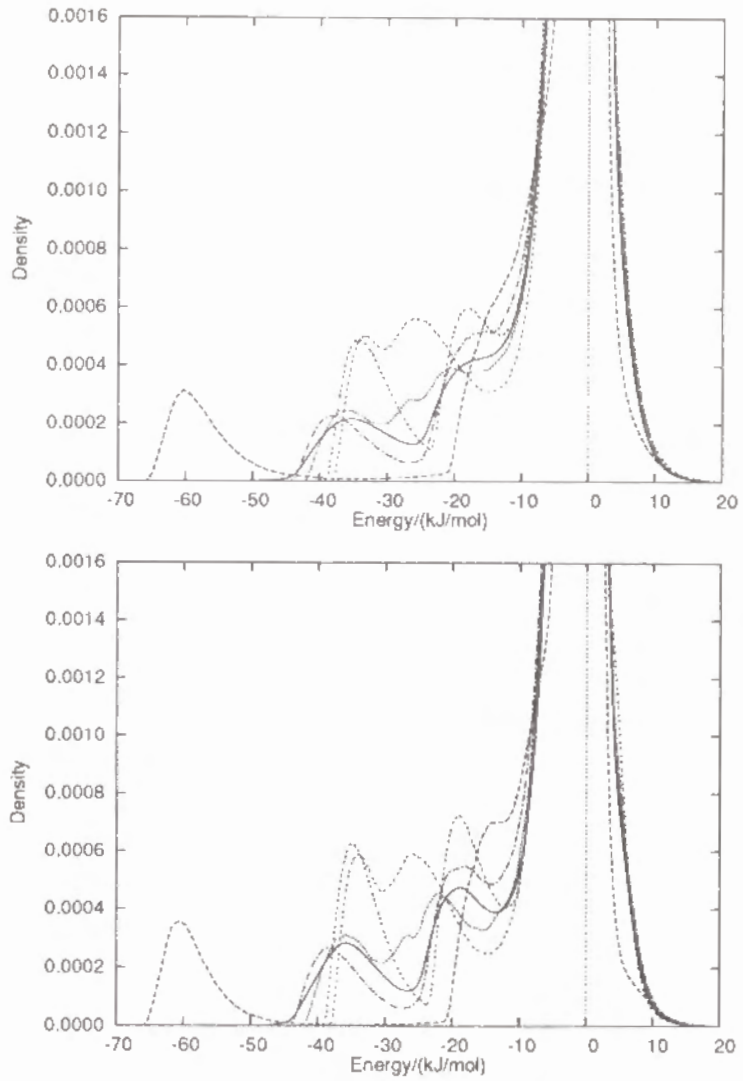

Figure 8. Distribution of the pair interaction potential energies between EG and water in an aqueous solution for the following models: flexible (solid line), *c-c-c* (**ccc**; dashed line), $e^{\pm}$-$g^{\pm}$-$g^{\mp}$ (**egg'**; dash-dotted line), *t*-$g^{\pm}$-$g^{\mp}$ (**tgg'**; dotted line), *t*-$g^{\pm}$-*t* (**tgt**; double-dashed line), *t-t-t* (**ttt**; triple-dashed line). The system has 54 EG molecules and 162 water molecules; **8a)** TOP: T=298.15K (system A-a), **8b)** BOTTOM: T=233.15K (system A-d).

Table 9. Average number of intermolecular hydrogen bonds between EG and water molecules for both the flexible model and rigid models in system A. The hydrogen-bonding energy is assumed to be -12 or -14 kJ/mol.

	-12.0kJ/mol					
	Flexible	*c-c-c*	$e^{\pm}$-$g^{\pm}$-$g^{\mp}$	*t*-$g^{\pm}$-$g^{\mp}$	*t*-$g^{\pm}$-*t*	*t-t-t*
a	2.51	2.33	2.56	2.75	3.54	3.28
b	2.67	2.38	2.73	2.95	3.44	3.36
c	2.72	2.44	2.91	3.03	3.47	3.33
d	2.77	2.44	2.81	2.94	3.59	3.57
	-14.0kJ/mol					
	Flexible	*c-c-c*	$e^{\pm}$-$g^{\pm}$-$g^{\mp}$	*t*-$g^{\pm}$-$g^{\mp}$	*t*-$g^{\pm}$-*t*	*t-t-t*
a	2.21	1.89	2.20	2.47	3.33	2.94
b	2.38	1.94	2.39	2.66	3.22	3.04
c	2.45	1.98	2.55	2.75	3.27	3.03
d	2.52	1.99	2.48	2.69	3.41	3.30

Table 10. Diffusion coefficient (D) and rotational relaxation time (τ_s) of water molecules for the flexible model and rigid-EG models in system A. The unit for D is $\times$ 10^9 m^2/s and for τ_s is picoseconds.

	Diffusion Coefficient					
	Flexible	*c-c-c*	$e^{\pm}$-$g^{\pm}$-$g^{\mp}$	*t*-$g^{\pm}$-$g^{\mp}$	*t*-$g^{\pm}$-*t*	*t-t-t*
a	1.50	1.46	0.99	0.97	0.56	0.66
b	0.84	0.67	0.60	0.37	0.36	0.36
c	0.20	0.48	0.30	0.42	0.09	0.15
d	0.15	0.31	0.27	0.14	0.02	0.14
	Rotational Relaxation Time					
	Flexible	*c-c-c*	$e^{\pm}$-$g^{\pm}$-$g^{\mp}$	*t*-$g^{\pm}$-$g^{\mp}$	*t*-$g^{\pm}$-*t*	*t-t-t*
a	3.65	3.80	4.19	4.44	5.08	4.58
b	5.09	5.83	5.43	6.24	6.43	6.10
c	8.76	6.55	7.62	7.12	8.96	7.92
d	9.96	8.27	8.21	9.11	11.02	10.25

the flexible model are smaller than those of the *c*-*c*-*c*, $e^{\pm}$-$g^{\pm}$-$g^{\mp}$ and *t*-$g^{\pm}$-$g^{\mp}$ models and are roughly the same as that for the *t*-*t*-*t* model. The results of the rotational relaxation time show the same tendency. This is caused mainly by coupling of water motions with the internal degrees of freedom of a flexible EG molecule. The higher the temperature, the more frequently the rotation of the dihedral angle in the EG molecules takes place. When a water molecule is adjacent to an HO group of EG, the associated dihedral angle is able to rotate to make a transition to a new topography of the intermolecular potential energy hypersurface for EG-water. As a result, the internal degrees of freedom of the water molecules are affected slightly by the flexible EG molecules. On the other hand, at lower temperatures the dihedral angle of an EG molecule can not rotate easily, so that the values of the diffusion constant and the rotational relaxation time are close to those for the $e^{\pm}$-$g^{\pm}$-$g^{\mp}$ and *t*-$g^{\pm}$-$g^{\mp}$ models.

CONCLUSIONS

Conformational equilibria for EG have been calculated from MD simulations. In the case of a non-polar flexible molecule, such as butane, the *gauche* conformation with respect to angle α in the liquid phase is more stabilized than that in the gas phase. This is explained in terms of a simple packing effect in the condensed phase. EG molecules strongly favour the folded form in the gaseous state, caused by intramolecular interactions, especially intramolecular hydrogen bonds. It must be expected that the presence of hydrogen bonds with solvent water alters these equilibria. A comparison of the aqueous solution of EG with the Xe solution and the gaseous state of EG shows that there is a preference for the *trans* form with respect to angle α in the aqueous solution in spite of the occurrence of intramolecular hydrogen bonds. The intermolecular hydrogen bonds with water molecules give rise to a small

shift in the equilibrium of the dihedral angle α toward the *trans* conformation in contrast to the case for non-polar flexible molecules. In an EG molecule, a single intramolecular hydrogen bond or a doubly connected cyclic intramolecular hydrogen bond is expected to exist.

The average population of EG molecules with double intramolecular hydrogen bonds in aqueous solution is almost the same as that in Xe solution, in contrast to the population of single intramolecular hydrogen bonds. The average lifetime of intramolecular hydrogen bonds of EG in Xe solution is twice as long as that in an aqueous solution. However, no large difference is seen in the short time behavior of the intramolecular hydrogen bonds.

Some rigid-EG models are also examined. From a comparison of a flexible EG model with rigid-EG models, the internal degrees of freedom of an EG molecule are seen to have an obvious effect on the intermolecular hydrogen bonds. The translational and rotational degrees of freedom of water molecules with the flexible EG model are somewhat less restricted than for the rigid-EG models. Owing to the internal degrees of freedom of EG, when an EG molecule in water forms a strong interaction with another molecule, its hydrogen bonds can easily switch to another water molecule, to other EGs or to itself in order to achieve a more stable state. The internal degrees of freedom, therefore, have a minor effect on the solvent.

GENERAL CONCLUSIONS

This chapter summarizes molecular dynamics studies on torsional motions of flexible molecules in condensed phase. We performed the molecular level simulations of dense chain molecules under a variety of applied conditions; adopted n-butane as the simplest flexible molecule among n-alkanes and ethylene glycol (1,2-ethanediol, EG) as the simplest polyol molecule for constraint Molecular Dynamics (constraint MD) simulations. Conformational equilibria and torsional motions of these molecules were investigated.

In chapter I, the scheme of constraint MD algorithm used in the present study was given with the equations of motion. Some improvements for efficient computations were achieved in the coding of these iterative procedures.

In chapter II, conformational equilibria for n-butane, which are found to depend on the models used and the conditions of simulation, have been investigated by MD simulations. The intermolecular interactions cause the shift of the equilibrium toward the *gauche* form. This is explained in terms of a simple packing effect in condensed phase. This shift of the *trans* conformational population is not large (i.e., 3~5%).

From the result of RDF's, the structure of liquid n-butane can be to great extent represented only by the repulsion part of the potential (RLJ model). However, comparing the dihedral angle distribution of the RLJ model with that of the LJ model, the shift toward an increase in the *gauche* form is more enhanced in the system of molecules interacting via the repulsive interaction than the LJ interaction. Therefore, the whole liquid structure including the dihedral distribution is sensitive to the attractive part of the intermolecular interaction as well as

the repulsive part.

Torsional motions for individual n-butane molecule have been analyzed by MD simulations in chapter III. Detailed examination of the various cases of intramolecular rearrangement using simple model reveals the coupling between intra- and inter-molecular interactions. In the liquid state, the profile of the total intramolecular potential energy of n-butane is altered by the solvent-induced contribution. In one case of intramolecular rearrangement, the intermolecular interaction from the surrounding solvents makes the solute molecule to be less stable conformation, and lowers the height of potential barrier. This leads to a facile rearrangement.

From the results of non-dihedral potential model, in which no dihedral potential is included, the *cis* conformation in the liquid state is more stabilized than the *gauche* conformation, and is much more stabilized than the *trans* one. This is caused by the solvent induced contribution. Therefore, the chain molecule has a tendency to become 'fold' or small in size in the liquid state.

Chapter IV was devoted to MD calculations for aqueous solution of EG. Conformational equilibria for EG have been calculated from MD simulations. In the case of non-polar flexible molecule, such as n-butane molecule, a more compact form in the liquid state is more stabilized than that in the gas phase. EG molecules favor more strongly the folding form in gaseous state by an intramolecular hydrogen bond. As is expected, the presence of intermolecular hydrogen bond alters the conformational equilibria significantly. The intramolecular hydrogen bonds are fairly dependent on solvent species which have some HO groups. From a comparison of aqueous solution of EG with a solution with solvent Xe, there is a preference for the *trans* form in the aqueous solution in spite of the occurrence of intramolecular hydrogen bond.

The intermolecular hydrogen bonds with water molecules lead to the small shift of the equilibrium of the dihedral angle α (-O-C-C-O-) toward the *trans* form in contrast to the non-polar flexible molecules. The average population of EG with double intramolecular hydrogen bonds in aqueous solution is almost the same as that in Xe solution, in contrast to that of single intramolecular hydrogen bonds. The averaged lifetime of intramolecular hydrogen bonds of the EG in the Xe solution is twice as long as that in an aqueous solution. However, no large difference is seen in the short time behavior of intramolecular hydrogen bonds.

The influence of flexibility on liquid properties have been studied. Comparing a flexible EG model with rigid-EG models, it is found that the EG molecule is able to change its hydrogen bond partner which is either water or EG molecule. Therefore, internal rotation of an EG molecule affects the solvent 'softly' through the intermolecular hydrogen bonds.

The coupling of intermolecular interactions with intramolecular interactions undoubtedly gives rise to some interesting static dynamical properties in the flexible chain molecules. The flexibility changes the solvent structures even for a non-polar molecule. Dynamic properties and torsional motions are sensitive to the intramolecular potential functions.

REFERENCES

Abraham, R.J. and Bretschneider, E. (1974). *In Internal Rotation in Molecules* (edited by Orville-Thomas, W.J.) Wiley-Interscience, New York.

Allen, M.P. and Tildesley, D.J. (1987). *Computer simulation of liquids* Oxford Univ. Press, New York.

Almarza, N.G., Enciso, E., Alonso, J., Bermejo, F.J. and Alvarez, M. (1990). Monte Carlo simulations of liquid n-butane. *Mol.Phys.* **70**, pp 485-504.

Andersen, H.C. (1983). Rattle : A "Velocity" version of Shake algorithm for Molecular Dynamics calculations. *J.Comput.Phys.* **52**, pp 24-34.

Bastiansen, O. (1949). *Acta Chem.Scand.* **3**, p 415.

Bowen, H. and Sutton, L. (1958). *Tables of Interatomic Distances and Configurations in Molecules and Ions.* The Chemical Society, London.

Brown, D. and Clarke, J.H.R. (1990). A direct method of studying reaction rates by equilibrium Molecular Dynamics: Application to the kinetics of isomerization in liquid n-butane. *J.Chem.Phys.* **92**, pp 3062-3073.

Buckley, P. and Giguère, P.A. (1967). Infrared studies on rotational isomerism. I. Ethylene glycol. *Can.J.Chem.* **45**, pp 397-407.

Chandler, D. and Pratt, L.R. (1976). Statistical mechanics of chemical equilibria and intramolecular structures of nonrigid molecules in condensed phases. *J.Chem.Phys.* **65**, pp 2925-2940.

Ciccotti, G and Ryckaert, J-P. (1986). Molecular Dynamics simulation of rigid molecules. *Compt.Phys.Rep.* **4**, pp 345-392.

Ciccotti, G., Ferrario, M and Ryckaert, J-P. (1982). Molecular dynamics of rigid systems in Cartesian coordinates. A general formulation. *Mol.Phys.* **47**, pp 1253-1264.

Douheret, G., Pal, A., Høiland, H., Anowi, O. and Davis, M.I. (1991). Thermodynamic properties of (ethan-1,2-diol + water) at the temperature 298.15K I. Molar volumes, isobaric molar heat capacities, ultrasonic speeds, and isentropic functions. *J.Chem.Thermodyn.* **23**, pp 569-580.

Edberg, R., Evans, D.J. and Morris, G.P. (1986). Constrained Molecular Dynamics: Simulations of liquid alkanes with a new algorithm. *J.Chem.Phys.* **84**, pp 6933-6939.

Edberg, R., Evans, D.J. and Morris, G.P. (1987). Conformational kinetics in liquid butane by nonequilibrium Molecular Dynamics. *J.Chem.Phys.* **87**, pp 5700-5708.

Elliott Jr, J.R. and Kanetkar, U.S. (1990). Theory and simulation of chain-molecule fluid structure. *Mol.Phys.* **71**, pp 871-882; Elliott Jr, J.R., Kanetkar, U.S. and Vasudevan, V.J. (1990). Attractive-force effects in chain molecular fluids. *ibid.* **71**, pp 883-895.

Enciso, E., Alonso, J., Almarza, N.G. and Bermejo, F.J. (1989). Statistical mechanics of small chain molecular liquids. I. Conformational properties of modeled n-butane. *J.Chem.Phys.* **90**, pp 413-421; Statistical mechanics of small chain molecular liquids. II. Structure and thermodynamic properties of modeled n-butane liquid. *ibid.* **90**, pp 422-430.

Evans, D.J. (1977). On the representation of orientation space. *Mol. Phys.* **34**, pp 317-325.

Evans, D.J. and Murad, S. (1977). Singularity free algorithm for Molecular Dynamics simulation of rigid polyatomics. *Mol.Phys.* **34**, pp 327-331.

Flory, P.J. (1969). *"Statistical Mechanics of Chain Molecules"*, Wiley-Interscience, New York.

Franks, F. (1982). *Water Vol.7* Plenum Press, New York.

Forsyth, M. and MacFarlane, D.R. (1990). A Study of Hydrogen Bonding in Concentrated Diol/Water Solutions by Proton NMR. Correlations with Glass Formation. *J.Phys.Chem.* **94**, pp 6889-6893.

Goldstein, H. (1980). *Classical mechanics (2nd edn)* Addison-Wesley, New-York.

Hansen, J.P. and McDonald, I.R. (1986). *Theory of simple liquids (2nd ed.)* Academic Press, New York.

Hooft, R.W.W., van Eijck, P. and Kroon, J. (1992). Use of molecular dynamics methods in conformational analysis. Glycol. A model study. *J.Chem.Phys.* **97**, pp 3639-3646.

Hsu, C.S., Pratt. L.R. and Chandler, D. (1978). Statistical mechanics of small chain molecules in liquids. II. Intermolecular pair correlations for n-butane. *J.Chem.Phys.* **68**, pp 4213-4217.

Huot, J-Y., Battistel, E., Lumry, R., Villeneuve, G., Lavalle, J.F., Anusiem, A. and Jolicoeur, C. (1988). A Comprehensive Thermodynamic Investigation of Water-Ethylene Glycol Mixtures at 5, 25, and 45 °C. *J.Solution.Chem.* **17**, pp 601-636.

Jorgensen, W.L., Binning, R.C.,Jr. and Bigot, B. (1981). Structures and properties of organic liquids: n-butane and 1,2-dichloroethane and their conformational equilibria. *J.Am.Chem.Soc.* **103**, pp 4393-4399.

Jorgensen, W.L. (1981). Pressure Dependence of the Structure and Properties of Liquid n-Butane. *J.Am.Chem.Soc.* **103**, pp 4721-4726.

Jorgensen,W.L. (1986). Optimized Intermolecular Potential Functions for Liquid Alcohols. *J.Phys.Chem.* **90**, pp 1276-1284.

Jorgensen, W., Chandrasekhar, J., Nadura, J.D., Impey, R.W. and Klein, M.L. (1983). Comparison of simple potential functions for simulating liquid water. *J.Chem.Phys.* **79**, pp 926-935.

Jorgensen, W.L., Impey, R.W. and Klein, M.L. (1983). Comparison of simple potential functions for simulating liquid water. *J.Chem.Phys.* **79**, pp 926-935.

Krueger, P.J. and Mettee, H.D. (1965). *J.Mol.Spectrosc.* **18**, p 131.

Lambrakos, S.G., Boris, J.P., Oran, E.S., Chandrasekhar, I. and Nagumo, M. (1989). A modified Shake algorithm for maintaining rigid bonds in Molecular Dynamics simulations of large molecules. *J.Comput.Phys.* **85**, pp 473-486.

Miyamoto, S. and Kollman, P.A. (1992). SETTLE: An analytical Version of the SHAKE and RATTLE Algorithm for Rigid Water Models. *J.Comput.Chem.* **13**, pp 952-962.

Nagy, P.I., Dunn III, W.J., Alagona, G. and Ghio, C. (1991). Theoretical Calculations on 1,2-Ethanediol. Gauche-Trans Equilibrium in Gas-Phase and Aqueous Solution. *J.Am.Chem.Soc.* **113**, pp 6719-6729.

Ohmine, I., Tanaka, H. and Wolynes, P.G. (1988). Large local energy fluctuations in water. II. Cooperative motions and fluctuations. *J.Chem.Phys.* **89**, pp 5852-5860.

Podo, F., Nemethy, G., Indovina, P.L., Radics, L. and Viti, V. (1974). Conformational studies of ethylene glycol and its two methyl ether derivatives. I. Theoretical analysis of intramolecular interactions. *Mol. Phys.* **27**, pp 521-539.

Pratt, L.R. and Chandler, D. (1977). Theory of the hydrophobic effect. *J.Chem.Phys.* **67**, pp 3683-3704.

Pratt, L.R., Hsu, C.S. and Chandler, D. (1978). Statistical mechanics of small chain molecules in liquids. I. Effects of liquid packing on conformational structures. *J.Chem.Phys.* **68**, pp 4202-4212.

Pratt, L.R., Rosenberg, R.O., Berne, B.J. and Chandler, D. (1977). Comment on the structure of a simple liquid solvent near a n-butane solute molecule. *J.Chem.Phys.* **73**, pp 1002-1003.

Raghavachari, K. (1984). Rotational potential surface for alkanes: Basis set and electron correlation effects on the conformations of n-butane. *J.Chem.Phys.* **81**, pp 1383-1388.

Rapaport, D.C. (1983). Hydrogen bonds in water. Network organization and lifetimes. *Mol.Phys.* **50**, pp 1151-1162.

Rebertus, D.W., Berne, B.J. and Chandler, D. (1978). A Molecular Dynamics and Monte Carlo study of solvent effects on the conformational equilibrium of n-butane in CCl_4 . *J.Chem.Phys.* **70**, pp 3395-3400.

Ryckaert, J-P. (1985). Special geometrical constraints in the molecular dynamics of chain molecules. *Mol.Phys.* **55**, pp 549-556.

Ryckaert, J-P. and Bellemans, A. (1978). Molecular Dynamics of Liquid Alkanes. *Discuss.Faraday Soc.* **66**, pp 95-106.

Ryckaert, J-P. and Ciccotti, G. (1986). Andersen's canonical-ensemble molecules dynamics for molecular with constraints. *Mol.Phys.* **58**, pp 1125-1136.

Ryckaert, J-P., Ciccotti, G. and Berendsen, H.J.C. (1977). Numerical integration of the Cartesian equations of motion of a system with constraints: Molecular Dynamics of n-alkanes, *J.Comput.Phys.* **23**, pp 327-341.

Saaty, T.L. (1961). *Elements of Queueing Theory with Applications*, McGraw-Hill.

Scherer, J.R. and Snyder, R.G. (1980). Raman spectra of liquid n-alkanes. II. Longitudinal acoustic modes and the gauche-trans energy difference. *J.Chem.Phys.* **72**, pp 5798-5808.

Scott, R.A. and Scheraga, H.A. (1966). Conformational Analysis of Macromolecules. II. The Rotational Isomeric States of the Normal Hydrocarbons. *J.Chem.Phys.* **44**, pp 3054-3069.

Stidham, H.D. and Durig, J.R. (1986). Far infrared spectrum and conformational potential function of n-butane. *Spectrochim.Acta.* Part A **42**, pp 105-111.

Tanaka, H. and Gubbins, K.E. (1992). Structure and thermodynamic properties of water-methanol mixtures: Role of the water-water interaction. *J.Chem.Phys.* **97**, pp 2626-2634.

Toxvaerd, S. (1987). Comment on constrained molecular dynamics of macromolecules, *J.Chem.Phys.* **87**, pp 6140-6143.

Toxvaerd, S. (1988). Molecular Dynamics of liquid butane. *J.Chem.Phys.* **89**, pp 3808-3813.

Toxvaerd, S. (1990). Molecular dynamics calculation of the equation of state of alkanes. *J.Chem.Phys.* **93**, pp 4290-4295.

van Alsenoy, C., van Enden, L. and Schäfer, L. (1984). Ab initio studies of structural features not easily amenable to experiment. *J.Mol.Struct.* **108**, pp 121-128.

van Gunsteren, W.F. (1980). Constrained dynamics of flexible molecules *Mol.Phys.* **40**, pp 1015-1019.

Verlet, L. (1967). Computer "experiments" on classical fluids. I. Thermodynamical properities of Lennard-Jones molecules. *Phys.Rev.* **159**, pp 98-103.

Warshel, A. and Lifson, S. (1970). Consistent force field calculations. II. Crystal structures, sublimation energies, molecular and lattice vibrations, enthalpies of alkane. *J.Chem.Phys.* **53**, pp 582-594.

Weeks, J.D., Chandler, D. and Andersen, H.C. (1971). Role of repulsive force in determining the equilibrium structure of simple liquids. *J.Chem.Phys.* **54**, pp 5237-5247.

Wielopolski, P.A. and Smith, E.R. (1986). Dihedral angle distribution in liquid n-butane: Molecular Dynamics simulations. *J.Chem.Phys.* **84**, pp 6940-6942.

Woller, P.B. and Garbisch, E.W.,Jr., (1972). The Conformational Analysis of n-Butane. *J.Am.Chem.Soc.* **94**, pp 5310-5314.

Zichi, D.A. and Rossky, P.J. (1986). Molecular conformational equilibria in liquids. *J.Chem.Phys.* **84**, pp 1712-1723.